# ACOUSTIC INVESTIGATION OF THE SHOALING DYNAMICS OF SARDINE *Sardinops sagax* POPULATIONS: IMPLICATIONS FOR ACOUSTIC SURVEYS.

DISSERTATION

Submitted in fulfilment
of the degree of
Master of Science
at the
University of Cape Town

by
Janet Claire Coetzee

April 1997

## ABSTRACT

The total allowable catches (TACs) of both anchovy and sardine in South africa are determined by assessment methods which rely on absolute estimates of recruitment and spawner biomass each year. The validity of the TAC set for each species each year is heavily dependent on the accuracy and precision of the biomass estimates. The method used for both anchovy and sardine has been acoustic surveys on a random stratified grid covering the known range of the species. These surveys have, however, been designed according to the life history patterns of anchovy, which result in a particular occupation of the pelagic environment. This study investigated the shoaling dynamics of sardine at various scales in both the horizontal and vertical dimension in an attempt to ascertain whether these surveys are adequate to characterise the occupation of space by sardine.

Hydro-acoustic data collected during 5 meso-scale surveys in 1994 and 1995 was used to study the shoaling dynamics of sardine, *Sardinops sagax* on the western Agulhas Bank of South Africa. Results of this study indicate the presence of spatial structure in sardine aggregations at both the shoal and meso-scale level. Spatial structure at the meso-scale level was very small and indicated the need for adapting the current survey strategies by decreasing inter-transect spacing substantially. A very clear structure was observed within shoals indicating non randomness and organised and synchronised activity within sardine shoals. A clear diurnal cycle in sardine density was also observed with densities being lower at night than during the day. Geostatistical selectivity curved also suggested dispersion of sardine at night, although some degree of shoaling still persisted. Definite diel vertical migration of sardine was apparent and the potential problem of underestimation of sardine biomass at night was highlighted. In addition, information present in the digitized backscattered signal was used to study the shoaling characteristics of sardine. A Principal Component Analysis successfully reduced the number of variables needed to describe sardine shoal characteristics to three main factors. These factors appeared to be spatially and temporally stable and indicated the possibility of making use of shoal characteristics to aid identification of pelagic species in the future.

## ACKNOWLEDGEMENTS

This study was completed under the auspices of the Benguela Ecology Programme with the support of the Sea Fisheries Research Institute. Both organizations are thanked for their contributions throughout the course of this study. Professor John Field and Ian Hampton, my two supervisors are kindly thanked for their support, motivation and inspiration. I am also indebted to Manuel Barange who provided me with information and advice on much of the statistical data analyses. I thank him too for his continuous guidance during this study. The officers and crew of the F.R.S.*Africana*, F.R.S.*Algoa* and R.V. *Dr. Fridtjof Nansen* are thanked for their cooperation throughout the surveys. Members of the RAM surveys group of the SFRI are acknowledged for their assistance in data collection and processing on board the research ships. Finally, I thank Vic for his support and encouragement and for putting up with all the stress!

## CONTENTS

Page

# CHAPTER 1.

# INTRODUCTION

## 1.1 CLUPEOID FISHERIES OF THE WORLD

The small pelagic fishes of which clupeoids such as anchovy, herrings and sardines form the major part, are of great importance in the world's fisheries. Annually they account for about one third of the world's total fisheries catches with a joint economical value of several billion dollars thereby making a major contribution to protein resources and economies of the world (Blaxter and Hunter, 1982). In 1992, seven of the top ten species landed were small pelagic fishes (Figure 1.1). The largest fishery in the history of the world was for Peruvian anchoveta of which sixteen million tonnes was landed in 1970 (Castillo and Mendo, 1987; cited in Blaxter and Hunter, 1982). Interruptions in the supply of clupeoids have serious implications world-wide because they are traded internationally as food for both human and animal consumption and as industrial products such as fertilizer and paints. In addition the supply of fish meal derived from these small pelagic fishes also has an effect on the international soybean market (Thompson, 1990).

A few species inhabiting relatively cool waters of eastern boundary currents and Japan make up most of the world's catch. In 1992, four cool-water species (anchoveta, Chilean jack mackerel, South American sardine and South African anchovy and sardine) accounted for 16 percent of the world's marine catch (FAO, 1994). A larger number of species live in tropical waters, but they are generally less productive. They are still important often forming the basis of subsistence fisheries where other sources of animal protein are not available or too expensive. Although there is still scope for further development of the fisheries of some tropical species, cool water species are already fully developed and many are believed to be overexploited.

Fishery records that extend back for hundreds of years, paleoecological records for thousands

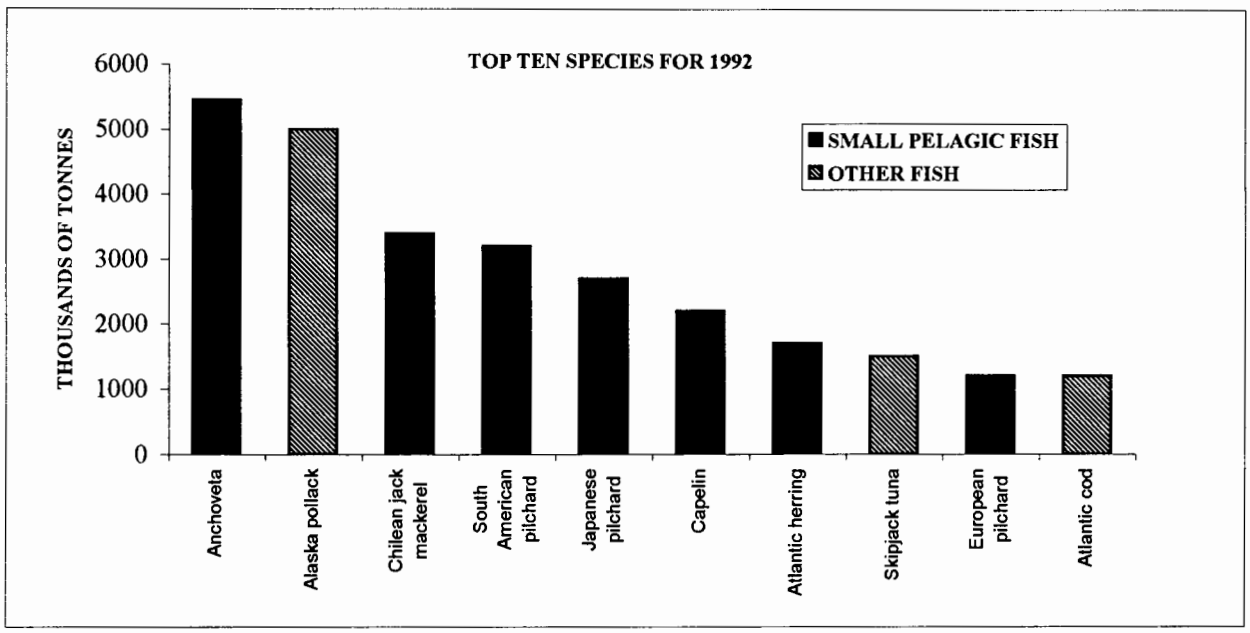


Fig 1. World landings of the top ten species during 1992 (from FAO yearbook, 1992)

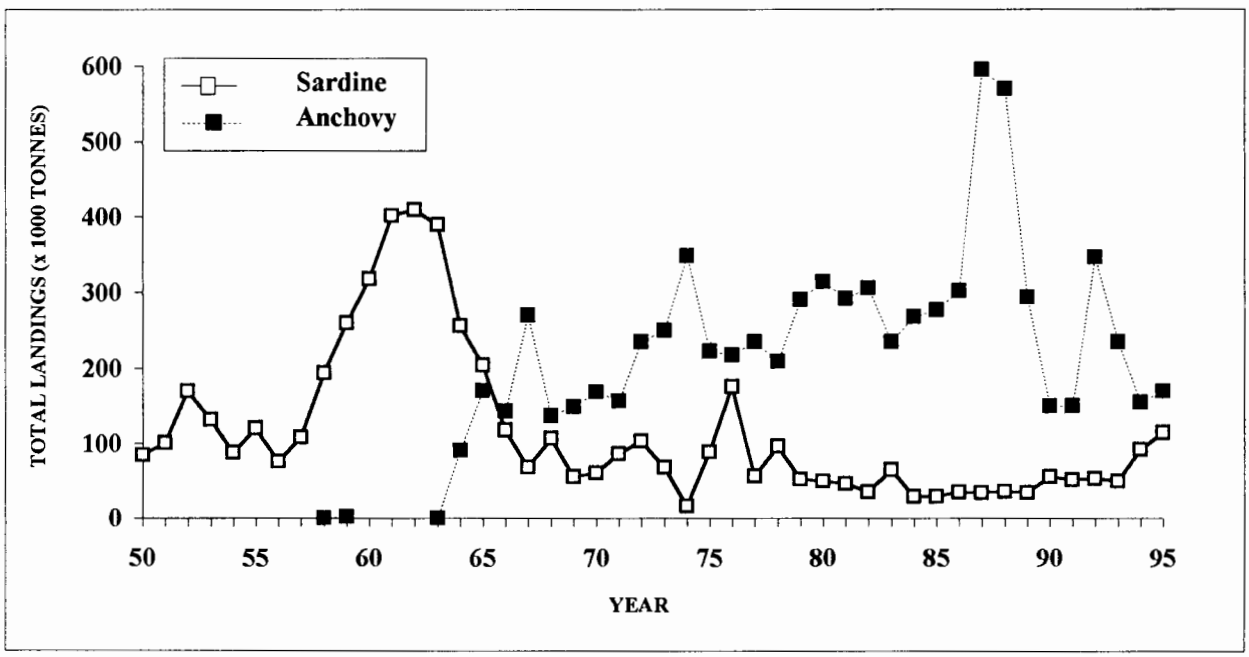


Fig 2. Landings of anchovy and sardine in South Africa from 1950 to 1995.

of years and genetic assessments over evolutionary time all indicate great variations in the productivity of small pelagic fish populations. Clupeoid populations around the world have undergone remarkable increases, followed by sudden and disastrous declines, which have caused the collapse of several fishing industries. A well-known example is that of the Peruvian anchoveta *Engraulis ringens* which expanded from a small fishery in the late 1950's to one of 8-12 million tonnes in 1966-72, and then drastically plummeted to 2 million tonnes or less by 1973 (Blaxter and Hunter, 1982). The decline was associated with a recruitment failure caused by a natural phenomenon, El Niño, combined with a management policy which led to overfishing. A probable combination of overfishing and natural changes also caused declines in other clupeoid stocks during the last few decades i.e.,the Californian sardine *Sardinops caerulea*, Japanese sardine *S. melanosticta,* South African sardine *S. sagax* and Atlantic herring *Clupea harengus* (Blaxter and Hunter, 1982). In every case, economic effects of these dramatic changes were significant on both national and international scales.

Most clupeoids are highly mobile, have short, plankton-based food chains and are short lived. They mature sexually in their first or second year, are highly fecund, and can spawn year round if conditions are suitable. These biological characteristics make them highly sensitive to environmental forcing and extremely variable in their abundance (GLOBEC, 1994).

## 1.2 CLUPEOID STOCKS OF SOUTH AFRICA

In the South - East Atlantic, clupeoids form the basis of important commercial pelagic fisheries off Namibia and South Africa's west and south coasts (Armstrong and Thomas, 1989). These clupeoids of which anchovy and sardine have periodically dominated, have supported the purse seine fisheries in both regions from as early as the late 1940's. Off the Western Cape, this industry really prospered from the late 1950's with sardine dominating the escalating catches until 1964, with a peak catch of 410 000 tonnes in 1962 (Crawford *et al.*, 1987). This sustained fishing pressure and a lack of proper management, probably coupled with poor recruitment, led to a rapid decline in the landings of sardine by the mid 1960's and fishing strategies of the purse seine fleet had to be changed to target on the less utilized anchovy resource (Armstrong and Thomas, 1989).

Anchovy catches have since dominated the catches of the purse seine fishery off South Africa, fluctuating between 150 000 tonnes and 600 000 tonnes. In contrast the sardine catches remained low yielding on average 71 000 tonnes annually between 1966 and 1985 (Figure 1.2). Recent assessments of the abundance of the sardine resource indicate an increase in sardine abundance probably as a result of the strict management policy adopted by the South African authorities with co-operation from the fishing Industry. In 1995 for the first time, the relative estimated sardine biomass was higher than that of anchovy (Pelagic Working Group, SFRI, unpublished reports). It is expected that with continued growth of the sardine population, anchovy will become less important (as the target species) and more effort will be put into the development of a sardine fishery and the management thereof (Barange and van der Lingen, 1996). Currently, the South African pelagic fishing industry represents about a fifth of the value of the fishing industry of South Africa and about 50 percent of the total clupeoid landings in the South - East Atlantic region (FAO, 1993).

## 1.3 ASSESSMENT OF CLUPEOID BIOMASS IN SOUTH AFRICA

Prior to 1984, recommendations on Total Allowable Catch (TAC) of anchovy and sardine were based on catch-per-unit-effort (cpue) indices and Virtual Population Analysis (VPA) of commercial catch data (Hampton, 1992). From these results in the early 1980's, it was considered at that time that both anchovy and sardine had been overexploited (Armstrong *et al.*, 1983; Butterworth, 1983).

In 1982, however, the Sea Fisheries Research Institute obtained the facility to conduct hydro acoustic surveys of pelagic fish with the commissioning of the F.R.S.*Africana* (Hampton *et al.*, 1985). Hydro acoustic estimates of fish abundance had become common practice in many countries since the early 1970's (MacLennan and Simmonds, 1992). This means of assessment has proved to be the most efficient way of providing a direct and synoptic measure of the abundance of pelagic fish populations which is independent of the fishery.

In South Africa the first reliable acoustic estimate of anchovy spawner biomass was obtained in November 1984 and the first assessment of anchovy recruitment followed in May/June of

the next year (Hampton, 1985). In addition, the daily egg-production method (DEPM) has been used simultaneously to estimate the anchovy spawner biomass since 1984 (Shelton *et al.*, 1992). Anchovy spawner biomass has therefore been estimated both by acoustics and by the (DEPM) every November since 1984 and anchovy recruitment every autumn by means of acoustic surveys (Hampton, 1992).

Acoustic estimates of sardine biomass were also obtained during the course of the yearly anchovy spawner biomass surveys since November 1984. The sardine biomass results of the earlier surveys were, however, not considered reliable because of large sampling errors. Recently, however, more acceptable precision has been achieved, probably as a consequence of the increasing size of the sardine population (Hampton, 1992). Sardine recruitment has also been estimated as a by product of most of the annual autumn anchovy recruitment surveys since 1984. Most of these estimates were considered to be too low as the entire geographic range of sardine recruits had not been covered. Currently these recruitment surveys are extended to cover the entire sardine recruit distribution and the results of all acoustic surveys are utilized in the final calculations of the recommended TAC for both anchovy and sardine. Further methodological details and particulars of the equipment and survey grids used to obtain these estimates may be found in Hampton (1987) and Hampton (1992).

The results of the spawner biomass estimates obtained for anchovy and sardine since 1984 are presented in Figure 1.3. Anchovy biomass has fluctuated greatly between 1.7 million tonnes and 400 thousand tonnes during the last 12 years. The anchovy spawner biomass has decreased substantially since 1991 and recent November estimates of anchovy spawner biomass are the lowest it has been since 1984. In contrast the sardine biomass has remained lower than the anchovy biomass for all of the surveys except the most recent two November surveys (Barange and van der Lingen, 1996). In general the sardine biomass has gradually increased from about 150 thousand tonnes in the late 1980's to the present level of close to 600 thousand tonnes.

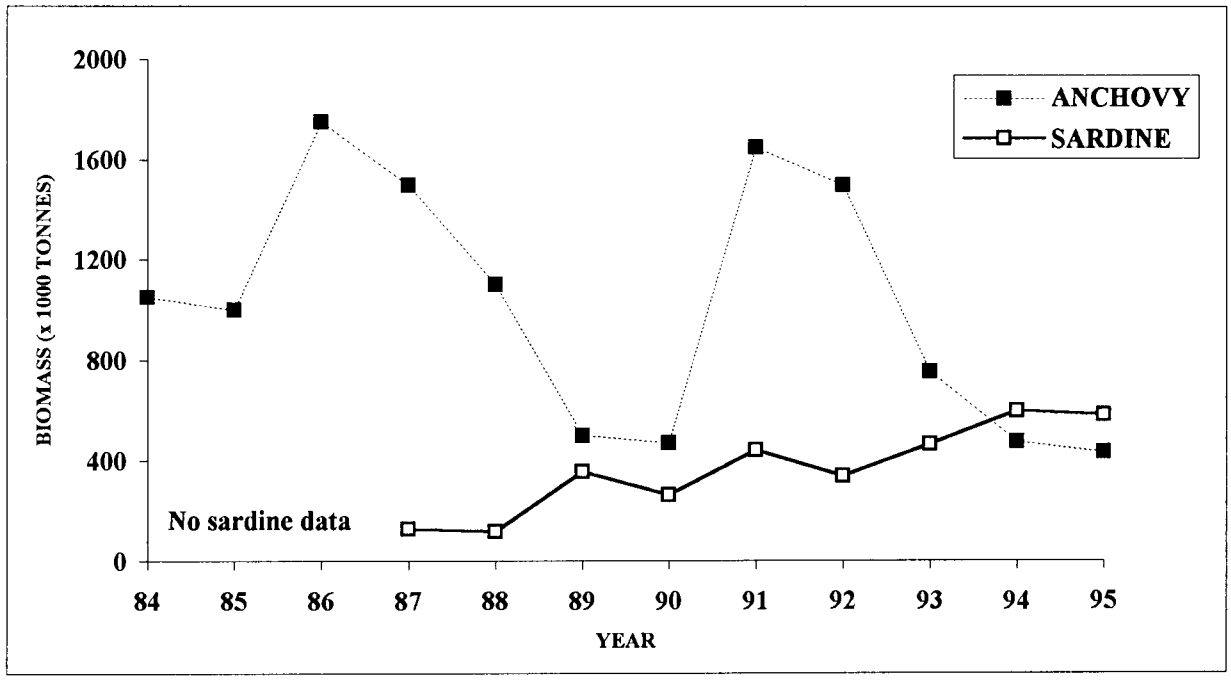


Fig 1.3. Relative acoustic abundance estimates for sardine and anchovy from 1984 to 1995.

## 1.4 BACKGROUND TO THIS STUDY

Although acoustic surveys form such an essential part of the management of the South African pelagic resource, it is recognised that acoustic surveys are highly sensitive to biases caused by effects of fish behaviour, particularly those which may reduce the acoustic detectability of fish. Fish in nature exhibit a variety of natural patterns of behaviour, adapted to the life of each particular species and to biological conditions. Acoustic surveys in South Africa were designed according to the particular life history patterns of anchovy, which results in a particular occupation of the pelagic environment. It remains to be seen if these surveys are adequate to characterise the occupation of space by sardine.

In acoustic surveys, numerous behavioural patterns have long been known to lead to various difficulties in correctly assessing fish biomass (Olsen, 1990; MacLennan and Simmonds, 1992; Fréon *et al.*, 1993). The following examples of behavioural biases may be of importance when assessing the biomass of sardine:

(i) Near surface shoaling - Acoustic sampling in the water column is restricted to the volume below the transducer. Fish above the transducer are not assessed. This is a potential source of bias whether the transducer is hull-mounted or mounted in a towed body. In this regard, diurnal variation in behaviour of pelagic organisms has been well documented (Hoar and Randall, 1978; Weston and Andrew, 1990). If extensive diurnal vertical migration does occur, the chance of not detecting fish close to the surface at night would lead to underestimation of the biomass.

(ii) Bottom or near bottom affinities - The ability of the acoustic system to sample near bottom is dependent on the extent of the "acoustic dead zone" (Ona and Mitson, 1996), which is determined by parameters such as pulse length, the transducer beamwidth and the distance between the transducer and the seabed. If fish were to migrate too close to the bottom , the biomass may only be partially estimated.

(iii) Schooling fish tend to aggregate in very high densities covering very small areas. This decreases the probability of encountering these high density areas during a large-scale survey. Survey reliability therefore largely depends on sampling a sufficient number of these high density areas.

(iv) Accurate hydroacoustic assessment of the biomass of a particular species has been limited by the difficulty to objectively differentiate among taxonomic groups of sound scatterers. Identification methods most commonly used are based on trawl sampling in close proximity to the acoustic targets and on visual interpretation of the echograms based on previous knowledge of species shoaling patterns. In many cases, however, these techniques have not enabled objective discrimination between co-occurring fish species (Rose and Leggett 1988). Species mixing in aggregations may also lead to biases in the proportion of the measured acoustic energy being allocated to a particular species. Hampton (1996) concluded that this error could be as large as 10 % in the case of South African anchovy during some surveys.

## 1.5 AIMS OF THIS STUDY.

Even with the best planning, certain biases may be unavoidable. Therefore, a knowledge of the biology and short-term and seasonal behaviour of sardine will provide some idea of the magnitude of this error. This will also enable the designs of these surveys to be improved so as to increase the precision of the sardine biomass estimate. The following chapters aim to investigate the shoaling dynamics of sardine in the light of the above mentioned probable biases and to study the manner in which sardine populations occupy the three-dimensional environment with the aim of improved understanding of their life history patterns.

# CHAPTER 2.

# MATERIALS AND METHODS

## 2.1 DATA COLLECTION AND EQUIPMENT

Data used for this study are acoustic data of fish density collected during four *ad hoc* acoustic surveys according to standard echo integration methodology (Maclennan and Simmonds, 1992). The equipment used for these purposes are the standard acoustic equipment used during all Sea Fisheries Research Institute acoustic surveys. These include a sphere-calibrated 38-kHz EK400 echo sounder and a custom built digital echo-integrator (Hampton, 1992). One of the surveys was done by the *R.V. Dr. Fridtjof Nansen* using a EK500 echo sounder interfaced to a Bergen Integrator. A mid water trawl (Engels 308) fitted with an anchovy cod-end liner of 8-mm mesh was used to identify acoustic targets during three of the surveys whilst a mid-water flytetral trawl was used during the *R.V. Dr. Fridtjof Nansen* survey.

In the absence of *in situ* estimates of target strength measurements of sardine, Halldórsson and Reynisson's (1983) expression for the weight-normalised target strength of herring *Clupea harengus* at 38 kHz as a function of length was used to convert back-scattering strengths to density. Hampton (1987) and Roel and Armstrong (1991) supply background and reasoning for the use of this particular target strength function. Recent measurements of *in situ* target strength of sardine in South Africa have, however, been made (Barange *et al.*, 1996). These results indicate an increase in sardine target strength per kg and therefore a decrease in fish density compared to that obtained from the above mentioned herring expression. For the purposes of this study, however, results should not be influenced by using either of the expressions.

Sardine abundance was calculated by converting mean surface back-scattering strength (MSBS) to density ($g.m^{-2}$) through the expression:

$$Density\ (g.m^{-2}) = 10^{0.1(MSBS - TS.kg^{-1})} * 1000$$

where $TS.kg^{-1} = -10.9 \log L_t - 20.9$

**or**

by converting $S_A$ values to density ($g.m^{-2}$) through the expression:

$$Density\ (g.m^{-2}) = 10^{0.1[(10\ \log(\frac{S_A}{4.\pi.1852^2})) - TS.kg^{-1}]} * 1000$$

where $TS.kg^{-1}$ is the same as before.

As all data were collected in areas where trawls indicated the presence of sardine only, it was not necessary to apply any weighting factors for proportional allocation of the acoustic energy between species. The mean density of each survey was calculated as a simple sample average of all ESDU's (elementary sampling distance unit) and multiplied by the total area covered in square kilometres to obtain a relative estimate of biomass.

## 2.2 SURVEY GRIDS

Four independent surveys done during the course of 1994/1995 were used for the collection of acoustic data. Listed in order of occurrence they were RAFOS II (Reproduction And Feeding of Sardine), intercalibration survey between the F.R.S. *Africana* and the R.V *Dr. Fridtjof Nansen*, RAFOS III and the sardine behaviour survey. All surveys took the form of meso-scale surveys in which systematic grids of parallel transects were surveyed. All surveys were also designed so as to cover each grid both during daylight and during darkness. The RAFOS III survey consisted of two separate meso-scale surveys which were sampled both during daylight and darkness thereby bringing the total number of individual coverages to ten. The transects during all surveys were approximately normal to the coast and their lengths varied between 10 and 15 nautical miles. Inter-transect spacing was kept as small as possible and varied from two to seven nautical miles. Inter-transect spacing for each individual survey was, however, kept constant. The surveys were all conducted on the Western

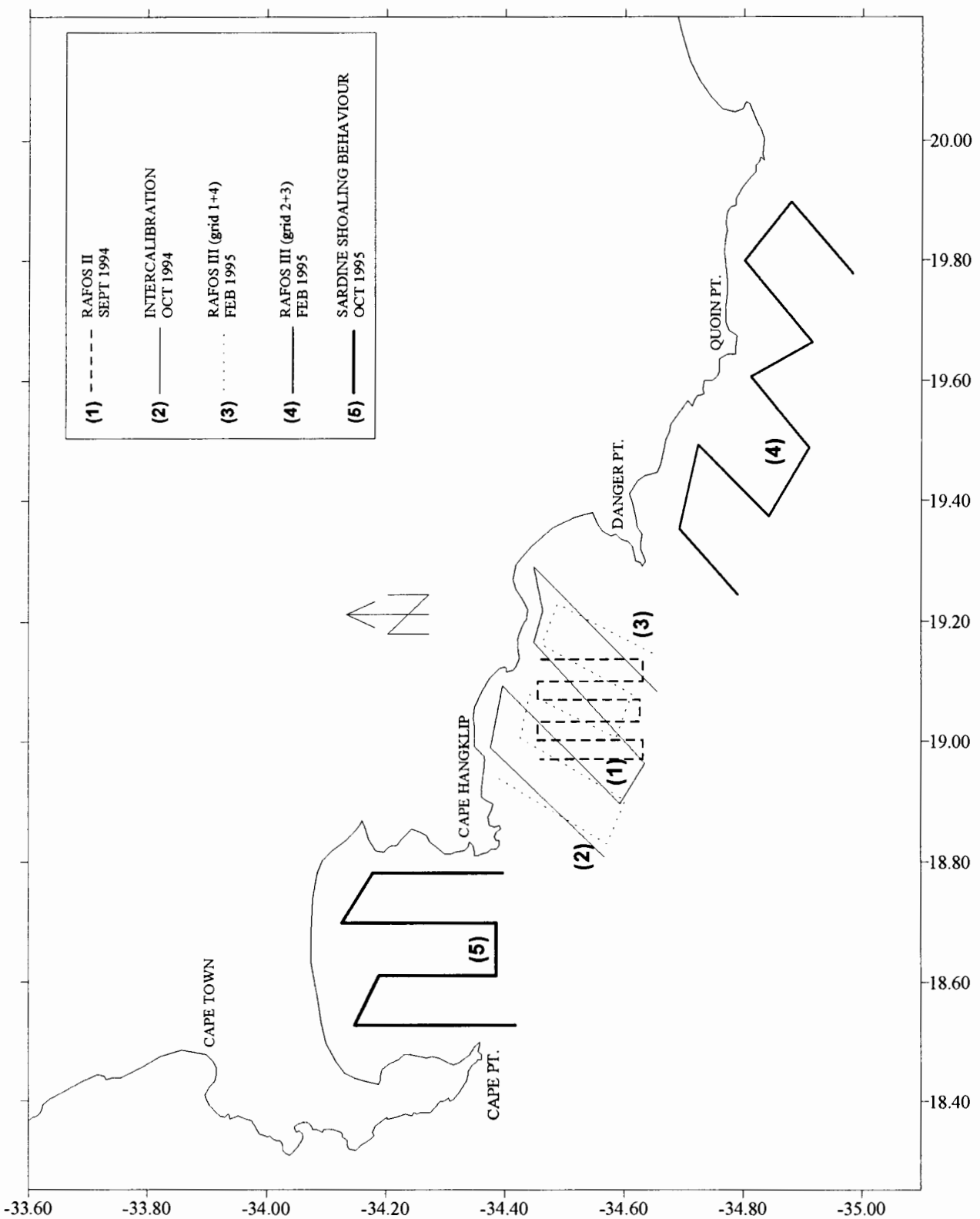


Figure 2.1. Geographic location and details of each survey grid

Agulhas Bank between Cape Point and Cape Agulhas. Three of the surveys were done in the Walker Bay area (between Cape Hangklip and Danger Point), one in the Quoin Point area, just South of Walker Bay, and the other inside False Bay (between Cape Point and Cape Hangklip). All of the surveys were done during the summer months i.e., September 1994, October 1994, February 1995 and October 1995. Detail of the positions and timing of each survey are shown in Figure 2.1.

## 2.3 METHODS USED TO RELATE SARDINE DISTRIBUTION TO TEMPERATURE.

Sea surface temperature (SST) data were used to investigate effects of temperature on the distribution of sardine. Data used in the analysis were collected during eight SFRI routine hydro acoustic stock assessment surveys between 1986 and 1993 as well as during 14 SARP (Sardine and Anchovy Recruitment Programme) surveys. The latter surveys were completed during 1993 and 1994. During the stock assessment surveys SST was recorded continuously from a 5 m deep water intake while the ship was underway. To accurately relate sardine distribution to the hydrographical conditions, we only used recordings of temperature where the percentage of sardine was higher than 70 %. During the SARP surveys, SST data were obtained at 10 nm intervals at 4 m depth during oblique bongo tows.

## 2.4 METHODS USED TO DESCRIBE SPATIAL STRUCTURE

Two methods were applied during this study:

2.4.1 Geostatistics. This is a group of statistical techniques developed to analyze spatial patterns of continuous variables. The variogram is the structural tool used. It measures the level of dissimilarity between points as a function of the distance separating them. An increase in the variance as distance between points increases indicates that closer points are more similar than more distant points and therefore there is spatial structure. If the variogram is flat, then close points are as dissimilar as more distant points and there is no structure.

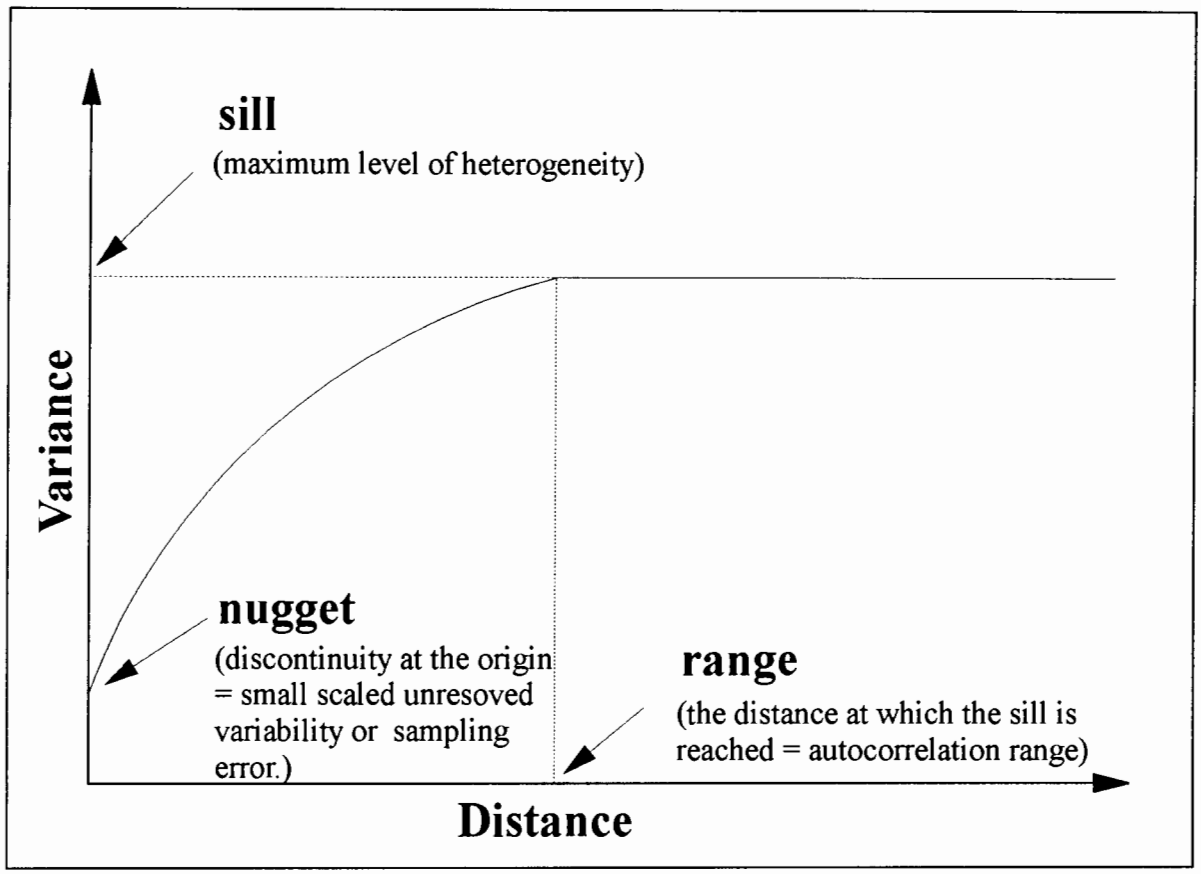


Fig 2.2. A basic representation of a variogram and a short discription of the main features.

A typical variogram, is shown and features thereof described in Figure 2.2. The variogram can be calculated in several directions to highlight structural anisitropies. Various variogram techniques were used to characterise aggregation patterns of sardine at the meso-scale level as well as within individual shoals.

2.4.2 Shoal analysis and patch estimation system (SHAPES). This is a Sea Fisheries Research Institute (SFRI) - developed software capable of identifying, extracting and statistically characterising fish shoals in an automated and objective manner from acoustic data. Shapes provides statistics for up to 17 school descriptors, including size and shape variables (i.e.,length, height, area, volume, perimeter, fractal dimension), variables describing internal features and energetic characteristics of the schools (i.e.,mean and standard deviation of the acoustic intensity, horizontal and vertical roughness, skewness and kurtosis of the acoustic energy) as well as relational statistics such as nearest neighbour distance and angle. Shapes was used to describe sardine aggregations and to feed data into a geostatistical analysis.

For the purposes of this study, the terms "school" and "shoal' are used in the same sense and no distinction is implied between them.

## 2.5 SARDINE SPATIAL ANALYSIS

As the analysis of the spatial structure is closely dependent on the scale at which the structures are observed, this study was done at small scale (shoal level) and at meso-scale (population level).

### 2.5.1 Horizontal patterns of dispersion

Each meso-scale survey was regarded as an instantaneous sample of a fixed spatial

distribution. All transects were re-integrated into one nautical mile segments. Acoustic back-scattering values were converted to density ($g.m^{-2}$) as described in section 2.1. Each value is therefore the mean density over one nautical mile (nm) of the digital echoes already integrated on the vertical. Each value is located at the centre of a one nm segment and therefore the values are 1 nm apart along the ships track. However, as they represent 1 nm segment integrations, the transects are continuously sampled. In order to calculate distances between values, the latitudes and longitudes were converted to nautical miles. Variograms were then computed using the EVA software (Petigas and Prampart, 1993) to investigate the spatial structure for each survey. Both isotropic (omnidirectional) and two-dimensional (along track and across track) experimental variograms were computed according to Matherton's (1971) variogram estimator:

$$\gamma(h)=\frac{1}{2N(h)}\sum_{i=1}^{N(h)}[Z(x_i+h) - Z(x_i)]^2$$

where $Z(x_i)$ is the density for the $i$-th data point, and $N(h)$ is the number of pairs of points which are a distance $h$ apart.

Day and night differences in spatial heterogeneity were measured by the skewness of the histograms of fish density. Because it is difficult to study how the shape of the histogram varies when the mean varies, geostatistical selectivity curves were used to compare the shapes of histograms (Petitgas, 1994). When surveys have different means, P(T) curves may be computed where P(z) is defined by:

$$P(z) = \frac{Q(T)}{m}$$

P(z) represents the percentage of the population abundance that is standing on the percentage T(z) of total surface. T(z) is defined by the densities greater than z. The P(T) curve is computed as follows:

$$Q(z_p) = \sum_{i=p}^{n} \frac{n_i}{n}.z_i \quad ; P(z_p) = \frac{Q(z_p)}{m} \quad ; T(z_i) = \sum_{i=p}^{n} \frac{n_i}{n}$$

where $n_i$ is the number of data in class i, n the number of data in the survey, $z_i$ the mean of class i and m the mean of the survey. The variations in shapes of the P(T) curves associated

with variations in the population abundance enable to characterise so called strategies for the occupation of space.

### 2.5.2 Spatial structure between schools

The spatial distribution of shoals extracted by SHAPES for analysis in previous sections was investigated. A 1 X 1 nm grid was superimposed on surface plots of the shoals and the number of shoals in each grid cell counted. In addition a Chi-square test based on expected Poisson statistics was done to test for randomness of shoals. Shoals per grid cell was also used in a geostatistical analysis to investigate the existence of structure between shoals in each of the surveys. For these purposes, distance was calculated using the relative positions of the grid cells. Each grid cell position was taken as the centre of the cell and therefore adjacent cells were 1 nm apart.

### 2.5.3 Shoal identification and description

Acoustic interval data was processed by shapes in the following manner. A data matrix consisting of $n$ columns (one per echo return) and $m$ rows (one per 1-m vertical depth channel) was generated for each 1 nm acoustic interval according to the methods described by Barange (1994). A threshold value was predetermined by comparing echo charts with the aggregations identified by shapes. This threshold value was used to filter each individual matrix to eliminate any unwanted "noise" such as that originating from plankton. A threshold value of 100 units corresponding to a minimum fish density of 0.1 individuals per $m^3$ for a 17 cm fish was chosen and used throughout the analysis. Filtered matrices were then subjected to a shoal-recognition process whereby a shoal was identified using algorithms based on super-threshold adjacent cell criteria which consisted of the following:

(i) a minimum number of columns - a shoal was recognised if adjacent super-threshold cells in the horizontal dimension occurred in a set minimum number of echo returns

(ii) a minimum number of rows - to be considered a shoal the number of adjacent super-threshold cells in the vertical dimension had to exceed the minimum value

(iii) a continuity factor which allowed for a maximum number of below- threshold adjacent cells.

The continuity factor served to smooth the small-scale variability between successive echo returns, whilst the minimum number of rows and columns was intended to discard isolated single super threshold cells. These values were set between 3 and 4 pings in the horizontal dimension depending on the vertical recording range and a vertical extent of at least 2 rows. This corresponded to a minimum shoal size of 10 meters long and 2 m high.

Once identified, shoals were extracted after careful scrutiny in conjunction with the original echo charts and any shoals which were too close to the surface or bottom so as not to be completely integrated, were discarded. Statistical indices as described earlier were then calculated for each shoal according to the algorithms described by Nero and Magnuson (1989), Reid and Simmonds (1993) and Barange (1994).

Before the calculation of averaging parameters, corrections to school shape variables to account for pulse length effects were performed. In addition, artifacts due to beam width were corrected for by removing pings that had not completely insonified the shoal on both sides. Formal definitions of these variables were presented by Barange (1994) and are included in Table 2.1. In this way, a new matrix was created for each survey which consisted of $p$ rows (one per identified shoal) and 17 columns (one for each shoal variable). Three additional variables related to fish density were calculated for each shoal i.e., density per surface area ($g.m^{-2}$), density per unit volume ($g.m^{-3}$) and packing density ($individuals.m^{-3}$). An example of one shoal extracted by shapes is shown in Figure 2.3. These variables were then used in a number of statistical analysis such as regressions, correlations and ANOVAS to describe differences and similarities between shoal parameters as observed during the various surveys. All statistical tests were done according to methods described by Zar (1984) or by using STATISTICA® data analysis software. In addition a principle component analysis was used to establish which variables best describe the school characteristics of sardine.

Table 2.1. Definitions of variables calculated by shapes and corrections made.

| Variable | Definition | Notes |
|---|---|---|
| Nearest neighbour angle | $\tan^{-1}( \lvert i_1-i_2 \rvert / (\lvert j_1-j_2 \rvert)*k)$ | where k is the number of meters per ping (calculated using vessel speed and ping rate) and i are rows and j are columns. |
| Nearest neighbour distance | $((i_1-i_2)^2 + ((j_1-j_2)*k)^2)^{0.5}$ | |
| $Height_{real}$ | $HEIGHT_{appar}$ - (c*γ/2) | where c = speed of sound, γ = pulse length, θ = the half angle of the beam, D = shoal mean depth and k as above. |
| $Length_{real}$ | $[(LENGTH_{appar} *k) - (2*\tan\theta*D)]*4/\pi$ | |
| Area (A) | $L * H * \pi$ | |
| Volume (V) | $[(\pi * L^2 * H)/4]$ | |
| Number of cells (N) | Σ(cells) | |
| Perimeter (P) | Σ(side - cells) | |
| Fractal dimension | (Ln (P/4)*2)/Ln(N) | |
| Pings to discard (each side) | (tan θ * D)/k | Where θ, D and k are as above. |
| Mean Echo intensity ($E_m$) | $(\Sigma \langle E_{ij} \rangle)/(N)$ | |
| Stdev of Echo intensity ($E_s$) | $\sqrt{\frac{\Sigma(\langle E_{ij}\rangle)^2 - \frac{(\Sigma\langle E_{ij}\rangle)^2}{n}}{n-1}}$ | |
| Coefficient of Variation ($E_{cv}$) | $(E_s)^2/E_m$ | |
| Coefficient of Horizontal Roughness | $Rh^2/E_m$ | $where\ Rh^2 = \frac{\Sigma(\langle E_{ij}\rangle - \langle E_{ij+1}\rangle)^2}{n-1}$ |
| Coefficient of Vertical Roughness | $Rv^2/E_m$ | $where\ Rv^2 = \frac{\Sigma(\langle E_{ij}\rangle - \langle E_{i+1j}\rangle)^2}{n-1}$ |
| Skewness ($g_1$) | $K_3/(E_s)^3$ | $where\ K_3 = \frac{N.\Sigma(\langle E_{ij}\rangle - E_m)^3}{(n-1)(n-2)}$ |
| Kurtosis ($g_2$) | $K_4/(E_s)^4$ - 3 | $where\ K^4 = \frac{[(N^3+N^2).\Sigma\langle E_{ij}\rangle^4] - [4(N^2+N).\Sigma\langle E_{ij}\rangle^3.\Sigma\langle E_{ij}\rangle] - [3.(N^2-N)(\Sigma\langle E_{ij}\rangle^2)^2 + [12N.\Sigma\langle E_{ij}\rangle^2.(\Sigma\langle E_{ij}\rangle)^2}{N(N-1)(N-2)(N-3)}$ |

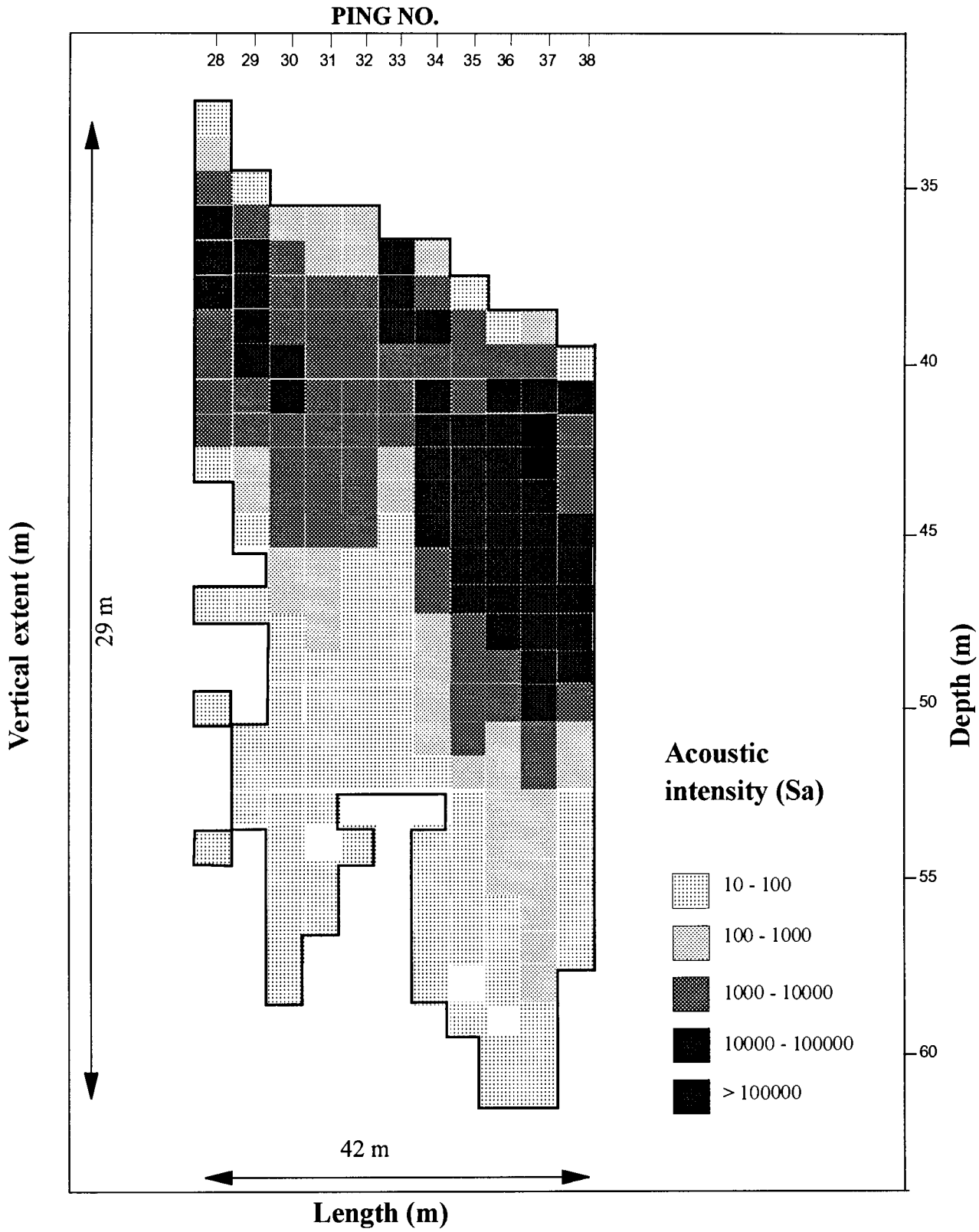


| Height (m) | Length (m) | Area ($m^2$) | Volume ($m^3$) | Perimeter (# cells) | Mean Intensity (Sa) | Horizontal Roughness | Vertical Roughness | Skewness | Depth (m) |
|---|---|---|---|---|---|---|---|---|---|
| 29.3 | 42.3 | 5430 | 80213 | 82 | 10497 | 42358 | 26049 | 2.1 | 49 |

Fig 2.3. An example of a shoal identified and analyzed by SHAPES with an example of the statistical output.

In each case the schools were assumed to be cylindrical with equal length and width. There is, however, no guarantee that the sampling transect passed through the middle of each school. It is most likely that schools will not be sampled through the centre, but the assumption is made that shoals will be encountered at random with increasing number of schools.

### 2.5.4 Internal school structure

The internal school structure of 12 large sardine shoals was investigated by the use of variograms. For each selected shoal, the matrix created by shapes consisting of $n$ columns and $m$ rows was imported into a spreadsheet and modified for use in a geostatistical analysis. A new matrix was thereby created for each shoal which consisted of $n$ columns (each representing the length of one ping in meters calculated from vessel speed and ping rate) and $m$ rows (one for each 1 m vertical channel). Each cell was then used as a sampling point of a systematic grid and fed into the geostatistical analysis. Two-dimensional variograms were computed for each shoal (horizontal and vertical dimensions) and a model fitted to each.

## 2.6 TEMPORAL DYNAMICS OF SARDINE

### 2.6.1 Vertical patterns of dispersion

The vertical distribution of sardine and particularly diel vertical migrations was investigated using the same 1 nm integrated acoustic intervals. The depth of the maximum backscattering strength for each interval was calculated as the mid-point of a 5 m vertical channel in which the echo return was the strongest. Although this depth calculated did not always reflect the true depth of the bulk of the fish distribution as was the case with big shoals which could extend down from the surface for 20 to 30 metres, it was the simplest and most unbiased method of obtaining a depth measurement for each interval. To investigate the existence of diel vertical migratory patterns all intervals were allocated day or night status. As all surveys took place in the summer months (between September and February) an approximate sunrise and sunset time corresponding to 04:00 GMT and 18:00 GMT was chosen as the split between day and night for all surveys. For instances where hourly depths were calculated each hour lasted from half an hour before the hour specified to half an hour after.

### 2.6.2 Diurnal variation in density

Acoustic back-scattering values for each 1 nm segment of transect were converted to density ($g.m^{-2}$) as described in Chapter 2.1. Densities were split into hour classes as described above. Non-parametric tests such as Kolmogorov-Smirnov, Wilcoxon and Mann-Whitney (Zar, 1984) were used to compare day and night mean densities. Densities were then logarithmically transformed in an attempt to normalize the distributions. Both Kolmogorov-Smirnov and Chi-squared goodness of fit procedures were used to test for log-normality. A multifactorial analysis of variance was performed to study the effect of the survey, the time and their interactions. Time was entered in two ways: firstly as day-night period and secondly as hour interval. In an attempt to smooth the effects of different mean survey densities, a relative acoustic density index was calculated for each elementary sampling distance unit (ESDU). This was in fact the ratio of the mean density of the ESDU to the mean acoustic density observed during the relevant survey. For these purposes the mean acoustic density of a survey was the mean of both coverages (day and night). It was therefore assumed that no change in distribution had occurred during the time lapse between successive coverages. This use of a relative acoustic density index for each survey assisted in providing a global stationarity for the distribution.

Following the example of Freon *et al.*(1993), the autocorrelation function (AFC) of each survey was studied in order to detect a diurnal cycle in acoustic density. In order to study the AFC with as many diurnal cycles as possible, an artificial time series of mean hourly densities was constructed using all the surveys. Missing values were inserted between surveys to maintain the 24 hour periodicity. Missing values were recognised during the computation of the AFC. The time series eventually corresponded to an uninterrupted survey lasting 132 hours and comprising eleven 12 hour cycles.

# CHAPTER 3.

# SPATIAL STRUCTURE OF SARDINE AT MESO-SCALE LEVEL

## 3.1 RELATIONSHIP BETWEEN SARDINE DISTRIBUTION AND TEMPERATURE

Hydrological features such as temperature fronts and thermoclines possibly have an important effect on the behaviour of sardine and would effect both their horizontal and vertical distribution. For that reason this study investigates how particularly the horizontal distribution of sardine relates to sea surface temperature.

As no clear hydrological features were apparent during any of the meso-scale surveys, sea surface temperature data from other surveys have been used to relate sardine distribution to temperature.

A frequency distribution of sea surface temperature where sardine were present in substantial quantities during the stock assessment surveys is presented in Figure 3.1. Only about 20 % of all sardine observations were made at sea surface temperatures of less than 14 °C. Most observations were made at sea surface temperatures of between 16 and 18 °C with a prominent maximum at 17 °C. Very few observations of sardine were made at sea surface temperatures exceeding 18 °C and none at SST's exceeding 20 °C. Investigations into the preferences of different size cohorts of sardine failed to reveal any clear patterns in their distributions relative to sea surface temperature.

Sea surface temperature contours superimposed on sardine distributions during 6 of the SARP (Sardine and Anchovy Recruitment Program) surveys are presented in Figures 3.2 (a - f). Figures 3.2 (a-c) and Figures 3.2 (d-f) show the distributions and sea surface temperature isotherms during early, mid and late summer of 1993 and 1994 respectively. A very distinct pattern is seen, particularly in the Cape Agulhas region, during both years.

In early summer (Figure 3.2 a and d) the distribution of sardine extends approximately 60 nm offshore. During this time no strong sea surface temperature fronts were observed with the

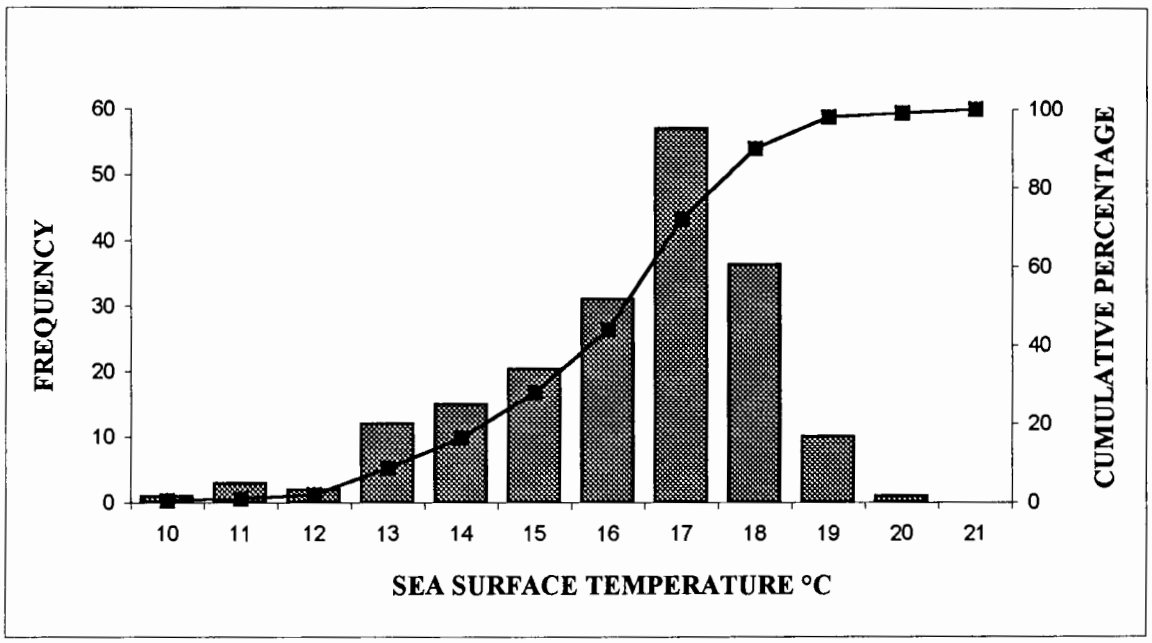


Fig 3.1. Frequency distribution of sea surface temperature where sardine were present during November spawner biomass surveys.

SST's being very uniform over the entire Western Agulhas Bank. The outer edge of the distributions roughly coincide with the 19 °C isotherms in both years.

During mid-summer of both years (Figures 3.2 b and e), a very pronounced temperature gradient is found close inshore, probably due to the influx of warmer Agulhas current water onto the shelf area. During both years, the 19 °C isotherm shifted from approximately 60 nm offshore in November to only 20 nm offshore during January and February. Corresponding to this hydrographic feature, the distribution of sardine changed drastically and was limited to a narrow band close inshore within 20 nm of the coast. Once again the 19° C isotherms were located in close proximity to the outer edge of the sardine distributions.

By late summer of both years (Figures 3.2 c and f), the distributions of sardine had again spread out over the shelf with the offshore edge of the distribution extending approximately 40 nm offshore. Once again, coincident with the distributions, the SST over the shelf area was more uniform than that found during mid-summer and the 19 °C had shifted further offshore.

It is therefore clear that sea surface temperature, and in particular, temperature fronts have a very strong influence on the spatial distribution of sardine and should be taken into account when studying any distributional or behavioural patterns.

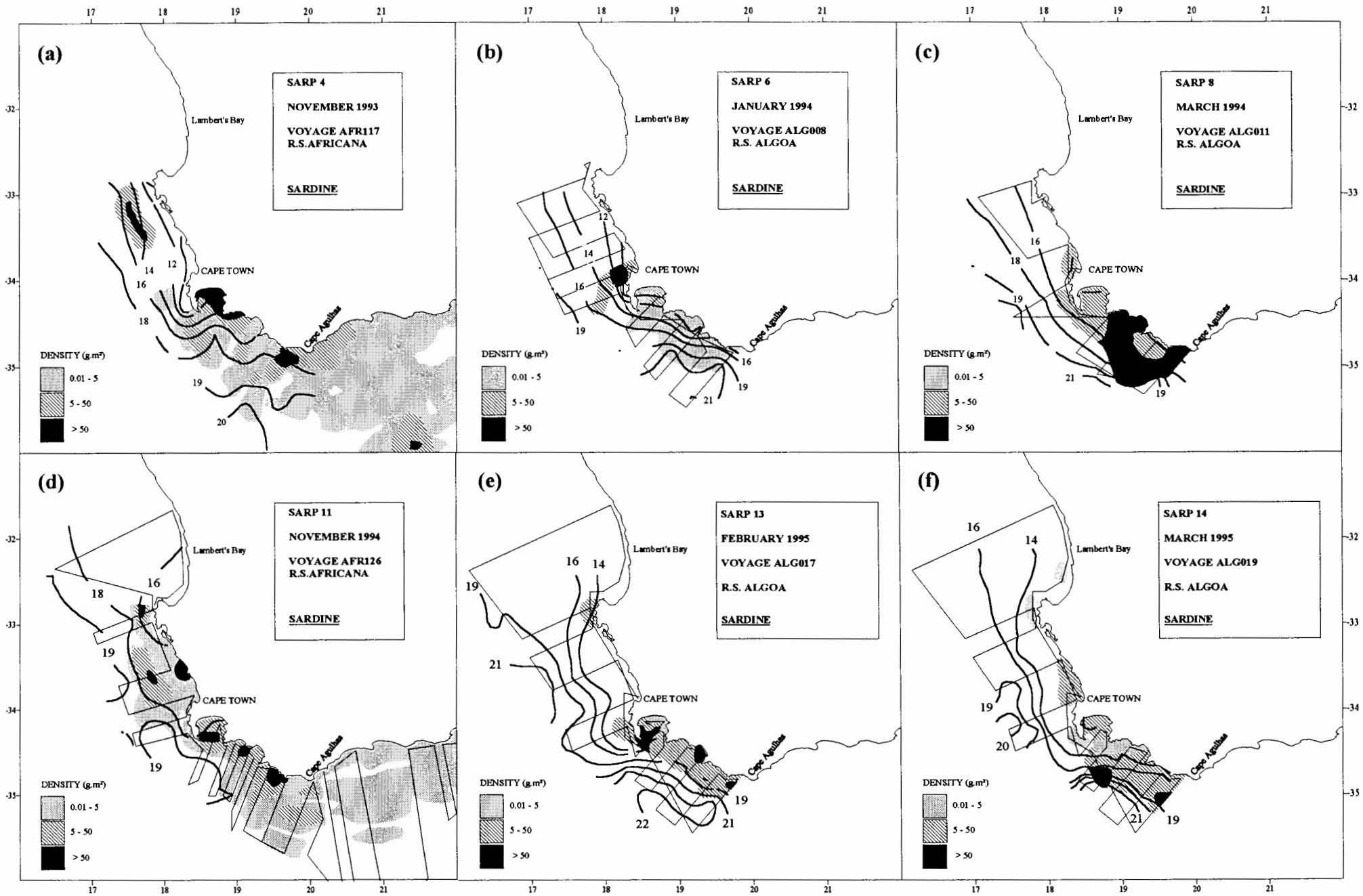


Fig 3.2. Distribution of sardine in relation to sea surface temperature during the summer months of SARP I (a-c) and II (d-f).

## 3.2 HORIZONTAL PATTERNS OF DISPERSION AND DAY-NIGHT VARIABILITY

A knowledge of the spatial structure of sardine populations and their strategies of occupying space is essential if accurate assessments of their biomass are to be made. Of particular concern are the apparent large differences in acoustic density estimated between day and night surveys covering the same area. The following section aims to determine the extent of the spatial structure of sardine during the four meso-scale surveys and how it changes with time.

A proportional representation of the densities measured during the four meso-scale surveys(1 nautical mile units) is shown in Figure 3.3 a and b. The values are represented by circles with the largest value being represented by the circle with the largest radius and all other values represented by circles with proportionally smaller radii. General observations for each survey are described below as an introduction to the structural analysis performed:

### (i) RAFOS II.

This survey consisted of 6 parallel transects approximately 10 nm long with an inter-transect spacing of 2 nautical miles. The first grid of the Rafos II survey which was completed during daylight hours shows mostly smaller values around the edges of the survey area with a group of larger values towards the centre of the area. Large differences in density are observed with the largest value being two orders of magnitude greater than the smallest value. The second grid was completed during darkness and in this case the values seem to be of a similar magnitude throughout the survey area with no grouping of larger values in any particular area. The densities are also somewhat lower than during the first coverage of this area.

### (ii) INTERCALIBRATION.

In the case of the intercalibration survey the first coverage of the survey grid was also performed during daylight whilst the second coverage was completed during darkness. The grid for this survey comprised 5 parallel transects spaced about 5 nm apart. The length of the transects varied between 8 and 12 nm. Once again the distribution of densities was more homogenous during the night survey with all values being of a similar

magnitude. During the day a few large values were recorded towards the centre of the survey area with lower values towards the edges. The densities recorded during the day survey tended to be higher than during the night survey.

(iii) SHOALING BEHAVIOUR.

During the shoaling behaviour survey the same grid was repeated twice although not split into day and night. The first two transects of the first grid (from left to right) were completed during daylight whilst the last two transects were completed during darkness. For the second coverage the first two transects (from left to right) were completed during darkness and the last two transects during daylight. Transects in this case were approximately 15 nm long with an inter-transect spacing of 5 nm. It is clear that the densities recorded during daylight are not as homogenous as those recorded during darkness. Values also tended to be much larger during the day than during the night in both cases.

(iv) RAFOS III (1 st survey).

During the RAFOS III (grid 1) survey, the same grid was surveyed both during darkness and during daylight. Inter-transect spacing during this survey was 5 nm and the length of the transects approximately 15 nm. Densities recorded during both coverages tended to be quite similar and proportionally lower than above mentioned surveys. Values were homogeneously spread throughout the survey area.

(v) RAFOS III (2 nd survey).

The RAFOS III (grid 2) survey was similarly also completed twice, during day and night. In this case transects were wider spaced than in the other surveys (7 nm) and had a length of approximately 10 nm. In both cases the largest densities were recorded towards the edge of the sampling area. Densities recorded during day and night were quite similar with large values being recorded during both coverages in similar areas.

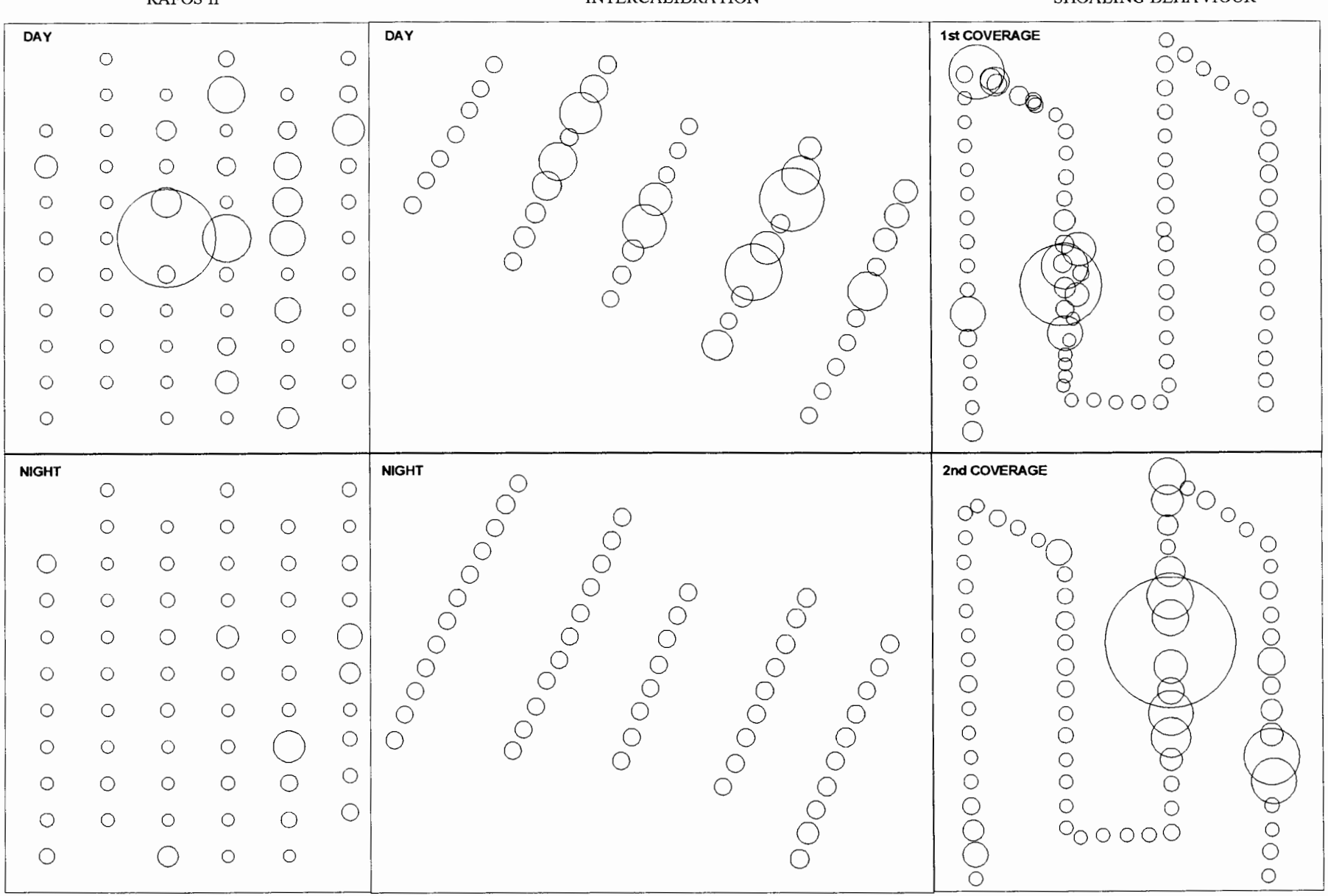


Fig 3.3(a). Proportional distribution of density (g/m²) for RAFOS II, the intercalibration and the shoaling behaviour survey. An increase in the radii of the circles represent increases in density. (sampling unit = 1 nm).

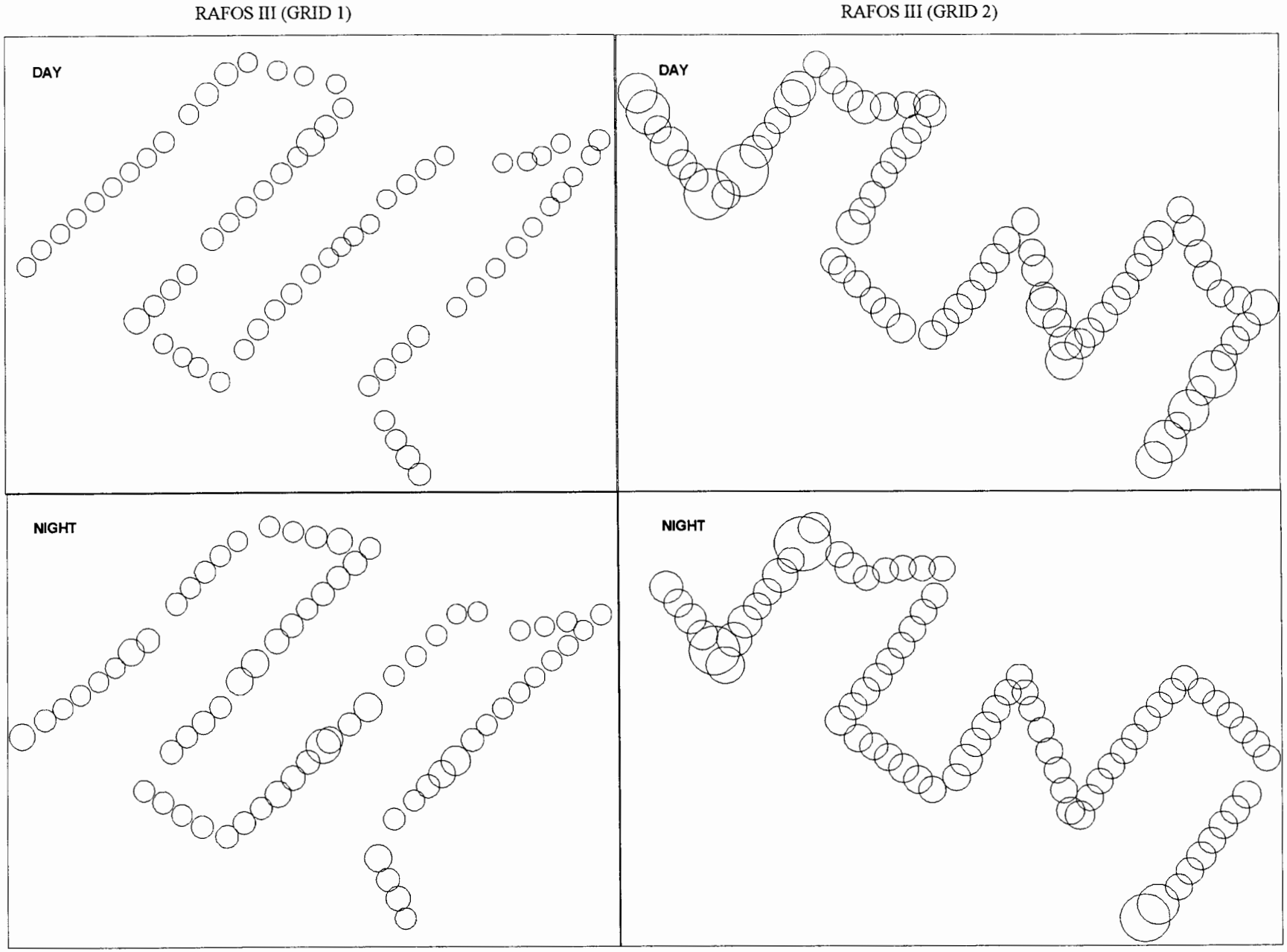


Fig 3.3 (b). Proportional representation of density (g/m²) for both RAFOS III surveys. An increase in the radii of the circles represent increases in density. (sampling unit = 1 nm).

Both isotropic and two dimensional intrinsic variograms were computed using these 1 nm density values to investigate the spatial structures of sardine distributions during these surveys. The analysis of each survey is presented below:

(i) RAFOS II (1 st coverage, day)

The histogram of fish density is shown in Figure 3.4(a). It is highly skewed with a very long tail. Only one value greater than 1000 $g.m^{-2}$ was recorded and although this value only accounts for 1.6 % of the total values, it contributes 25 % to the mean and 65 % to the total variance. The 18 highest values, those greater than 100 $g.m^{-2}$ represent only 30 % of the total data set but account for more than 90 % of the mean and 88 % of the variance.

The isotropic variogram and variogram model calculated for this data is shown in Figure 3.4(b). The variogram has a certain nugget effect, after which the variance increases to reach a maximum at a range of 5 nm. The subsequent decrease in variance is caused by the size and position within the grid of the high density values. These features reflect the degree of spatial continuity in the data. Two-dimensional variograms ($0^\circ$ and $90^\circ$) to check for anisotropies in the data (Figure 3.4 c) shows very little difference between the structure of the population along- and across-track. In both cases a nugget is present, although it is slightly larger in the direction of $0^\circ$ indicating larger unresolved small scale variability than in the $90^\circ$ direction. This is expected due to the inter-transect spacing being larger than the along-transect spacing. In both cases the sill is quite similar and the variograms decrease after reaching this point of maximum variance.

(ii) RAFOS II (2 nd coverage, night)

The frequency histogram of density is skewed to the right (Figure 3.5 a) with most of the values being less than 100 $g.m^{-2}$. Densities greater than 100 $g.m^{-2}$ accounted for only 13 % of the total data set, but represented 56 % of the mean and 85 % of the variance. The isotropic variogram computed on the density values is highly erratic and shows no structure (Figure 3.5 b). The variance decreases from the second lag to the third lag after which it increases slowly to reach a maximum at the seventh lag and then decreases again. No model is fitted to the data except for a straight line which is equal to the variance of the data. The two dimensional variogram

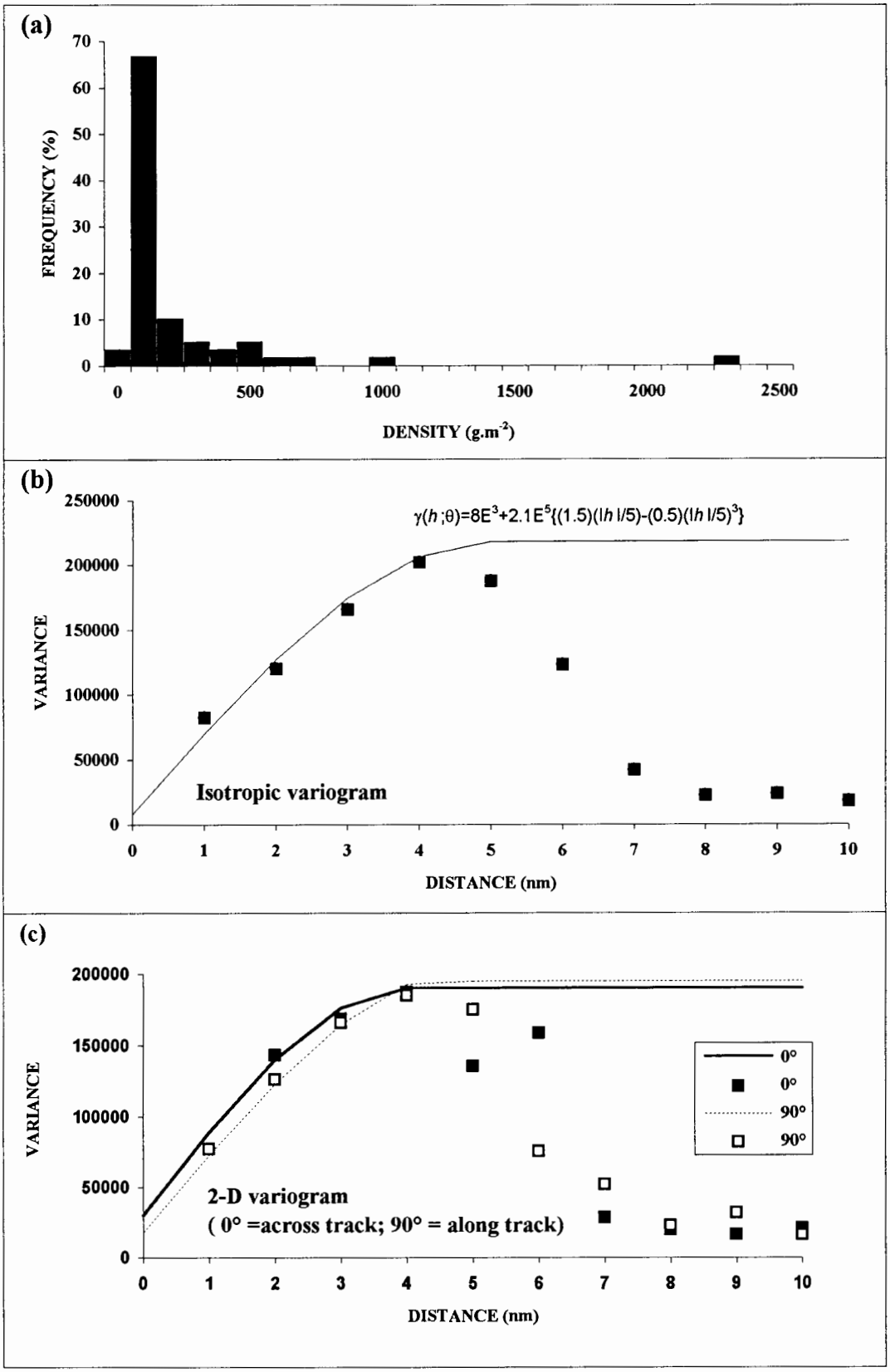


Fig 3.4. The frequency histogram of fish desity ($g.m^{-2}$) during the day coverage of the RAFOS II survey is shown in (a), the isotropic variogram in (b); and the 2-D variogram in (c).

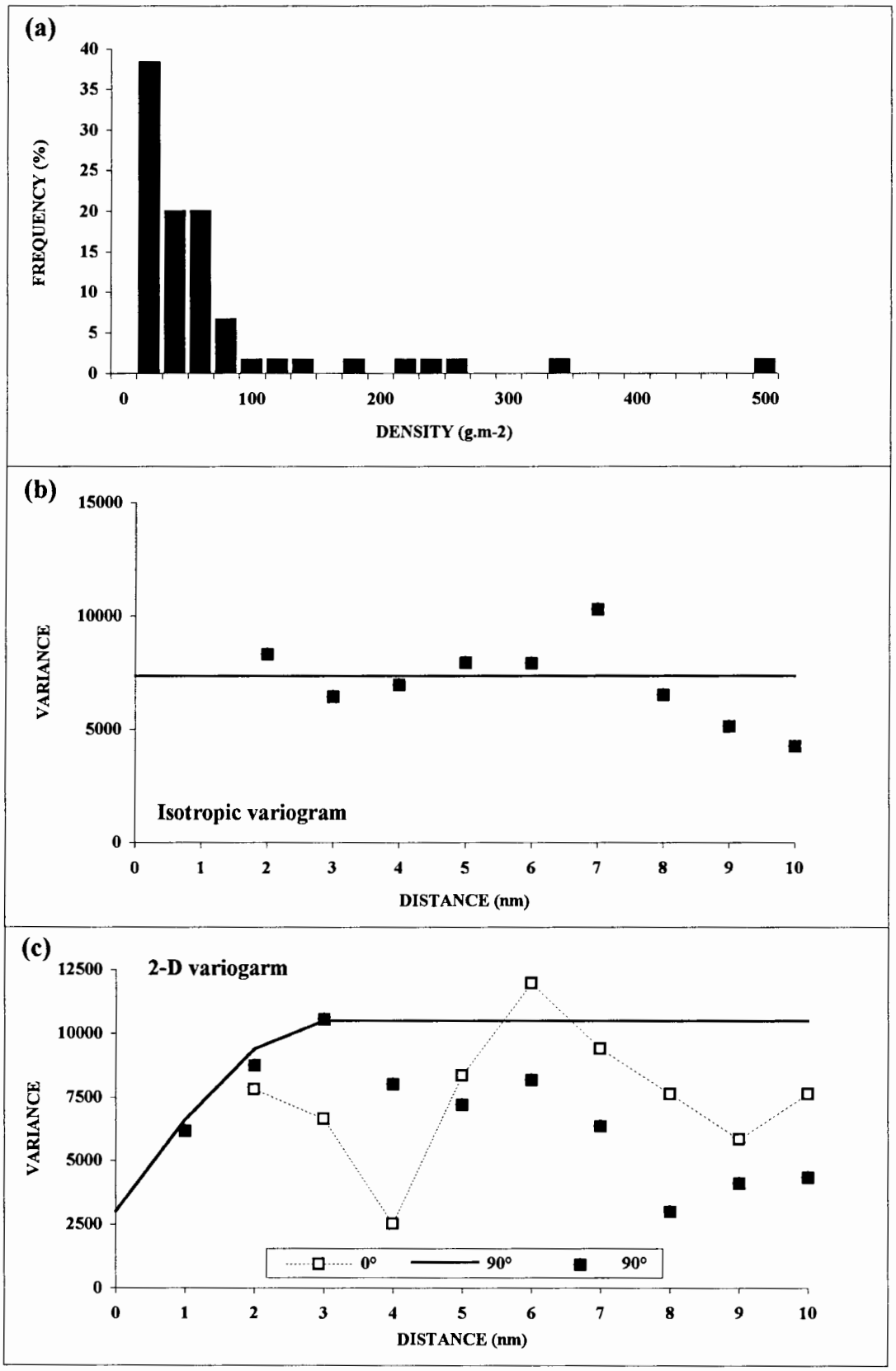


Fig 3.5. The frequency histogram of density for the night coverage of the RAFOS II survey is shown in (a); the isotropic variogram in (b) and the 2-D variogram in (c).

calculated for this data (Figure 3.5 c) showed a very small structure in the 90° direction (along track). The variogram increased quickly from a nugget to reach a maximum variance at a range of 3 nm after which it stabilized around the variance and then decreased. In the 0° direction, no structure at all was observed with the variogram first decreasing and then increasing with increasing distance. No model was fitted to this variogram.

(iii) Intercalibration survey (1 st coverage, day)

The frequency histogram of fish density recorded is shown in Figure 3.6 (a). Most of the density values are less than 100 $g.m^{-2}$ with only 37 % of the values being greater than 100 $g.m^{-2}$. These values, however, contribute 90 percent to the mean and 76 % of the total variance. The distribution is therefore very highly skewed to the right with a very long tail. The isotropic variogram calculated for this survey (Figure 3.6 b) possibly indicates a very small structure (range =2nm) and a large nugget effect. After reaching the maximum variance, the variogram stabilizes around the variance. When two-dimensional variograms are computed from the same data (Figure 3.6 c), very little structure is observed in both the along (90°) and across-track (0°) direction.

(iv) Intercalibration survey (2 nd coverage, night)

The frequency distribution of density is skewed to the right (Figure 3.7 a). Values less than 10 $g.m^{-2}$ represent 40 % of the data with values between 10 and 50 $g.m^{-2}$ making up the rest of the values. Only 1 value recorded was greater than 50 $g.m^{-2}$ and although it accounts for a small percentage of the total data set, it represents almost half (49 %) of the total variance. All variograms, both isotropic and two-dimensional, showed no spatial structure. The isotropic variogram is shown in Figure 3.7 (b).

(v) Shoaling behaviour survey (1 st coverage, day/night)

The frequency distribution of density for this survey is extremely skewed to the right (Figure 3.8 a). Only one value was higher than 1000 $g.m^{-2}$ and although forming such a small part of the data set it accounts for 50 % of the total variance and contributes 17 percent to the mean. The

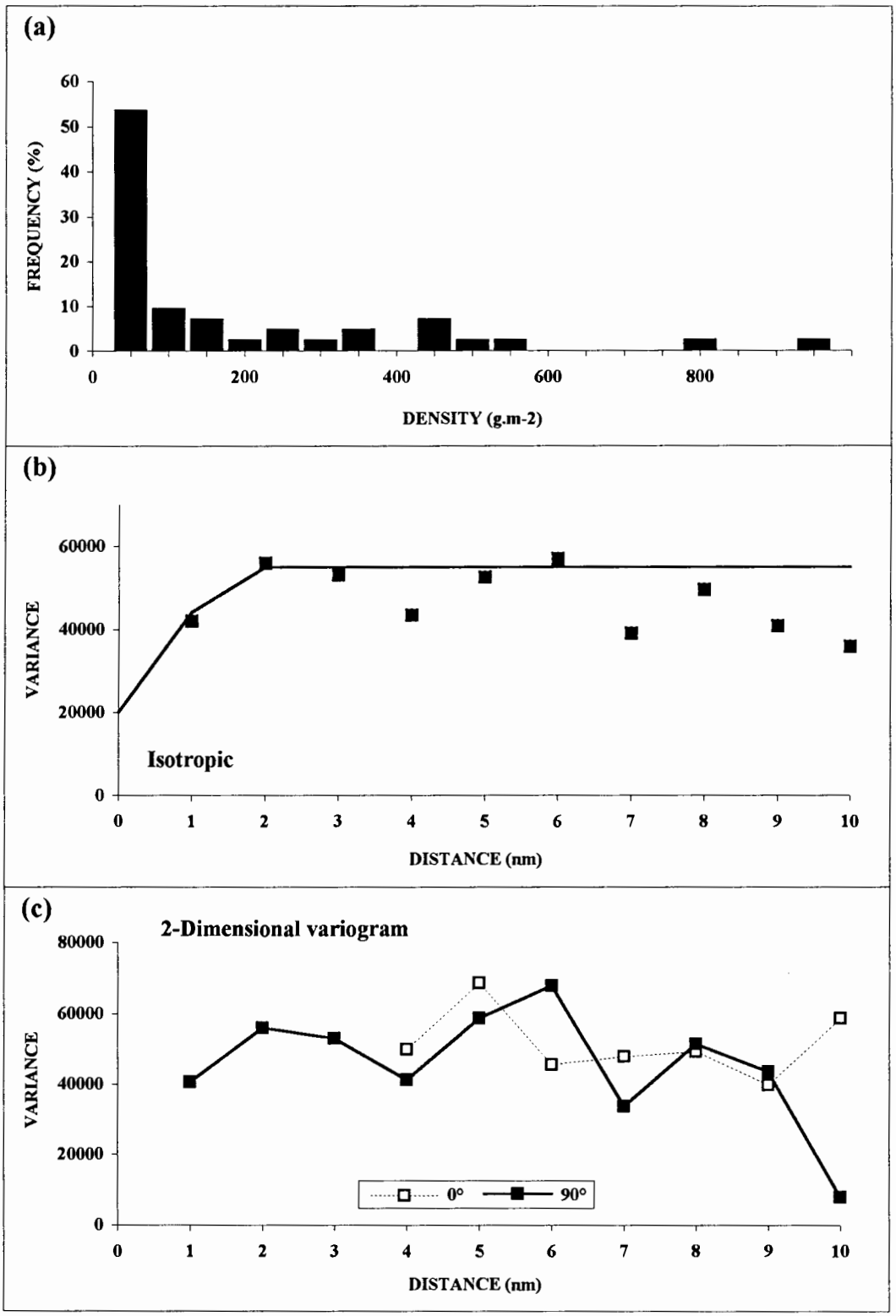


Fig 3.6. The histogram of fish density ($g.m^{-2}$) for the day coverage of the intercalibration survey is shown in (a), the isotropic variogram is shown in (b) and the two-dimensional variogram is shown in (c).

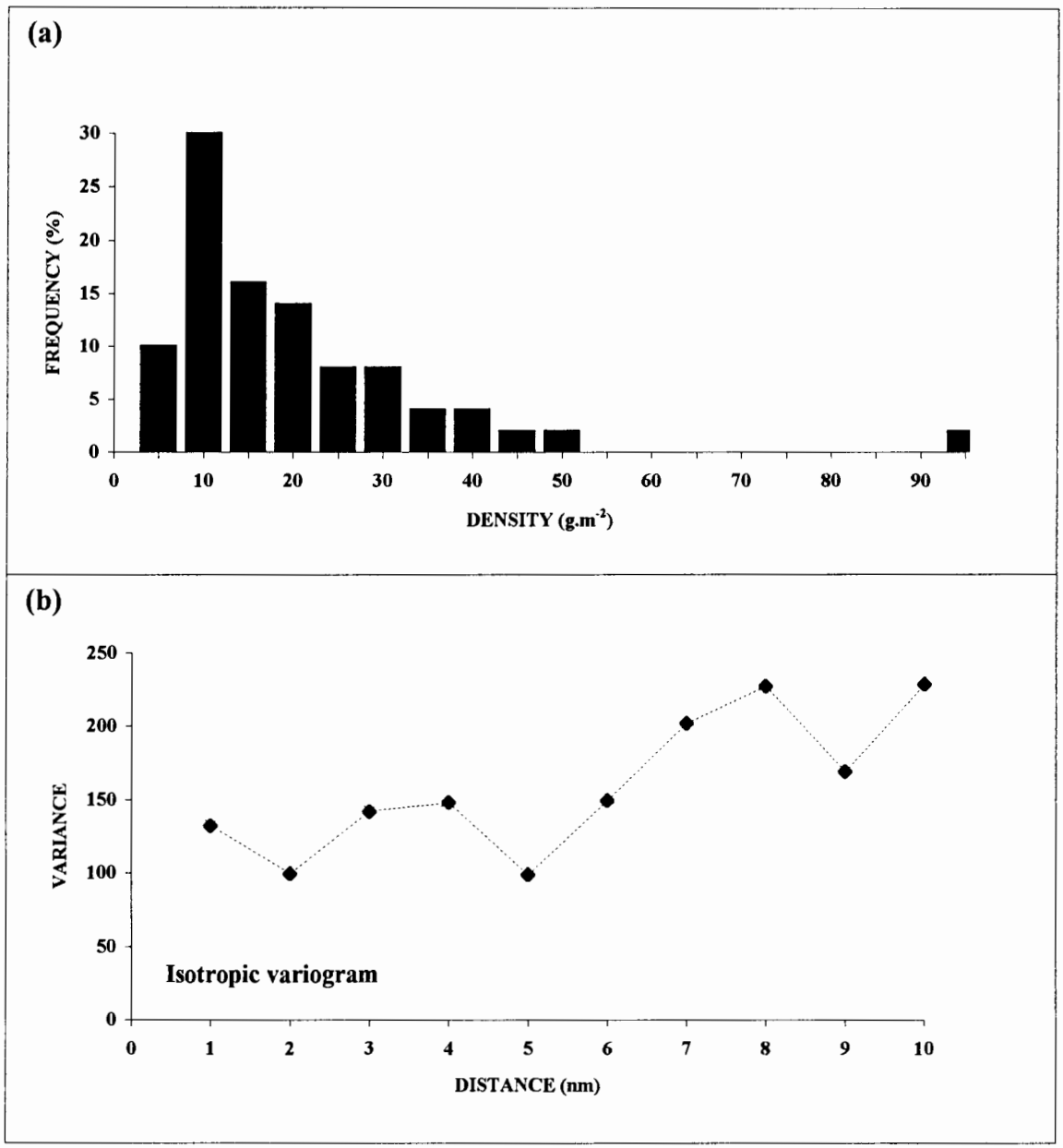


Fig 3.7. The frequency distribution of fish density ($g.m^{-2}$) during the night coverage of the intercalibration survey is shown in (a) and the isotropic variogram is shown in (b).

bulk of the values were less than 100 $g.m^{-2}$ and although making up a large portion of the data set, they account for less than 10 % of the total variance and represent only 20 percent of the mean.

An isotropic variogram was computed (Figure 3.8 b) and showed a very high nugget effect as a result of the one isolated high value recorded. No structure could be inferred with the variance being maximum for the first lag and then decreasing for subsequent lags. The two-dimensional variogram (Figure 3.8 c) computed once again showed no structure in the 0° (across-track) direction. The variogram was very erratic fluctuating greatly for most lags. In the 90° (along-track) direction, however, some spatial structure was present, with the variogram increasing slowly to reach a maximum variance at a range of 6 nm, despite the large nugget effect. This anisotropy is most likely due to the sampling grid followed, with values along the transects being more closely spaced than those in between transects.

(vi) Shoaling behaviour survey (2 nd coverage, night/day)

The frequency distribution of density ($g.m^{-2}$) is presented in Figure 3.9 (a). The distribution is extremely positively skewed with the values ranging from a minimum of 0.12 $g.m^{-2}$ to a maximum of 2718 $g.m^{-2}$. In fact only one value is higher than 1000 $g.m^{-2}$, but although it accounts for a small proportion of the total data set, it contributes 21 % to the mean and 65 percent to the variance. Most of the values have a density of less than 100 $g.m^{-2}$ and therefore the mean value of 176 $g.m^{-2}$ is strongly weighted by values greater than 100 $g.m^{-2}$.

The isotropic variogram computed is shown in Figure 3.9 (b). The variogram does not reveal any clear structure, being dominated by the effect of the one isolated high-density area. The maximum variance is reached at a lag of 6 nm, indicating the size of the sector where high densities were encountered. A two-dimensional variogram was also computed (Figure 3.9 c). The variogram of the 90° (along-track) direction reflects the patterns already evidenced in the isotropic variogram. The cross-track variogram (0°) is erratic as can be expected given the large inter-transect spacing and the small number of transit lines.

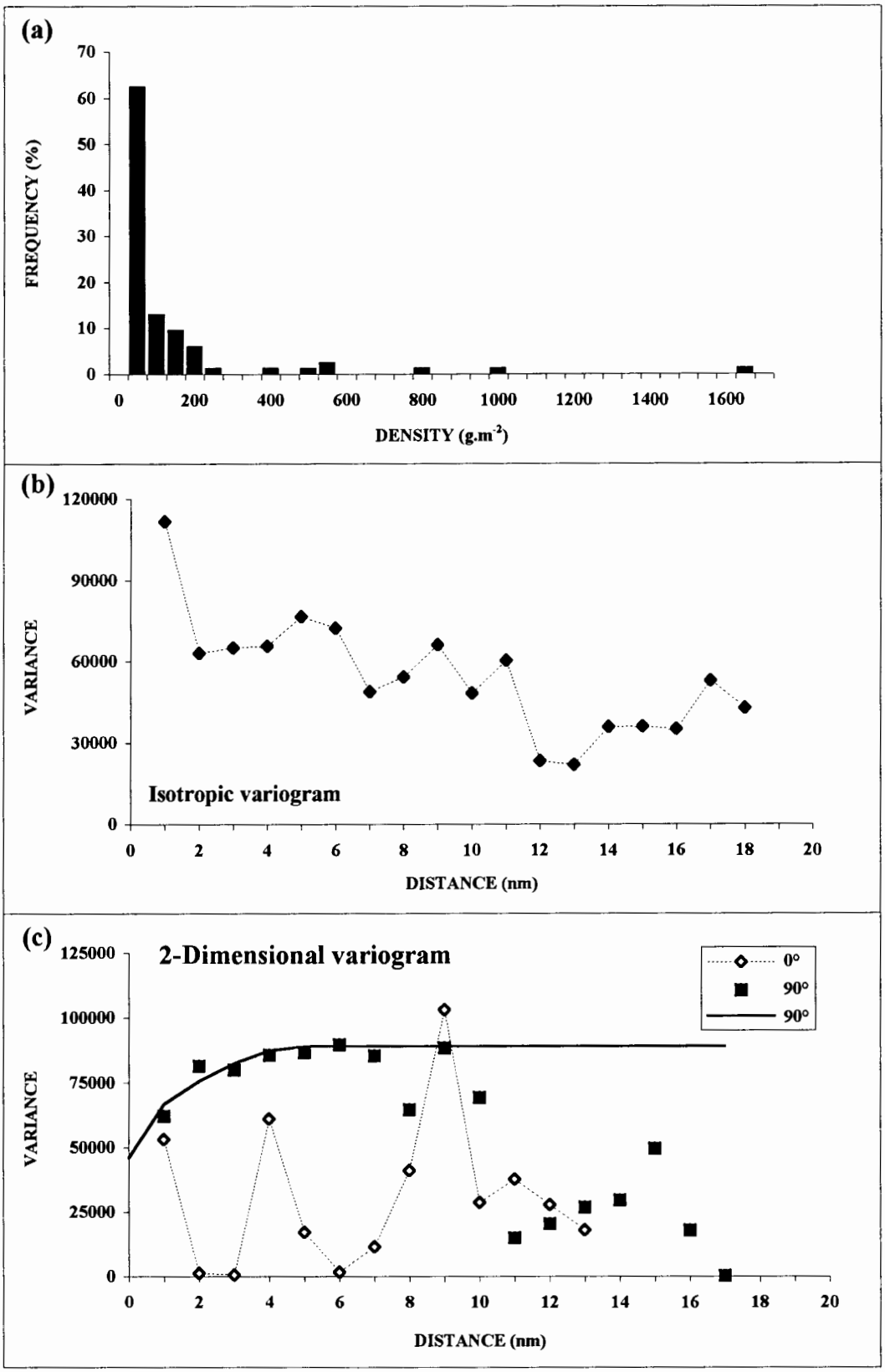


Fig 3.8. The frequency histogram of fish density ($g.m^{-2}$) during the first coverage (day/night) of the shoaling behaviour survey is shown in (a), the isotropic variogram is shown in (b) and the two-dimensional variogram is shown in (c).

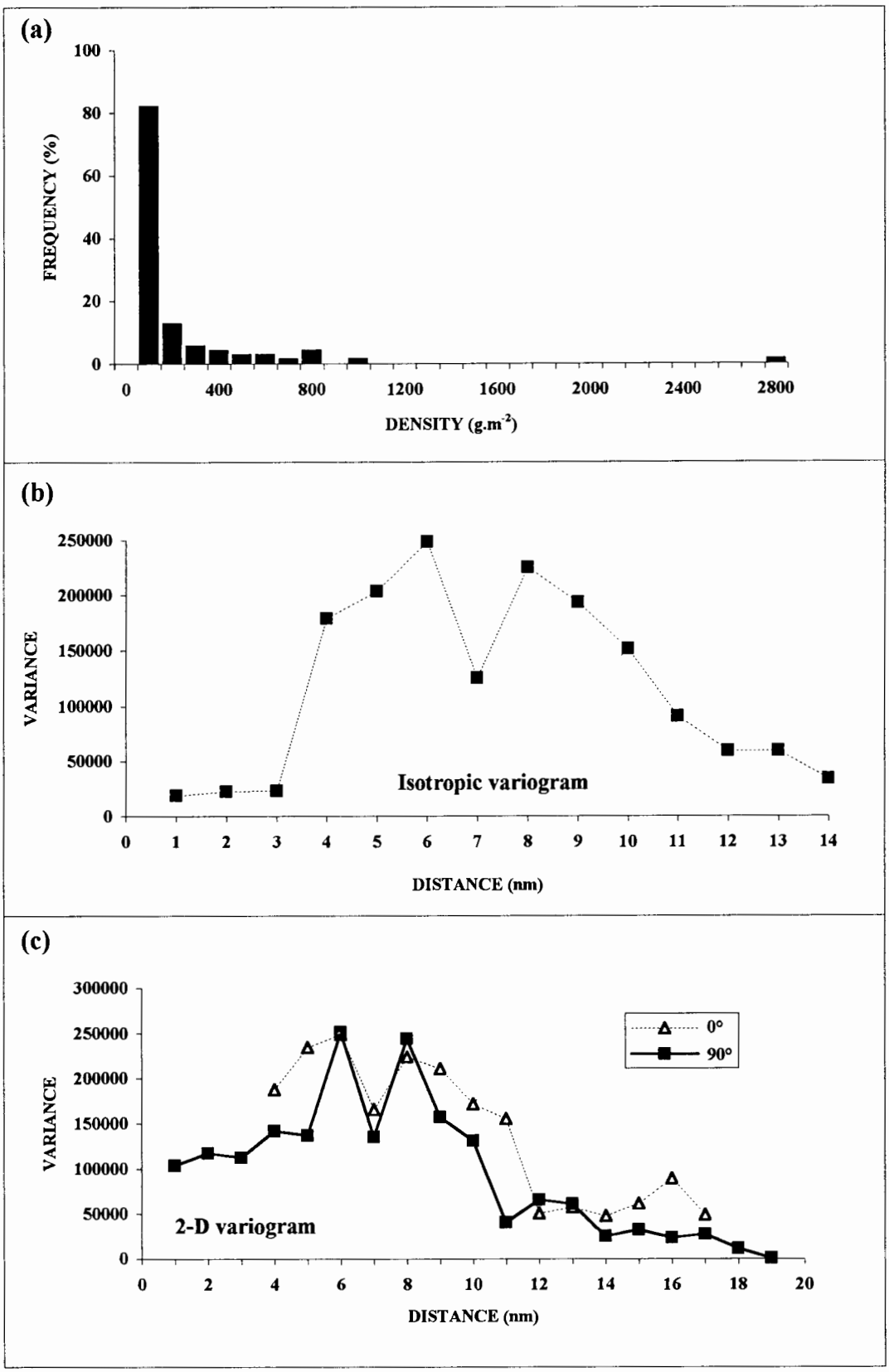


Fig 3.9. The frequency distribution of fish density ($g.m^{-2}$) of the second coverage of the shoaling behaviour survey (night/day) is shown in (a), the isotropic variogram is shown in (b) and the two-dimensional variogram is shown in (c).

(vii) RAFOS III (First grid, Day)

Although the histogram of fish density is skewed to the right (Figure 3.10 a), the range in values is considerably smaller than in most of the other surveys with the maximum recorded density being 138 $g.m^{-2}$. Only two values were higher than 100 $g.m^{-2}$ but they accounted for 45 % of the total variance. Almost 50 percent of the data points had density values of less than 10 $g.m^{-2}$ and the mean density of the data set was 21 $g.m^{-2}$.

An isotropic variogram computed on this data (Figure 3.10 b) shows spatial autocorrelation of the data for a range of 6 nm. A nugget effect is noted. The variance increases slowly with increase in distance from the nugget for the first 6 lags where it reached a maximum. Two-dimensional variograms calculated for points along the track (45°) and across the track (135°) reveal structure in both directions (Figure 3.10 c). The structure along the track is slightly smaller (3 nm) than that across the track (5 nm). The nugget effect is also higher in the 45 ° direction than in the 135° direction.

(viii) RAFOS III (First grid, Night)

Density ($g.m^{-2}$) varied from less than 1 $g.m^{-2}$ to a maximum of 235 $g.m^{-2}$. Unlike previous surveys the distribution is not strongly skewed although it is still far from normal (Figure 3.11a). Most of the values are between 10 and 100 $g.m^{-2}$ with 15 % of the values having a density of more than 100 $g.m^{-2}$. These higher values contribute 41 % of the mean and account for 66 percent of the total variance.

The isotropic variogram computed is shown in Figure 3.11 (b). A relatively large structure was observed with the variance increasing from a nugget to reach a maximum at a range of 9 nm. No large anisotropies were observed in the spatial structure. Two-dimensional variograms (45° and 135°) were calculated and show a nugget effect in both (Figure 3.11 c). The nugget was slightly higher in the along track direction (45°) as was the sill. The range was also slightly larger in the along track direction (8 nm) than in the across track direction (7 nm).

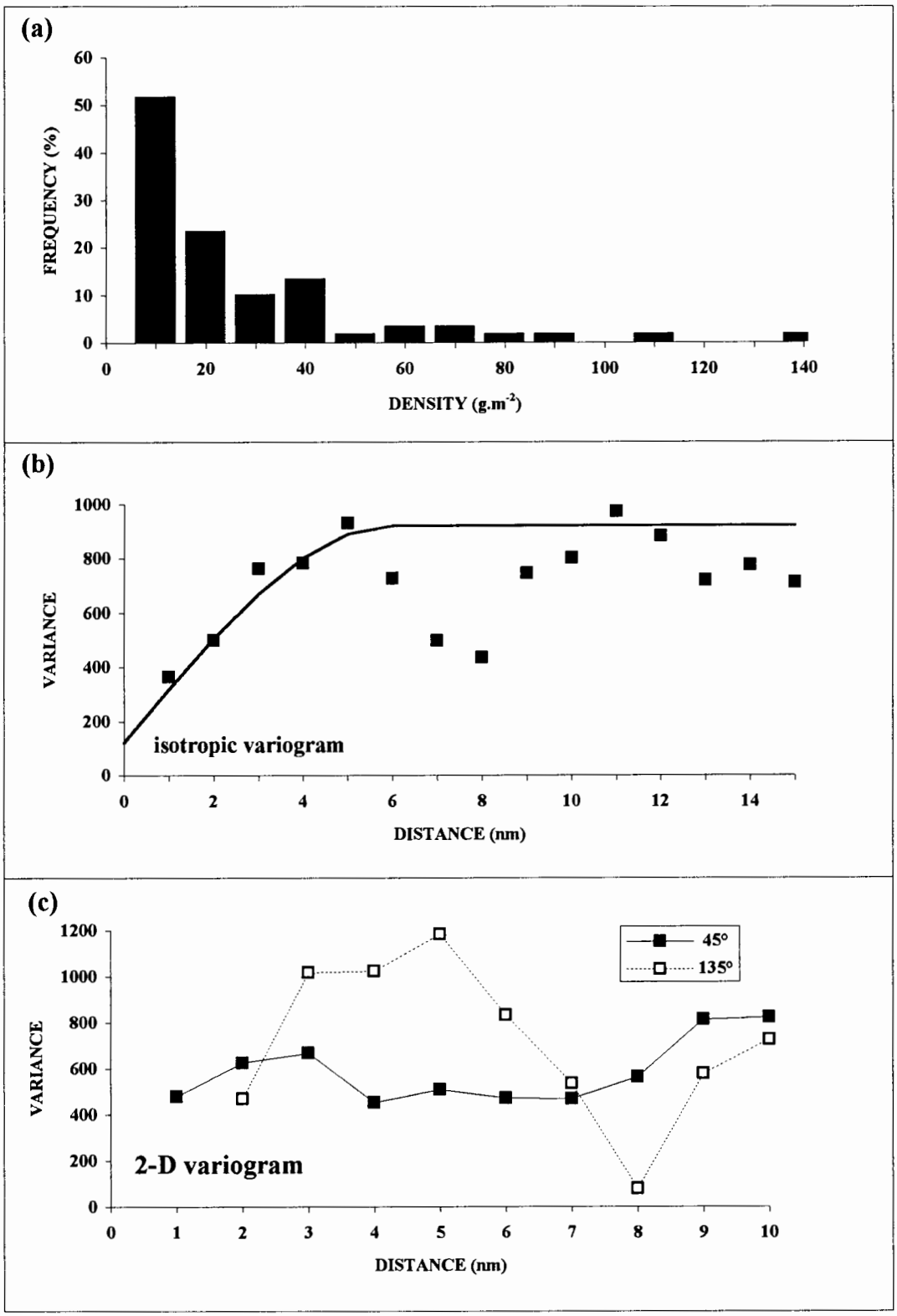


Fig 3.10. The frequency distribution of fish density ($g.m^{-2}$) for the first grid of the RAFOS III survey (day) is shown in (a), the isotropic variogram is shown in (b ) and the two-dimensional variogram is shown in (c). (45° = along-track and 135° = across-track)

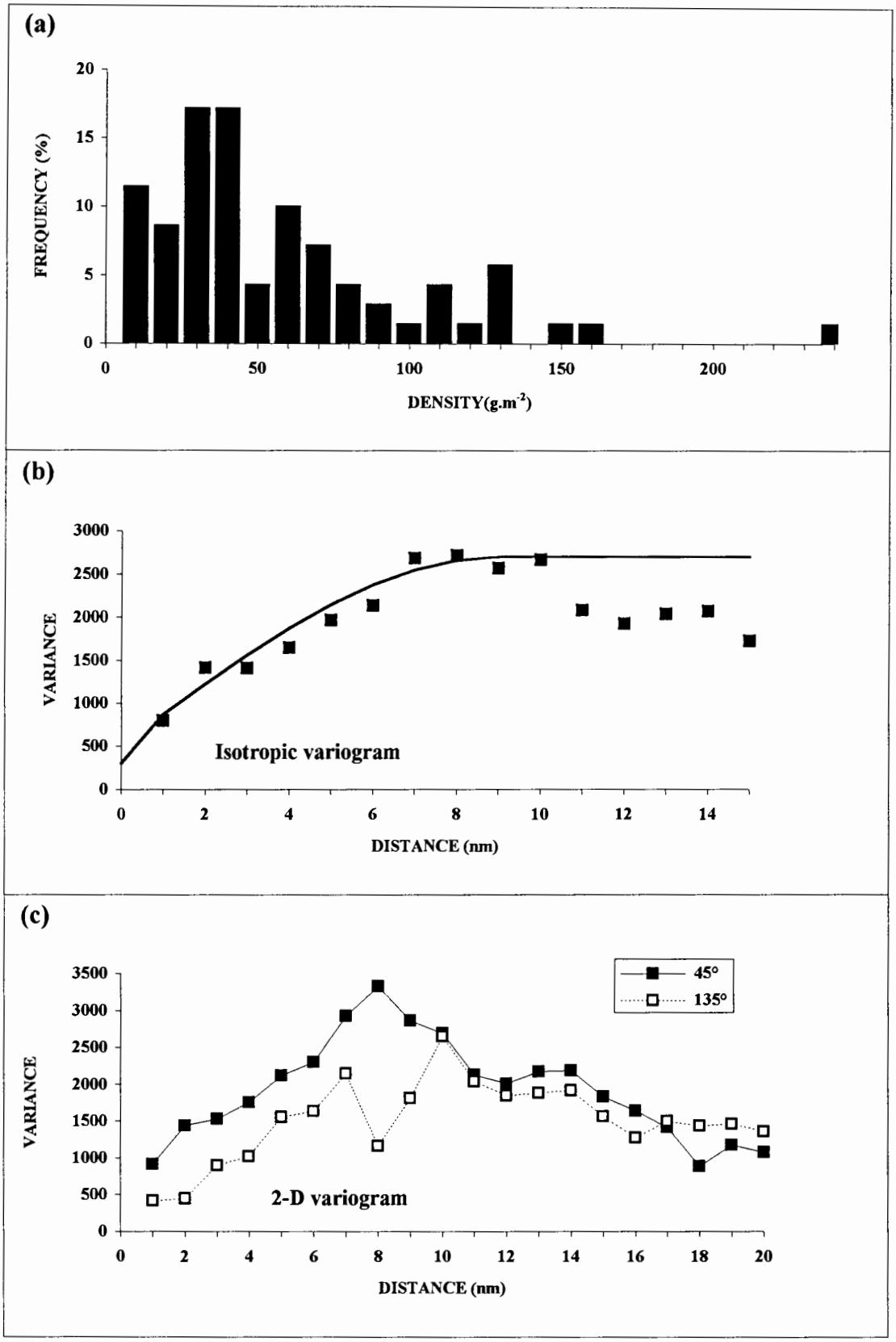


Fig 3.11. The distribution of fish density ($g.m^{-2}$) for the first grid of the RAFOS III survey (night) is shown in (a). The isotropic variogram is shown in (b) and the two-dimensional variogram is shown in (c). (45° = along-track; 135° = across-track).

(ix) RAFOS III (Second grid, day)

The frequency histogram of density is shown in Figure 3.12 (a). The histogram is strongly skewed to the right with values ranging from less than 1 $g.m^{-2}$ to a maximum of 311 $g.m^{-2}$. More than 60 % of the data points have a density of less than 50 $g.m^{-2}$, and the mean of the total data set is 55 $g.m^{-2}$. The values greater than 100 $g.m^{-2}$ strongly influence the mean, contributing more than 60 % to the mean and 76 percent to the total variance even though they account for less than 20 % of the total data points.

No spatial structure of fish density was observed during this survey. The isotropic variogram computed is shown in Figure 3.12 (b). The variogram is very irregular and does not increase with increasing distance. This is due to the largest values being on the edges of the survey area with small values in the centre of the survey area.

(x) RAFOS III (Second grid, night)

The histogram of fish density is again positively skewed as shown in Figure 3.13 (a). Most of the data points (80 %) have a density of less than 50 g.m-2, but although they form such a large part of the data set they only contribute about 30 % to the mean and account for less than 20 % of the total variance. Values greater than 100 $g.m^{-2}$ make up a small proportion of the data set, but contribute largely to the mean (49 %) and the variance (83 %).

The small-scale of the survey prevented an adequate coverage of the entire distribution of fish, with the result that little spatial structure could be resolved. The isotropic variogram Figure 3.13 (b) therefore is very erratic and does not bind.

The general conclusion reached from this study of the horizontal patterns of dispersion, is that the variograms did not reveal a significant change in the population structure between day and night. The main reason for this, however, is the fact that the surveys covered very small regions, and other factors independent of the spatial structure (e.g., migrations beyond the survey area) dominated the variogram patterns.

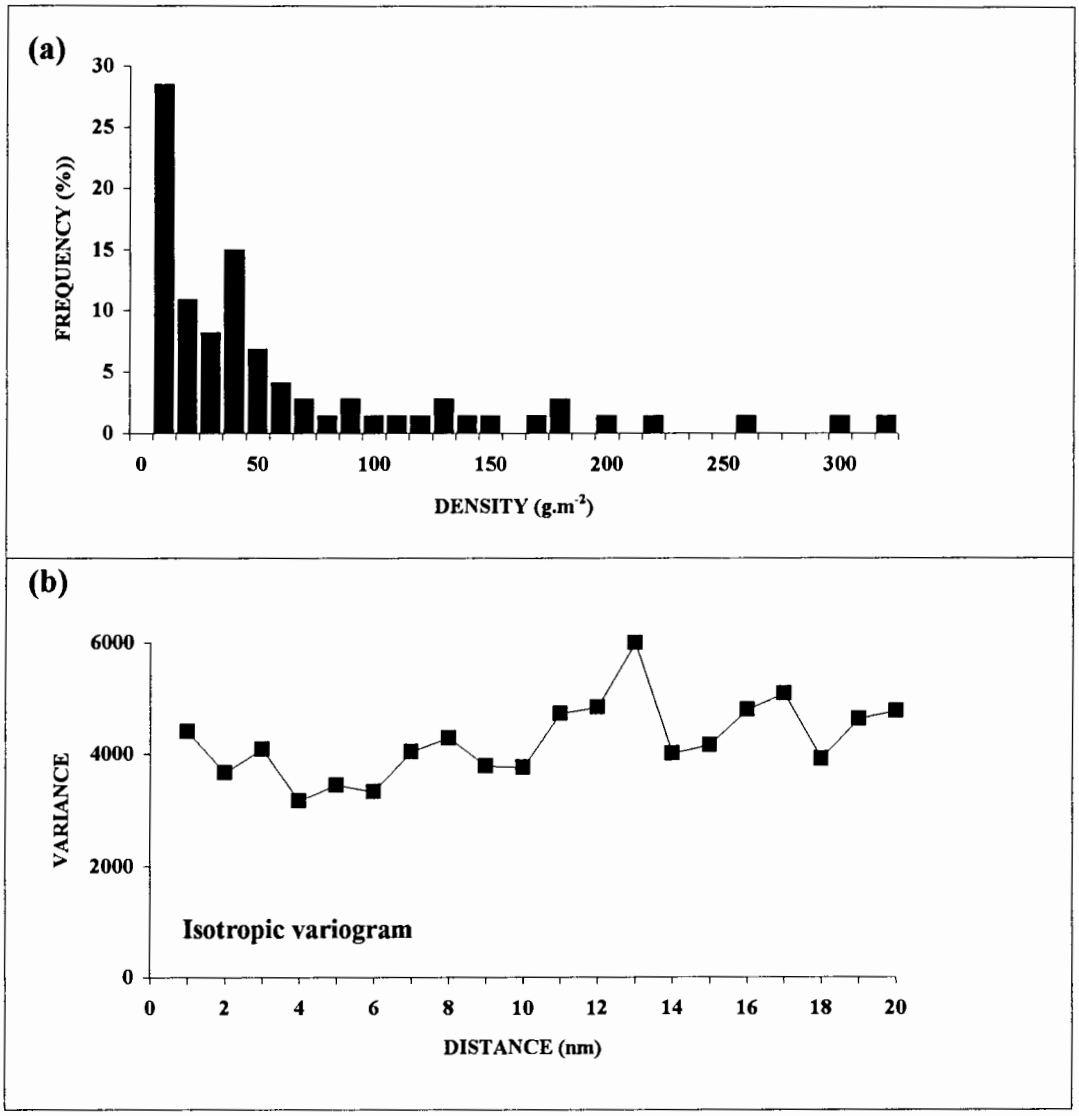


Fig 3.12. The distribution of fish density ($g.m^{-2}$) during the second grid of the RAFOS III survey (day) is shown in (a). The isotropic variogram is shown in (b).

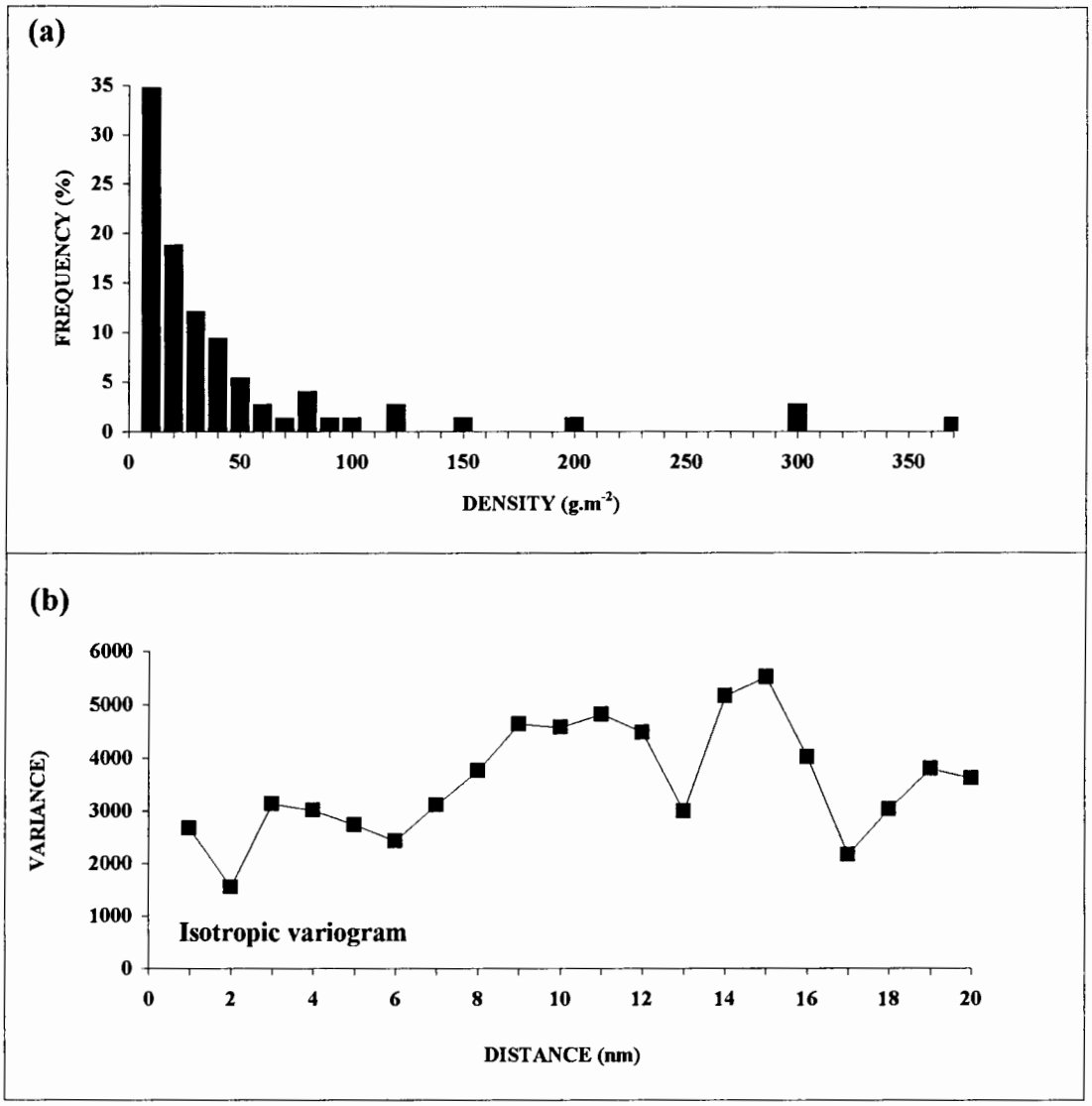


Fig 3.13. The distribution of fish density ($g.m^{-2}$) during the second grid of the RAFOS III survey (night) is shown in (a). The isotropic variogram is shown in (b).

Further investigation into the spatial heterogeneity of the day and night distributions using geostatistical selectivity curves (Figure 3.14) suggested more selectivity at night than during the day. Although both distributions are positively skewed, some very large values add considerably to the mean density during the day. During the night on the other hand, the curve is more convex indicating a larger contribution to the mean from smaller values. This indicates that during the night fish are more dispersed than during the day as the surface over which the population is present increases at night. The fact that a few high values are still present at night might also indicate that shoaling does not cease entirely at night.

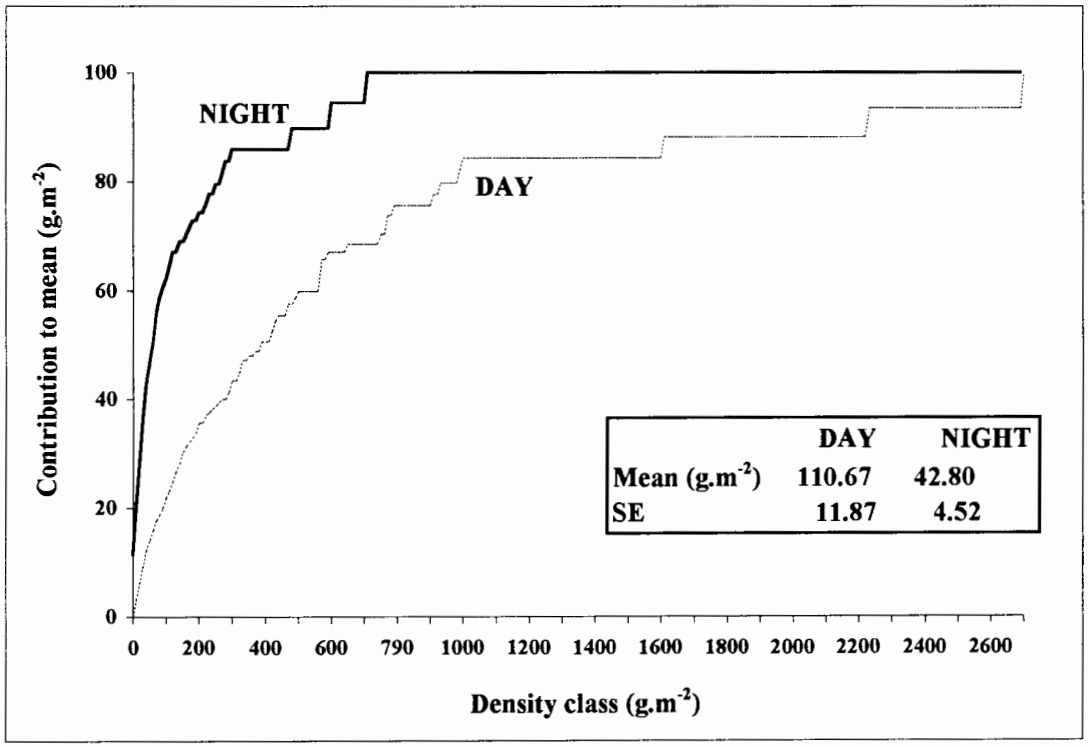


Fig 3.14. Cumulative rank frequency distributions of sardine in terms of their contribution to the mean survey density for night time and day time sampling.

## 3.3 SPATIAL STRUCTURE BETWEEN SHOALS.

As most of the biomass during the day is contained within shoals it is assumed that the structure of the distributions should reflect a structure between shoals too. To test this assumption, shoals per nautical mile were counted as described in section 2.5.2and used in a geostatistical analysis below.

The shoal plots with the 1 X 1 nm superimposed grids are shown in Figure 3.15. The top row of figures shows the position of shoals within the survey area. Surface area ($m^2$) was used to indicate the relative size of the shoals. Since shoal area will be dealt with in section 4.1, it will not be described here. The bottom row of figures represents the actual number of shoals present in each grid cell. Empty cells indicate areas which were not surveyed. These cells were omitted from all analyses. Cells with zero values indicate areas which were surveyed but contained no shoals. These cells were included in the analyses. It is clear that during the RAFOS II survey, a large cluster of shoals was observed in the upper and lower, central part of the grid with very few shoals situated in other parts of the grid. During the other three surveys shoals were present throughout most of the survey area. The grid cell counts of the RAFOS II and RAFOS III (grid 4) survey show a large proportion of cells contained no shoals. Very few zero values were, however present for the other two surveys. A distinct feature of the RAFOS II and intercalibration surveys is the relatively larger shoal size when compared to the other two surveys.

Frequency histograms of numbers of shoals per cell for each of the four surveys are presented in Figure 3.16. With the exception of the intercalibration survey, the histograms are strongly positively skewed. The mean number of shoals per grid cell did not differ significantly between survey with the minimum (2.68 shoals/cell) being that of the RAFOS II (grid 4) survey and the maximum (4.85 shoals/cell) being that of the RAFOS II (grid 2) survey. The frequency distribution of the RAFOS III (grid 2) survey was most skewed, due mostly to one cell containing a very high number of small shoals. The histogram of the intercalibration survey is only slightly skewed to the right and is closer to a normal distribution than the others.

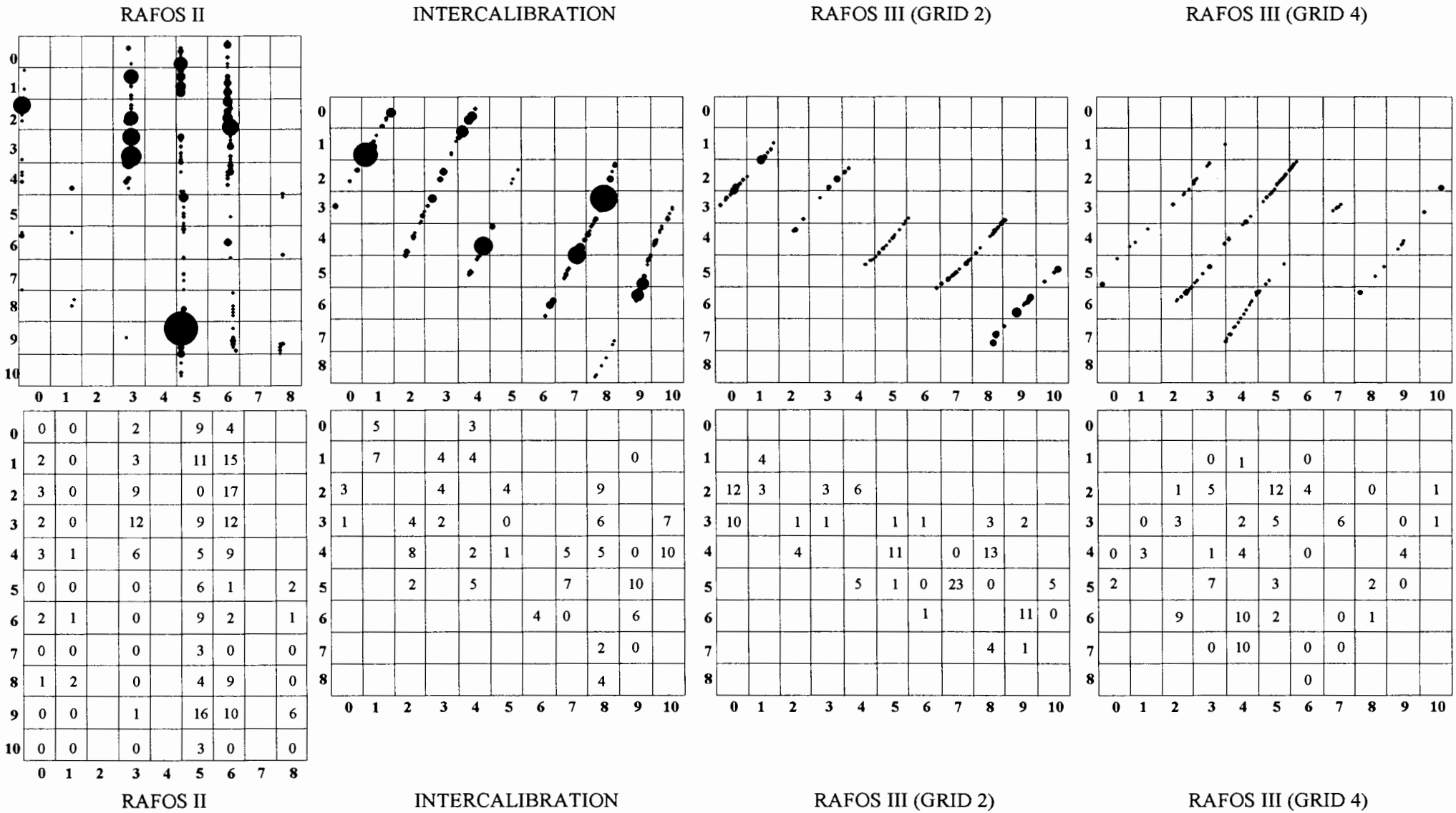


Fig 3.15. Shoal plots and grid cell counts for each survey. The top figures show the relative position and area of each shoal, whilst the bottom row of figures show the shoals counted per grid cell ( 1 X 1 n.mile).

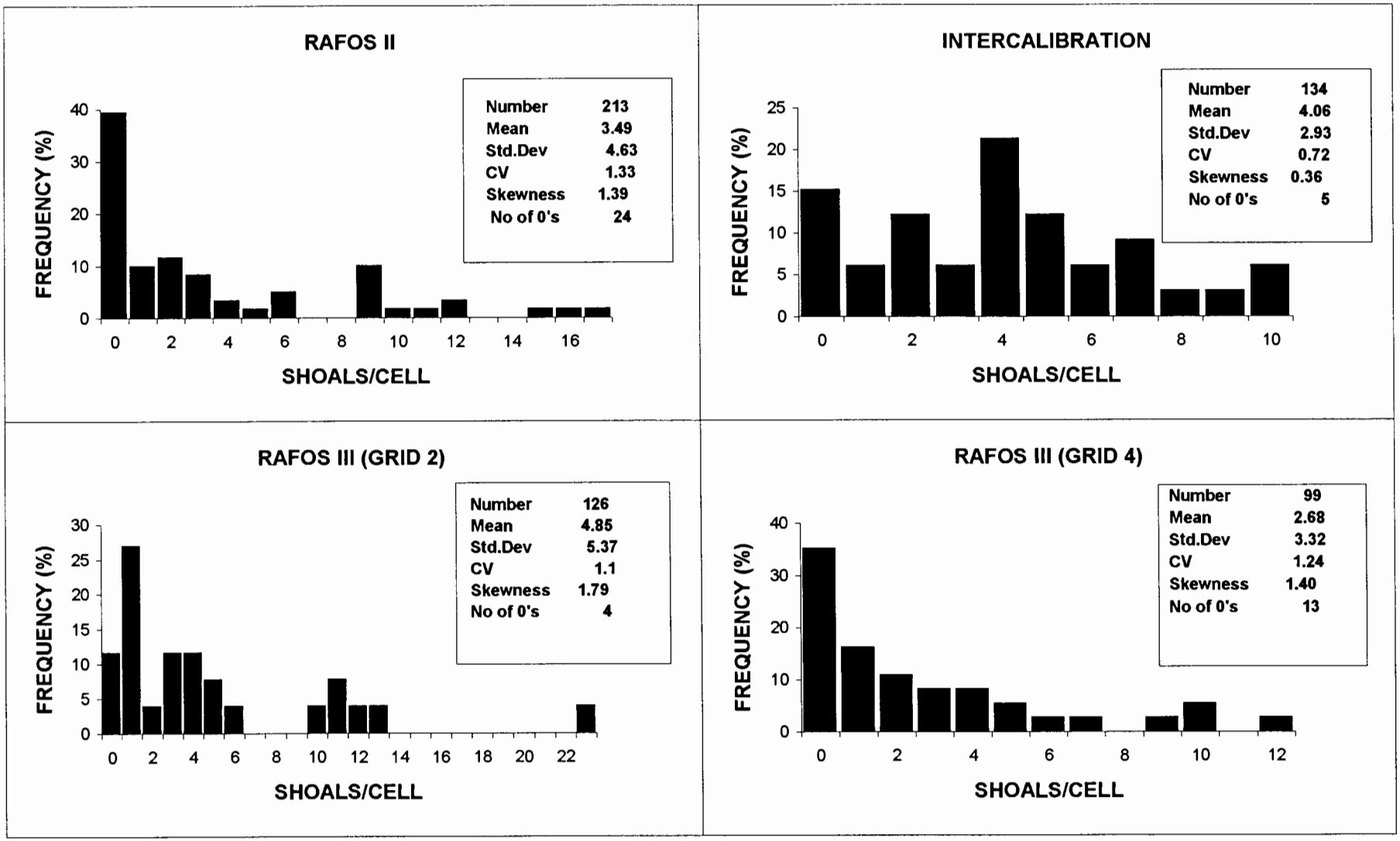


Fig 3.16. Frequency histogram and some summary statistics for shoal per nautical mile data.

A Chi-square goodness-of-fit test for a Poisson (i.e. random) distribution (Zar, 1984) revealed that shoals were not randomly distributed within the survey area for all four surveys. The results of this test are shown in Table 3.1. Except for the intercalibration survey, observed Chi-squared values were much larger than the expected values and the null hypothesis that shoals were randomly distributed was rejected at the 5 % level. The observed distribution of the intercalibration survey was close to the expected distribution, although the test still rejected the null hypothesis at the 5 % level.

Table 3.1. Chi-square ($\chi^2$) values and probability ($P$) levels for tests of randomness in the distribution of shoals during four surveys.

| Survey | # Shoals | # Cells | DF | $\chi^2$ | $\chi^2_{crit.}$ | $P$ |
|---|---|---|---|---|---|---|
| RAFOS II | 213 | 61 | 7 | 368.16 | 14.067 | $P < 0.001$ |
| Intercalibration | 134 | 33 | 6 | 13.52 | 12.592 | $0.05 > P > 0.025$ |
| RAFOS III (grid 2) | 126 | 26 | 7 | 87.18 | 14.067 | $P < 0.001$ |
| RAFOS III (grid 4) | 99 | 37 | 6 | 75.57 | 12.592 | $p < 0.001$ |

Because shoals were not randomly distributed, variograms to test for structure between shoals were computed. These are presented in Figure 3.17. All variograms were computed in both the along-track and across-track direction. Only along-track variograms are shown and interpreted due to very few pairs of data for most lags in the across-track direction. In the across track direction most lags had an insufficient number of data point pairs according to the geostatistical "rule of thumb" as described by Rossi *et al.*, (1992).

The variogram of the RAFOS II survey showed a large structure with a range of 7 nm and a relatively small nugget. This nugget could be due to either the size of the grid cells which do not resolve the small scale variability or to real small scale randomness at a distance less than that of the sampling resolution. A spherical model as indicated on the figure best described the structure. No structure was observed between shoals of the intercalibration survey. In this case the variance between the number of shoals at a short range is similar to that of shoals at a longer range. Results of the Chi-square test above indicated that of all the surveys, the distribution of shoals during the intercalibration survey diverged least from a random distribution. The

corresponding variogram therefore verifies this fact. The variogram computed for the RAFOS III (grid 2) survey showed no structure due to the effect of one outlier. The variogram shown in Figure 3.17 for this survey was calculated after exclusion of this highest value. This shows a small structure of 4 nm and a small nugget effect, once again described by a spherical model. A similar structure with a range of 5 nm was observed for the RAFOS III (grid 4 ) survey, although the nugget was higher. Three of the variograms therefore confirmed the finding of non-randomness of shoals as shown by the Chi-square test. In general, these variograms calculated from shoals per nautical mile correspond well with the two-dimensional variograms calculated using one nautical miles densities in section 3.2. In fact, the ranges of these variograms are slightly larger than those observed using the interval densities.

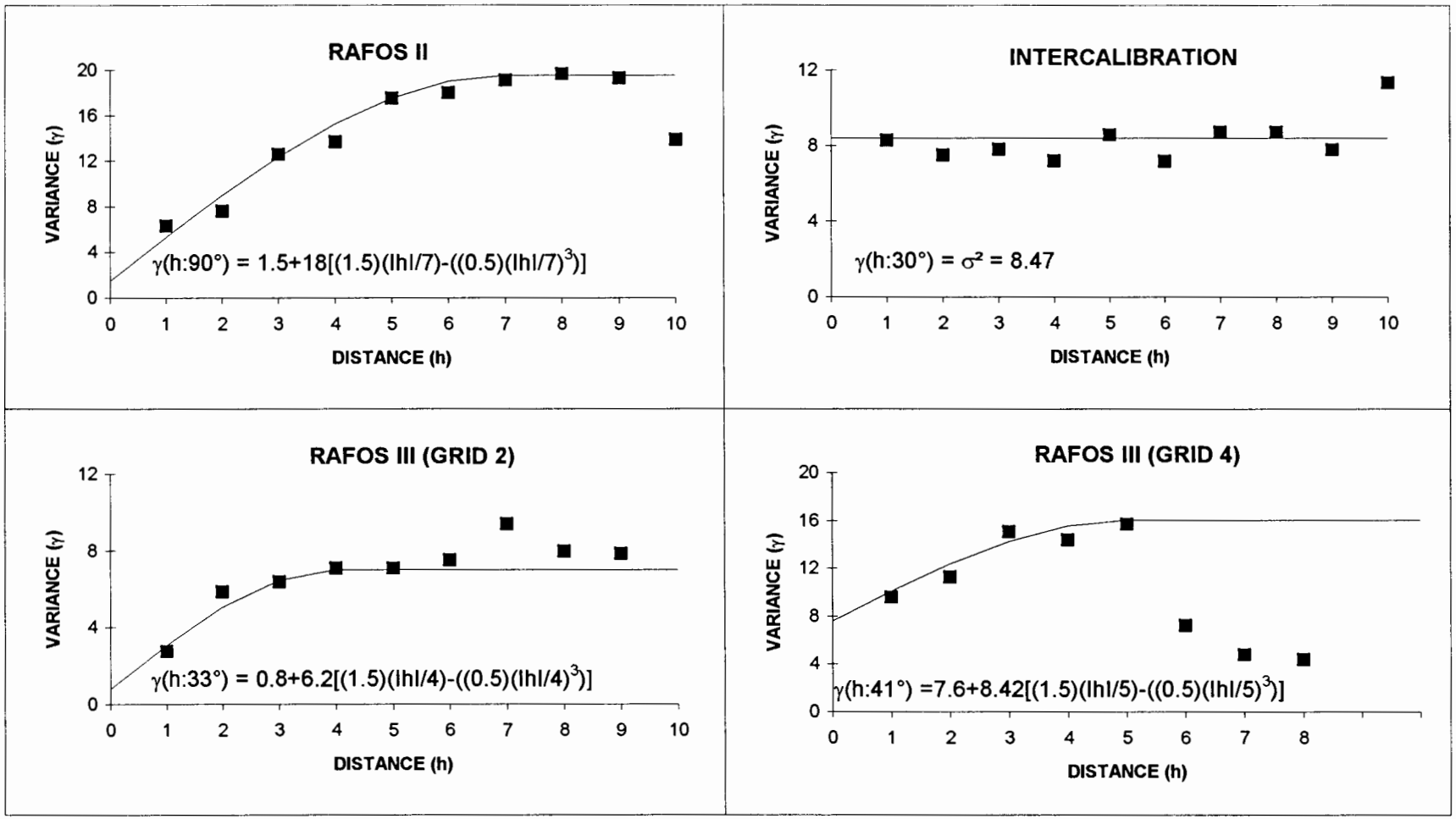


Fig. 3.17. 2-Dimensional variograms are shown for the shoal per nm data for each of the day surveys. Only the variograms relating to the along-track direction are, however, shown. Models describing the spatial structure are supplied on the appropriate figures.

# CHAPTER 4.

# SPATIAL STRUCTURE OF SARDINE SHOALS

## 4.1 Shoal statistics and description

Sardine tend to disperse in layers at night, making it very difficult to accurately differentiate between distinct schools especially when they are within a dense sound scattering layer. Only distinct schools recorded during daylight hours were therefore included in the analysis. Shoals from all day grids were used, except for the shoaling behaviour survey where incompatible file formats did not allow shoal extraction by SHAPES. In the case of the RAFOS III survey, two separate grids were sampled both during day and night. The first survey consisted of Grid 1 and 4 of which Grid 4 was the day coverage. The second survey consisted of Grid 2 and 3 of which Grid 2 was the day coverage. Only Grid 2 and 4 will therefore be used in this part of the analysis, together with the day coverage of the RAFOS II survey and the day coverage of the intercalibration survey.

A total of 573 distinct pilchard shoals were finally selected after careful scrutiny. The sample size varied among the surveys with the most shoals (214) originating from the RAFOS II survey and the least from the intercalibration survey (99). Large variations occurred both within surveys and between surveys for most of the calculated variables. Each shoal variable as well as relationships between shoal variables will be presented separately below.

### Shoal height

The frequency distribution of the height of the shoals indicates that approximately 60 % of the identified shoals were less than 10 m in height (Figure 4.1 a). In fact only 15 % of the shoals had a height greater than 20 m. The mean shoal height for all surveys was 11 m (SE =11), but varied from a minimum of 2 m (selected minimum) to a maximum of 69 m.

When the height of shoals recorded during the individual surveys are compared (Figure 4.1 b)

it is evident that in all cases the most shoals have a height of less than 15 m. It is, however, apparent that shoals recorded during the two RAFOS III surveys were generally of a lesser height than the shoals recorded during the remaining two surveys. This is further illustrated in Figure 4.1 (c) where all shoals recorded during the above mentioned RAFOS III surveys were less than 30 m in height. In the case of the RAFOS II and the intercalibration survey a few shoals with heights exceeding 30 m were recorded. The variance of height within these two RAFOS III surveys was also less than during the other two surveys (Table 4.1). The difference in mean height between the surveys was significant ($p < 0.0001$) with the variance between surveys being far greater than the within survey variance.

Table 4.1. Summary statistics calculated for shoal height and the results of the single factor analysis of variance of shoal height between surveys.

**SUMMARY**

| Groups | sum | mean | variance |
|---|---|---|---|
| RAFOS II | 2795.00 | 13.0 | 128.31 |
| RAFOS III (grid 2) | 925.50 | 7.4 | 27.78 |
| RAFOS III (grid 4) | 656.75 | 6.6 | 15.70 |
| INTERCALIBRATION | 2163.50 | 16.1 | 205.07 |

| Source of Variation | SS | df | MS | F-value | p | F *crit* |
|---|---|---|---|---|---|---|
| Groups | 7888.55 | 3 | 2629.52 | 25.09 | <0.0001 | 2.62 |
| Error | 59746.43 | 570 | 104.82 | | | |
| Total | 67634.99 | 573 | | | | |

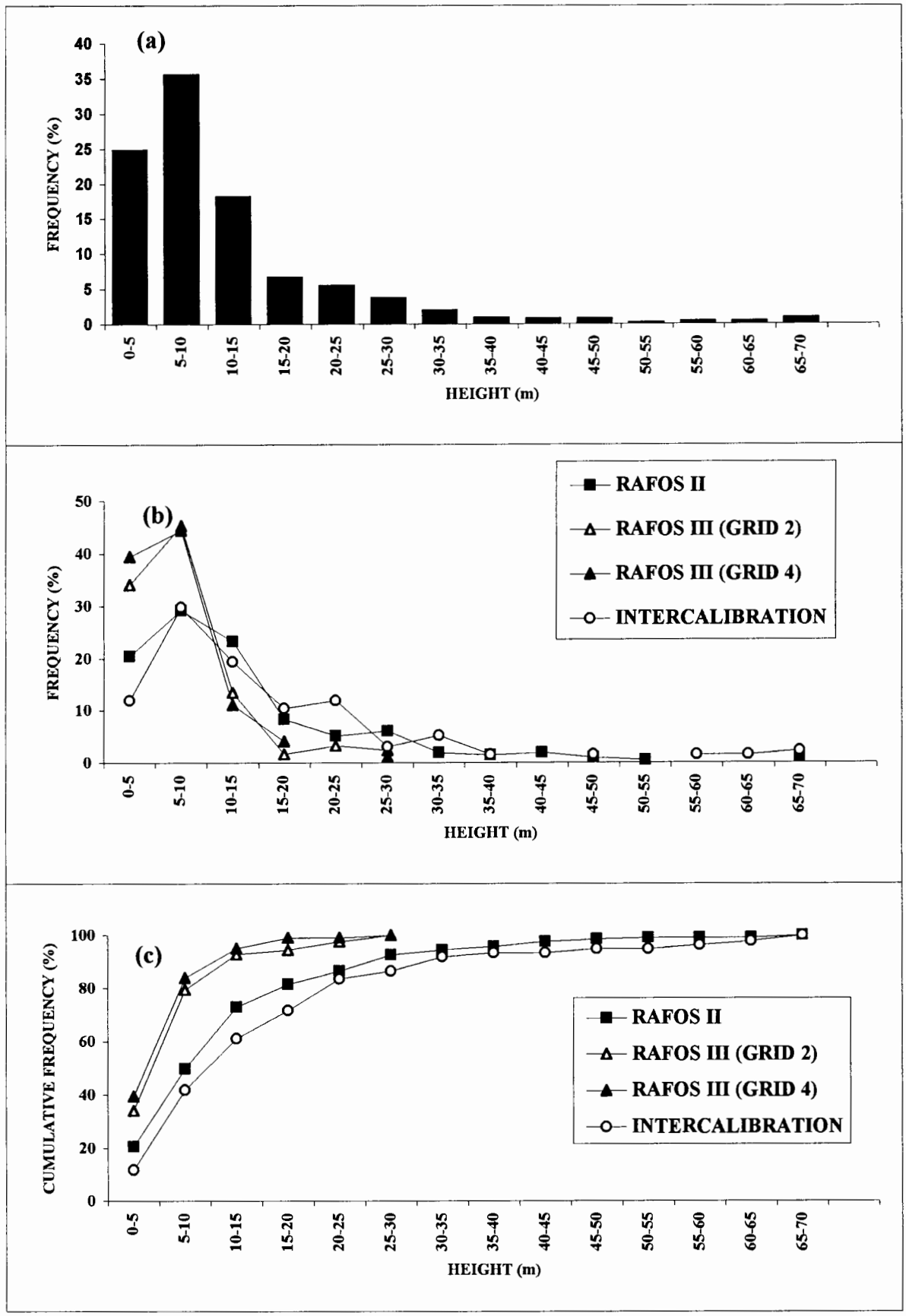


Fig 4.1. Frequency distributions of shoal height for all surveys (a), individual surveys (b) and cumulative frequency plots for each survey (c).

**Shoal length**

The mean shoal length calculated for all the surveys is 28 m (SD =29) but varies greatly from less than 10 m to a maximum of 250 m. Most of the shoals are, however, less than 30 m in length and account for about 70 % of the total. Shoals greater than 100 m in length are very few and only contribute about 3 % to the total (Figure 4.2 a). For the individual surveys there is not much difference in the frequency distribution of the shoal lengths with the majority of the shoals being less than 30 m for all surveys (Figure 4.2 b). Shoals less than 30 m in length account for more than 60 % of the total shoals for all individual surveys. There is, however, a difference in the distribution of larger shoals between the surveys. No shoals greater than 100 m in length were recorded during the two RAFOS III surveys, but only during the RAFOS II and intercalibration survey (figure 4.2 c). Although these larger shoals form a very small proportion of the total shoals for these two surveys, the difference in the sample means is still significant (p =0.001) with the between survey variation accounting for most of the variation (Table 4.2). As was the case for the height distribution, the variance in length is again much higher for the RAFOS II and intercalibration surveys than for the two RAFOS III surveys.

Table 4.2. Summary statistics and results of the single factor analysis of variance of shoal length.

SUMMARY

| Groups | sum | mean | variance |
|---|---|---|---|
| RAFOS II | 7026.13 | 32.68 | 1356.64 |
| RAFOS III (grid 2) | 3247.65 | 25.78 | 452.94 |
| RAFOS III (grid 4) | 1942.00 | 19.62 | 218.83 |
| INTERCALIBRATION | 4062.53 | 30.32 | 861.86 |

| Source of Variation | SS | df | MS | F-value | p | F *crit* |
|---|---|---|---|---|---|---|
| Groups | 12936.19 | 3 | 4312.06 | 5.09 | 0.001 | 2.62 |
| Error | 483010 | 570 | 847.39 | | | |
| Total | 495946.2 | 573 | | | | |

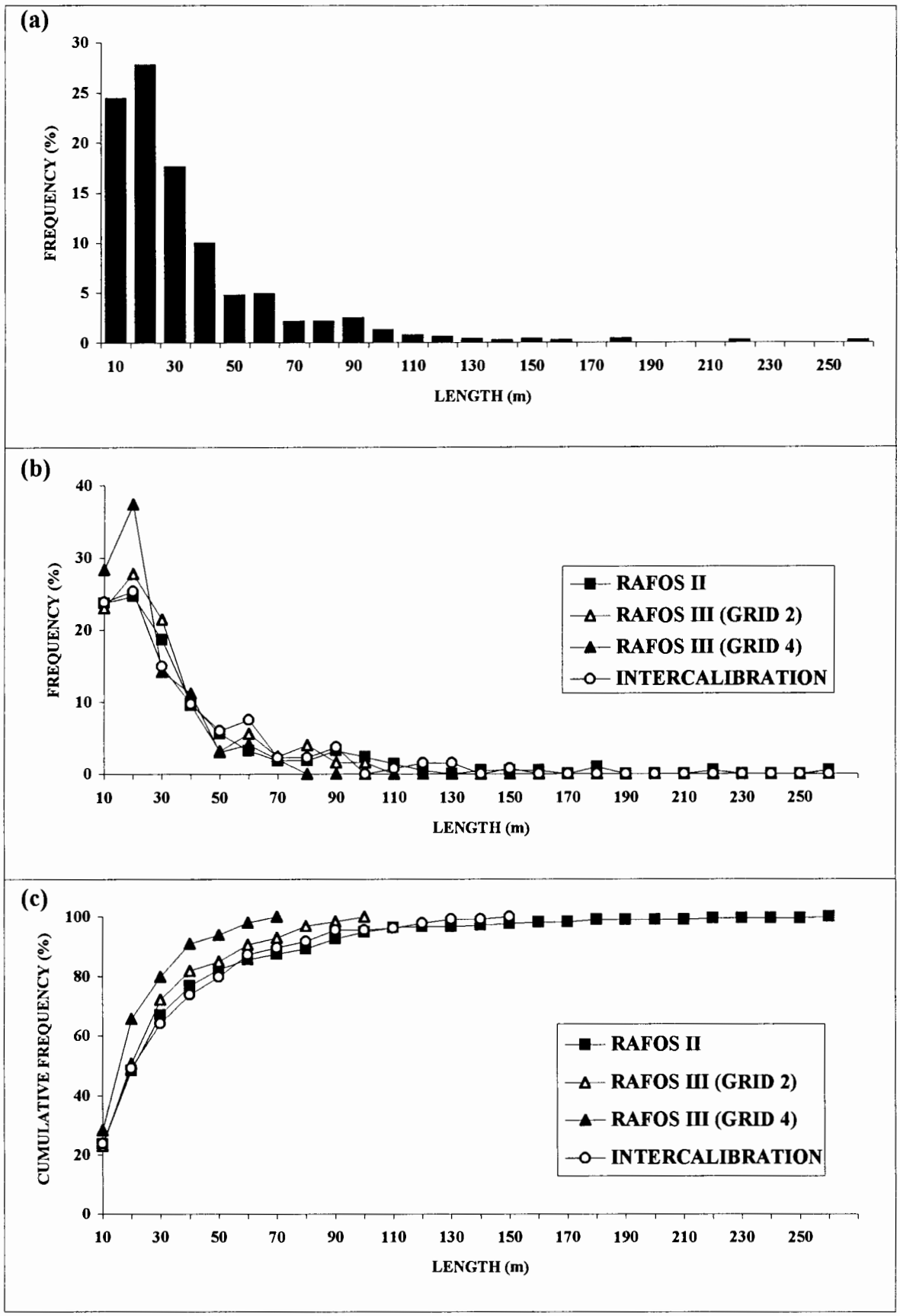


Fig 4.2. Frequency distributions of shoal length for all surveys (a), individual surveys (b) and cumulative frequency plots for each survey (c).

**Length vs height**

When length and height are correlated, a relatively strong correlation coefficient is found ($r = 0.47$). This correlation coefficient is significant when tested using a Student's t test ($P < 0.001$). In addition, a Fisher transformation (Zar, 1984) was performed on the data to check the validity of the results of the Student's t test and this also showed a significant correlation. (95 % confidence limits of r showed $0.34 < P < 0.53$). Individual surveys were also compared and the results are shown in Table 4.3.

Table 4.3. Comparison of correlation coefficients between shoal length and shoal height.

| SURVEY | RAFOS II | INTERCALIBRATION | RAFOS III(grid 2) | RAFOS III(grid 4) |
|---|---|---|---|---|
| r | 0.41 | 0.61 | 0.40 | 0.33 |
| n | 215 | 134 | 126 | 99 |

Correlation between length and height was highest for the intercalibration survey and very similar between the other 3 surveys. Results of a Chi-square analysis for differences in r between surveys was significant ($0.005 < P < 0.01$) A Tukey-type multiple comparison, however, revealed only a significant difference in r between the intercalibration survey and the rest, with no significant difference between the other 3 surveys.

Assuming (although not implied) a dependence of length on height, a linear regression was calculated and plotted (Figure 4.3) revealing a weak coefficient of determination ($R^2 = 0.22$) and a large standard error ($SE = 26.02$). The significance of the regression was tested (Zar, 1984) by way of a single analysis of variance (Table 4.4) and this indicated that the regression was indeed significant ($P < 0.0005$).

Table 4.4. Results of the ANOVA performed to test the significance of regressing length on height.

| Source | SS | df | MS | F-value | p | F *crit* |
|---|---|---|---|---|---|---|
| Regression | 108616.8 | 1 | 108616.9 | 160.4 | < 0.0005 | 3.84 |
| Residual | 387329.3 | 572 | 677.15 | | | |
| Total | 495946.2 | 573 | | | | |

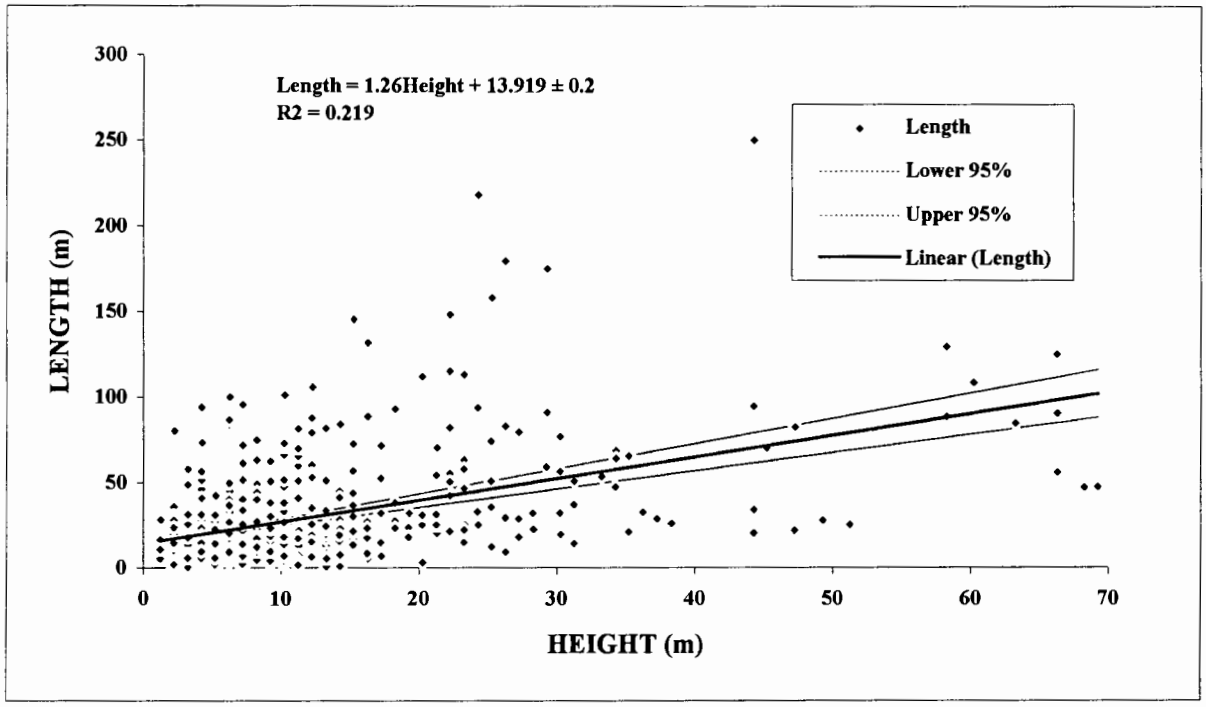


Fig 4.3. Linear regression of length on height for all shoals analyzed.

A regression of length on height was also done for each individual survey. The results of these regressions are shown in Table 4.5. The coefficient of determination was found to be highest for the intercalibration survey ($R^2 = 0.37$) but varied little between the other 3 surveys. An analysis of covariance was done to test for differences between the slopes as well as the elevations (Zar, 1984). This showed no significant differences for $\alpha(0.05)$ for both the slopes ($P > 0.25$) and the elevations ($0.05 < P < 0.10$) and therefore all survey regressions are assumed to be estimates of the same population regression and the common regression may be used as an estimate of the equation underlying all surveys.

Table 4.5. Results of linear regressions of length (L) on height (H) for each survey.

| SURVEY | RAFOS II | INTERCALIBRATION | RAFOS III (grid 2) | RAFOS III (grid 4) |
|---|---|---|---|---|
| r | 0.40 | 0.61 | 0.40 | 0.33 |
| $R^2$ | 0.16 | 0.37 | 0.16 | 0.11 |
| SE | 33.77 | 23.4 | 19.62 | 14.03 |
| Regression | L=1.31H+15.6 | L=1.25H+10.2 | L=1.39H+14.03 | L=1.22H+11.5 |

**Area**

The area of shoals analyzed varies considerably from less than 10 $m^2$ to a maximum of almost 35000 $m^2$. The mean area was estimated to be 1468 $m^2$, with a large standard deviation (SD = 3135). The frequency distribution of area is shown in Figure 4.4. Generally the data were strongly positively skewed with shoals less than 1000 $m^2$ accounting for 70 % of the total shoals and shoals greater than 2500 $m^2$ accounting for less than 10 % of the total. A logarithmic transformation was performed on the data and this did convert the positively skewed distribution into a more symmetrical one. A chi-square test also confirmed that the original distribution was log-normal ($0.75 < P < 0.9$). The distribution of the log transformed area data and the expected frequency for normality are shown in Figure 4.5.

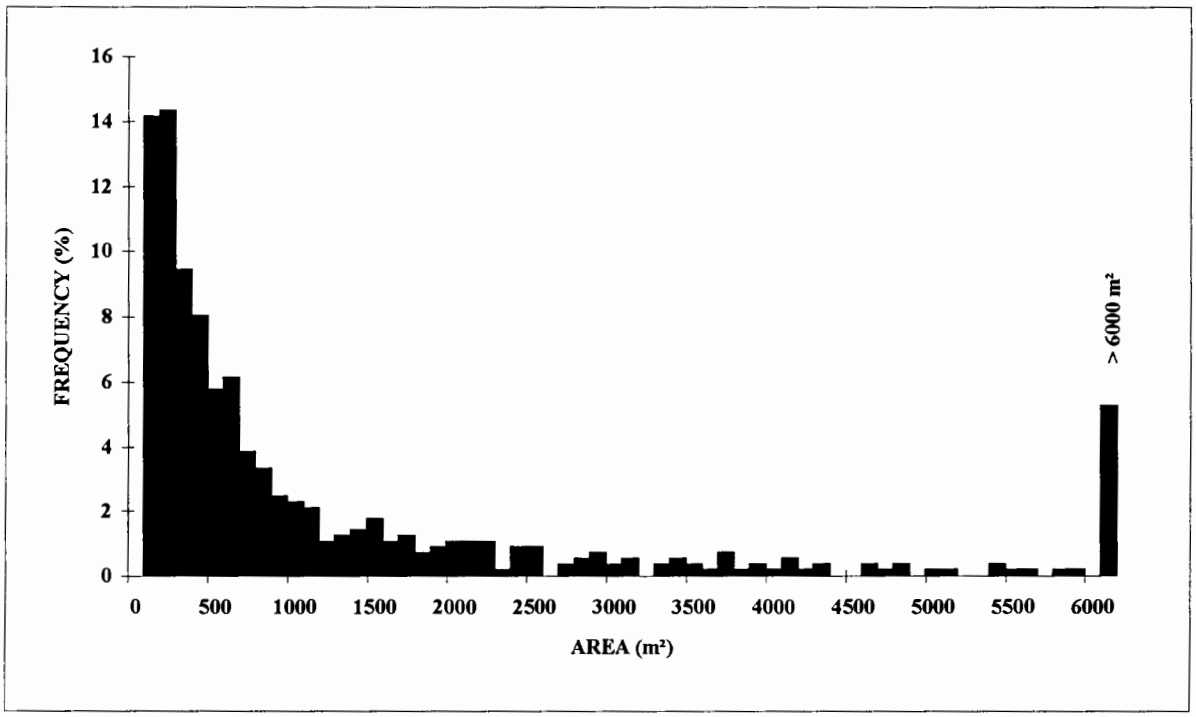


Fig 4.4. Frequency distribution of area of all shoals analyzed.

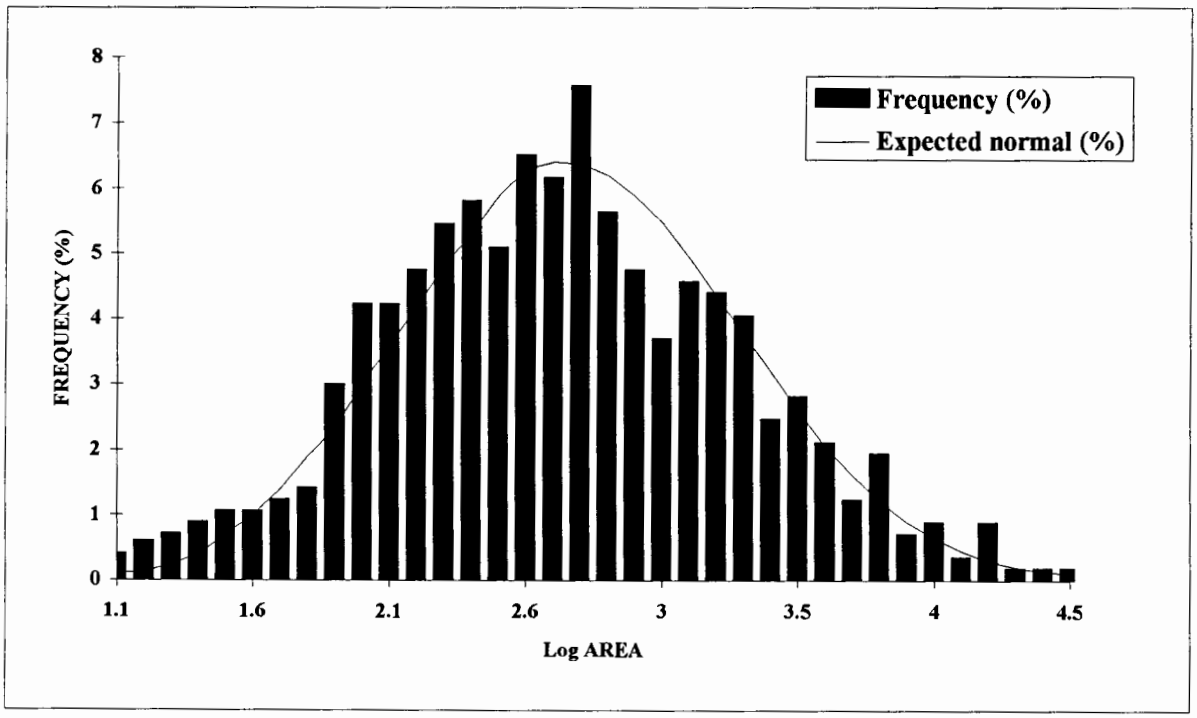


Fig 4.5. Distribution of the log-transformed area data and the expected normal frequency.

A comparison of the basic statistics calculated for the area data of each survey is shown in Table 4.6. The difference in mean area is notable, with the shoals recorded during the Rafos II and Intercalibration surveys having a much larger mean and maximum area than the remaining two surveys. When the frequency distributions of area is compared between surveys, all surveys are found to be strongly skewed to the right. Skewness ($g_1$) varied from a maximum of 4.74 in the case of the Rafos II survey to a minimum of 2.44 for the Rafos III (grid 4) survey.

An analysis of variance was performed on the transformed data to test for significance between the survey means. This indicated that the means were significantly different ($P < 0.0005$). A subsequent Tuckey test, however, revealed no significant difference between the Rafos II and intercalibration surveys or between the two Rafos III surveys. A significant difference, however, occurred between the two pairs of surveys ($\mu_{\text{Rafos II}} = \mu_{\text{intercalibration}} \neq \mu_{\text{Rafos III (grid 2)}} = \mu_{\text{Rafos III (grid 4)}}$).

Table 4.6. Basic statistics calculated for shoal area for each survey.

| Survey | G Mean | SD | CV | Min | Max | $g_1$ |
|---|---|---|---|---|---|---|
| Rafos II | 614 | 4.54 | 0.74 | 3.3 | 34801.4 | 1.05 |
| Intercalibration | 682 | 5.10 | 0.75 | 7.9 | 25903.0 | 0.63 |
| Rafos III (grid 2) | 361 | 4.06 | 1.12 | 4.1 | 7136.4 | 0.81 |
| Rafos III (grid 4) | 258 | 3.23 | 1.25 | 3.1 | 2810.7 | 0.27 |
| All surveys | 482 | 4.51 | 0.94 | 3.1 | 37801.4 | 1.06 |

**Volume**

The frequency distribution of the volumes recorded for all the shoals analyzed is shown in Figure 4.6. The volume ranged from a minimum of 10 $m^3$ to over 2 000 000 $m^3$. The distribution was extremely positively skewed with skewness ($g_1$) calculated for all the surveys being 10.69. The mean volume for all shoals was 29577.5 $m^3$ and a very high standard deviation was calculated (SD =127110). When the frequency distribution of volume was compared between surveys, it was found that all four distributions were skewed to the right and values of $g_1$ varied from 8.69 to 2.16 with the Rafos II survey being most skewed and Rafos III (grid 2) being least skewed.

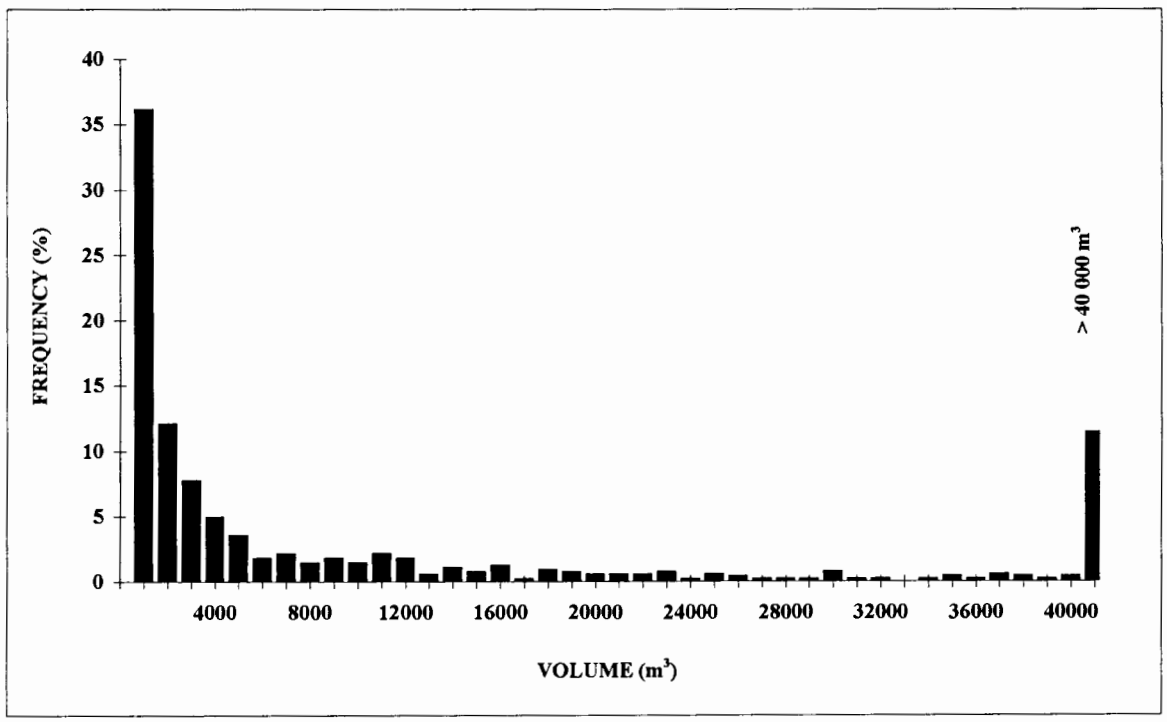


Fig 4.6. Frequency distribution of volume of all shoals analyzed.

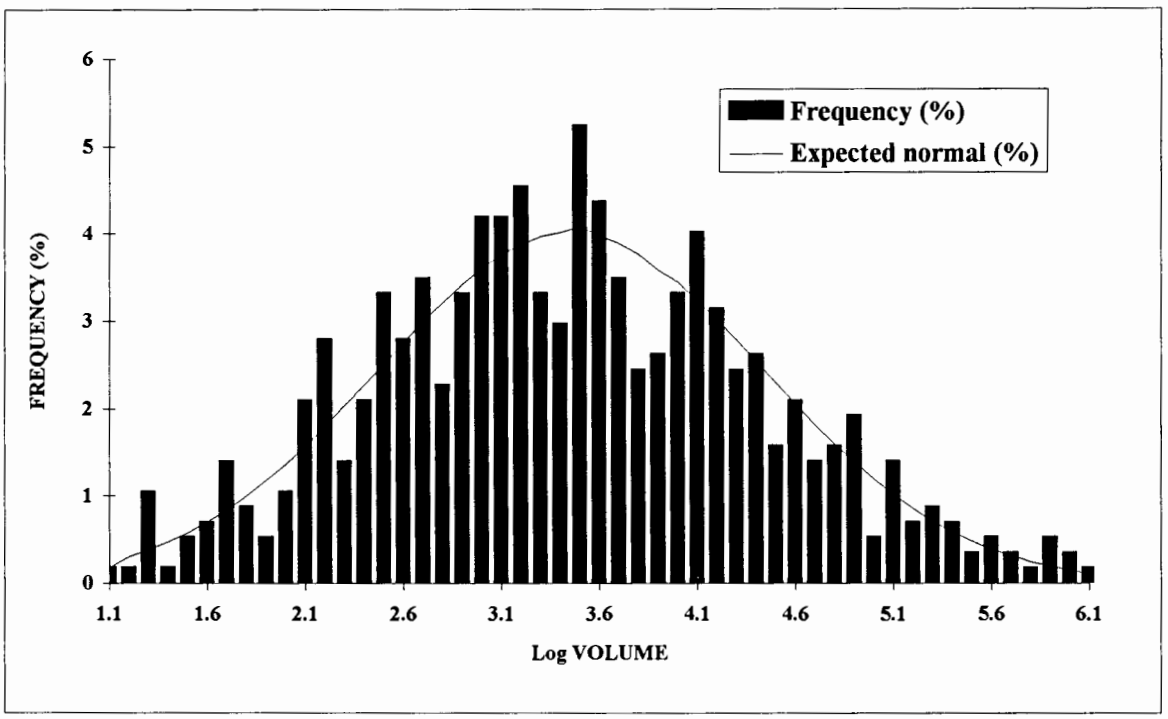


Fig 4.7. Distribution of the log-transformed volume data and the expected normal.

A logarithmic transformation of the data changed the distribution of volume into a more symmetrical distribution (Figure 4.7) and a chi-square test performed on the transformed data indicated that these data represent a normal population ($0.25 < P < 0.5$). A comparison of basic statistics of the transformed data describing volume measured during the four individual surveys is shown in Table 4.7.

Table 4.7. Various statistics calculated in respect of volume for each survey.

| Survey | G mean | SD | CV | Min | Max | $g_1$ |
|---|---|---|---|---|---|---|
| Rafos II | 3124 | 11.81 | 0.38 | 12.0 | 2178058.7 | 0.66 |
| Intercalibration | 3322 | 14.83 | 0.45 | 11.2 | 805941.0 | 0.44 |
| Rafos III (grid 2) | 1636 | 9.20 | 0.56 | 10.4 | 71095.2 | 0.39 |
| Rafos III (grid 4) | 917 | 7.68 | 0.83 | 12.3 | 43161.2 | 0.12 |
| All surveys | 2224 | 11.55 | 0.52 | 10.4 | 2178058.7 | 0.58 |

The geometric mean and standard deviation in shoal volume was found to be the highest for the intercalibration survey and least for the Rafos III (grid 4) survey.

An analysis of variance was also performed to determine differences between the survey means for the transformed data. A significant difference between surveys was found ( $P_{transformed} < 0.0005$).A Tukey test, however, revealed no significant difference between the RAFOS II and intercalibration surveys as well as between the two Rafos III surveys. A significant difference was, however, observed between the two pairs of surveys ($\mu_{\text{Rafos II}} = \mu_{\text{intercalibration}} \neq \mu_{\text{Rafos III (grid 2)}} = \mu_{\text{Rafos III (grid 4)}}$).

**Relationships between school area, school volume and school biomass**

Significant correlations existed between school area ($m^2$) and school biomass (kg) for all shoals analyzed. The results of the correlations are shown in Table 4.8 and plots of school biomass to corresponding school area and school volume are shown in Figures 4.8 and 4.9 respectively. The correlation appeared to be the strongest for the intercalibration survey where a correlation coefficient of 0.86 was calculated. All other surveys showed a correlation between school area and school

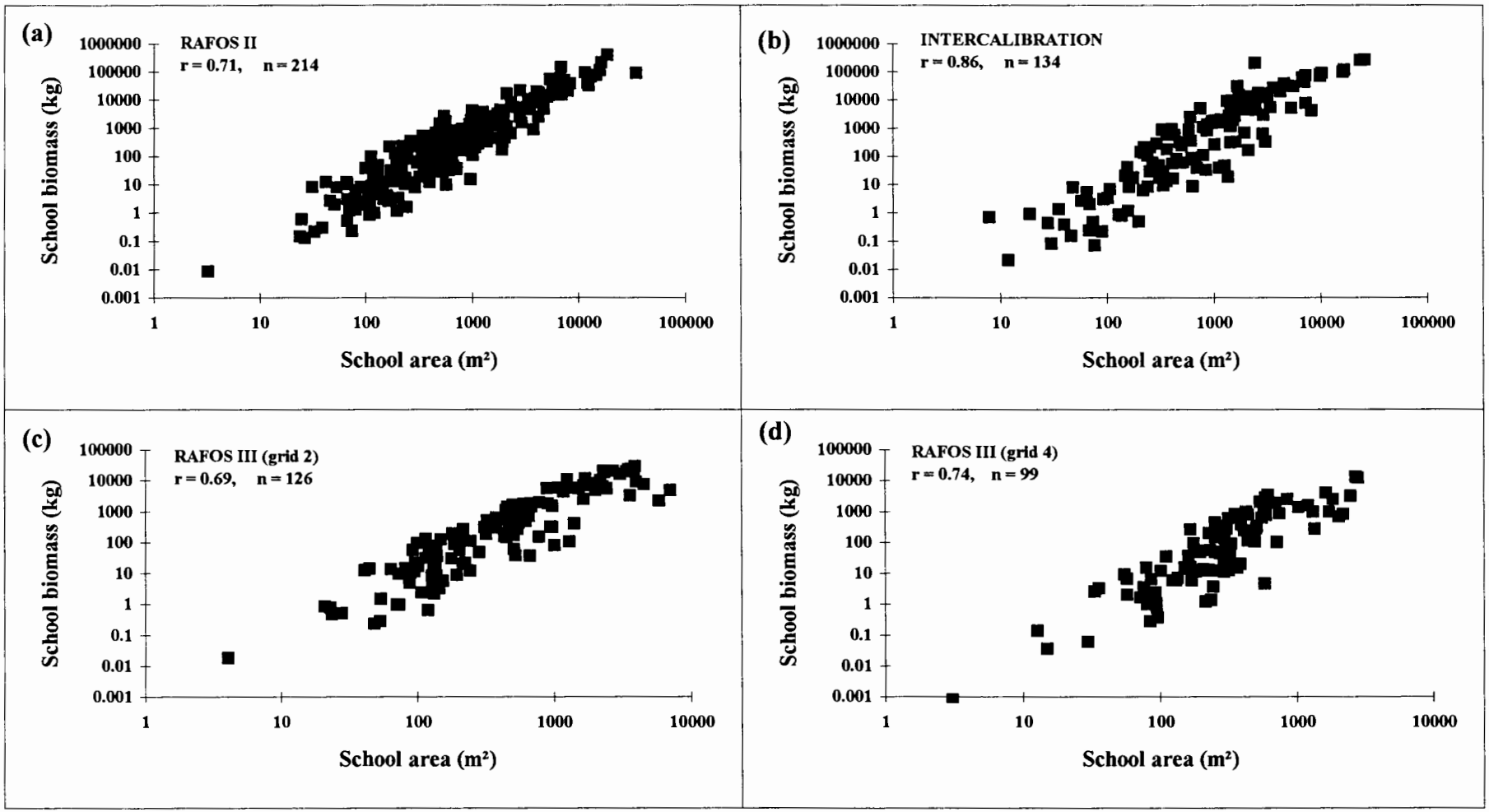


Fig 4.8. Relationships between school biomass and school area for each survey: (a) RAFOS II; (b) Intercalibration; (c) RAFOS III (grid 2); (d) RAFOS III (grid 4).

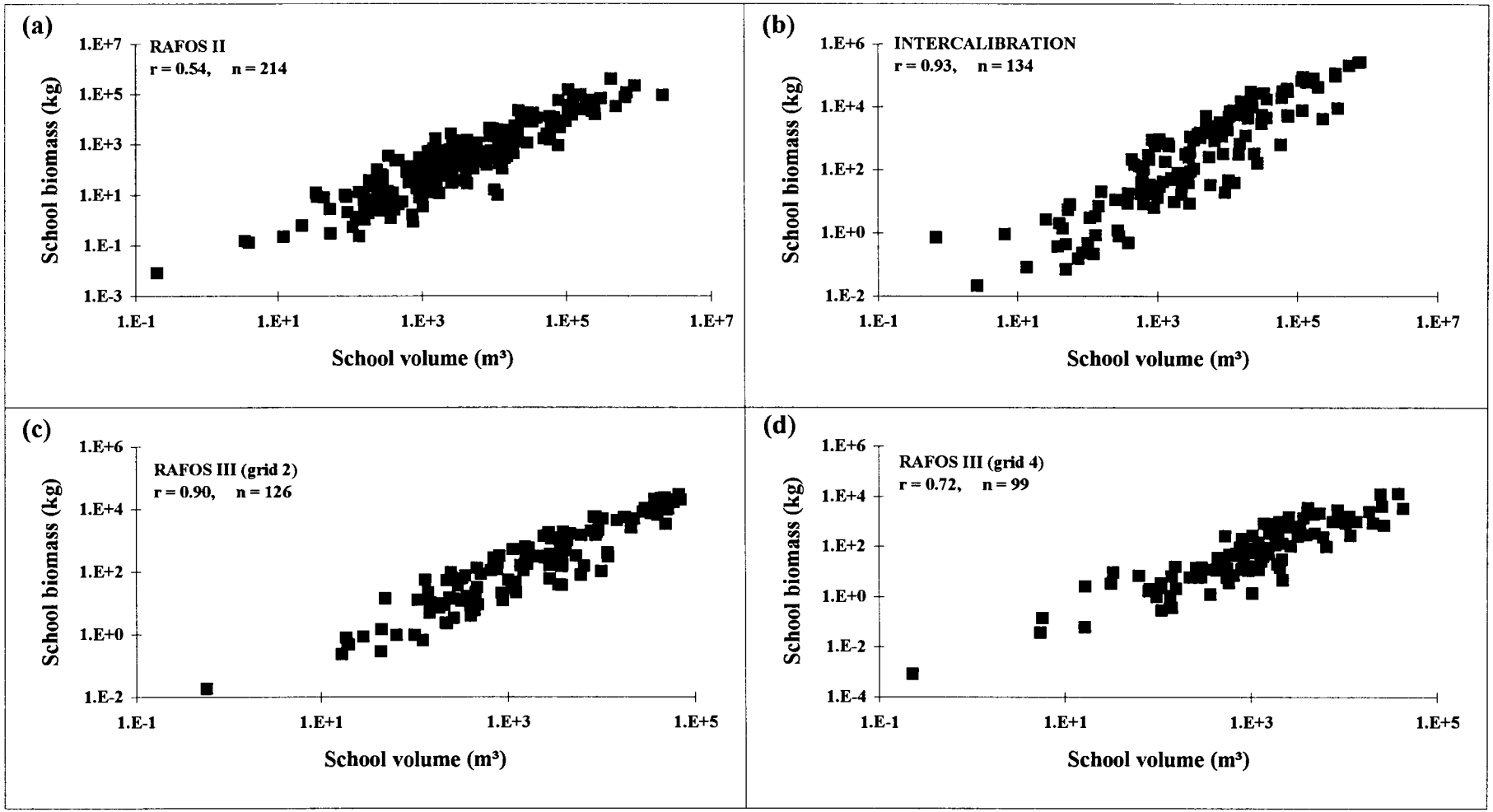


Fig 4.9. Relationships between school biomass and school volume for each survey: (a) RAFOS II; (b) Intercalibration; (c) RAFOS III (grid 2); (d) RAFOS III (grid 4).

biomass of greater than 0.69 ($P < 0.001$ for all surveys). When comparing school volume to school biomass, significant correlations were also found for all surveys. Once again the correlation was the strongest for the intercalibration survey ($r = 0.93$). The correlation coefficients between school volume and school biomass was greater than 0.54 for all surveys ($P < 0.001$).

Table 4.8. Results of the correlation between school area, school volume and school biomass for each survey.

| Survey | n | School area to biomass | | | School volume to biomass | | |
|---|---|---|---|---|---|---|---|
| | | r | $r^2$ | $s_r$ | r | $r^2$ | $s_r$ |
| Rafos II | 213 | 0.71 | 0.50 | 0.048 | 0.54 | 0.29 | 0.058 |
| Intercalibration | 134 | 0.86 | 0.74 | 0.044 | 0.93 | 0.86 | 0.032 |
| Rafos III (grid 2) | 126 | 0.69 | 0.48 | 0.065 | 0.90 | 0.81 | 0.039 |
| Rafos III (grid 4) | 99 | 0.74 | 0.55 | 0.068 | 0.71 | 0.50 | 0.072 |
| All surveys | 573 | 0.77 | 0.59 | 0.027 | 0.65 | 0.42 | 0.032 |

A chi-square test revealed a significant difference between the various survey correlation coefficients ($P < 0.001$) both for the area and volume correlations, but a subsequent Tukey-type multiple comparison showed the only significant different correlation coefficient for area to biomass was that of the intercalibration survey ($p_{\text{Rafos II}} = p_{\text{Rafos III (grid 2)}} = p_{\text{Rafos III (grid 4)}} \neq p_{\text{Intercalibration}}$). For the correlation between school volume and biomass a Tukey test revealed that the correlation coefficients of the intercalibration and Rafos III (grid 2) surveys were significantly different from the Rafos II and Rafos III (grid 4) surveys ($p_{\text{Rafos II}} = p_{\text{Rafos III (grid 4)}} \neq p_{\text{Rafos III (grid 2)}} = p_{\text{Intercalibration}}$).

Strong and significant regressions were calculated when relating school biomass to corresponding school area and school volume (Table 4.9). For both the area to biomass and volume to biomass regressions, there were no significant differences between the various slopes ($P > 0.1$ and $P > 0.25$ respectively), but the elevations differed significantly ($P < 0.0005$ and $P < 0.0025$ respectively).

Table 4.9. School area and school volume to school biomass regression equations.

| Survey | log (area) to log (biomass) | | | | log (volume) to log (biomass) | | | |
|---|---|---|---|---|---|---|---|---|
| | area | SE | Intercept | $r^2$ | volume | SE | Intercept | $r^2$ |
| Rafos II | 1.94 | 0.52 | -3.10 | 0.86 | 1.16 | 0.59 | -1.74 | 0.81 |
| Intercalibration | 1.99 | 0.55 | -2.90 | 0.83 | 1.29 | 0.48 | -1.95 | 0.87 |
| Rafos III (grid 2) | 2.22 | 0.62 | -3.73 | 0.77 | 1.30 | 0.59 | -2.21 | 0.79 |
| Rafos III (grid 4) | 2.11 | 0.69 | -3.57 | 0.82 | 1.26 | 0.72 | -2.04 | 0.81 |

$P < <0.0005$ for $\alpha$ 0.05

**Fractal Dimension and perimeter**

The fractal dimension (FD) is calculated from the perimeter length to area relationship and is a measure of shoal shape complexity. A fractal dimension value of 1 represents a square outline shape whilst a value of 2 denotes the most complex outline shapes. FD calculated for all schools, was generally low ($< 1.4$) indicating that the shape of the schools was quite regular. The distribution of fractal dimension is shown in Figure 4.10 and although the distribution is close to normal, it was slightly negatively skewed ($g_1 = -0.84$).

The mean fractal dimensions of the individual surveys were compared by an analysis of variance and this indicated a significant difference ($P < 0.0005$) between the survey means. A Tukey test, however, showed that the only significant different mean was that of the Rafos III (grid 4 survey). This survey had a mean fractal dimension of 0.86 indicating that shoals recorded during this survey were the most regular. The statistics calculated on fractal dimension for each survey are presented in Table 4.10.

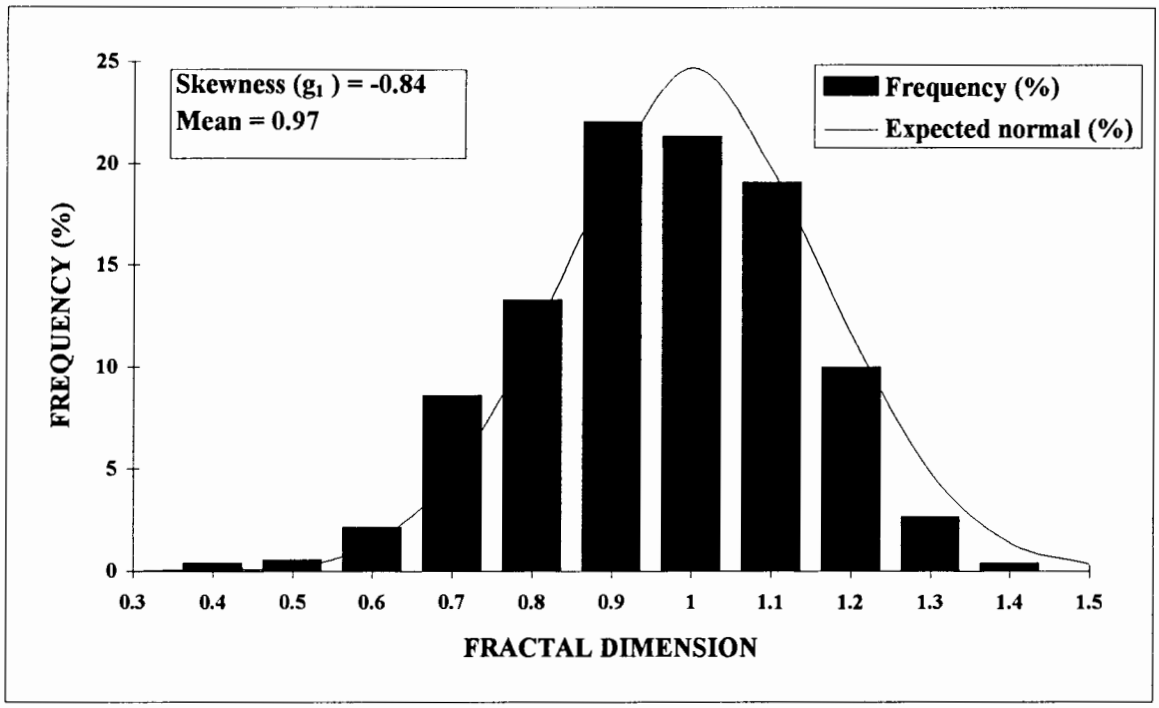


Fig 4.10. Frequency and expected normal distributions of fractal dimension.

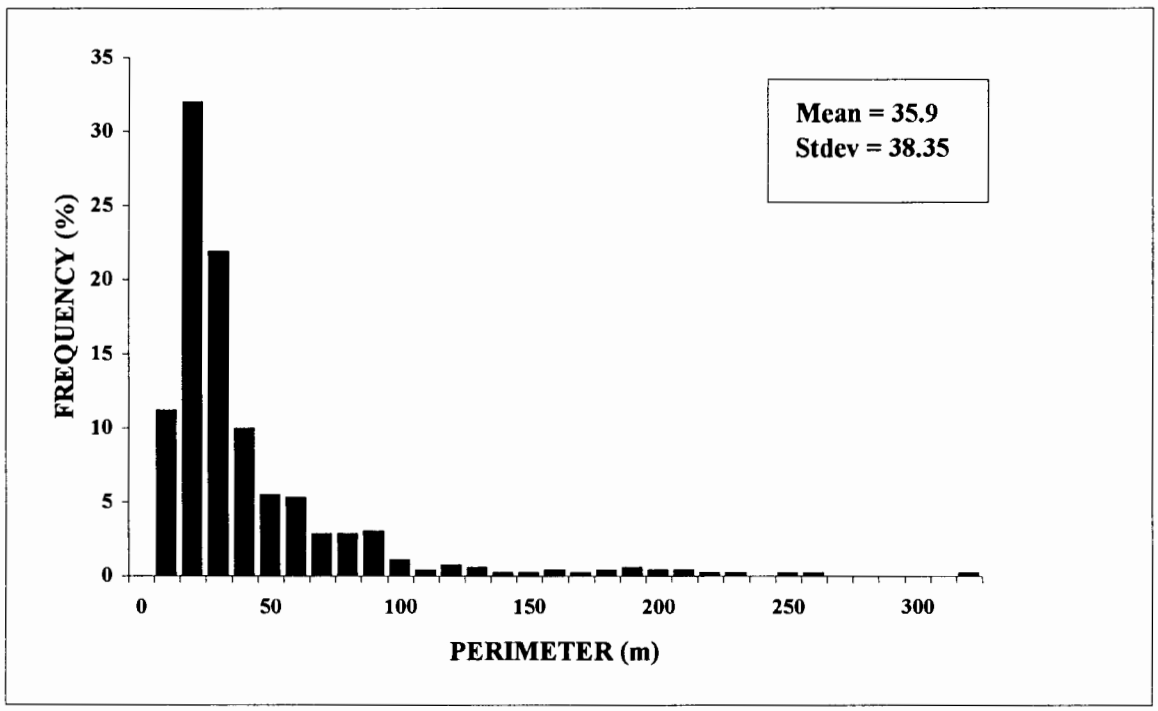


Fig 4.11. Percentage frequency distribution of perimeter of sardine shoals.

Table 4.10. Basic statistics calculated for fractal dimension for each survey.

| Survey | $\bar{x}$ | SD | CV | Min | Max | $g_1$ |
|---|---|---|---|---|---|---|
| Rafos II | 0.99 | 0.173 | 0.175 | 0.40 | 1.40 | -0.82 |
| Intercalibration | 1.02 | 0.137 | 0.134 | 0.67 | 1.38 | 0.59 |
| Rafos III (grid 2) | 0.95 | 0.162 | 0.170 | 0.54 | 1.34 | -0.76 |
| Rafos III (grid 4) | 0.86 | 0.145 | 0.167 | 0.42 | 1.16 | -1.02 |
| All surveys | 0.97 | 0.166 | 0.172 | 0.40 | 1.40 | -0.84 |

The perimeter (m) of shoals analyzed varied substantially from a minimum of below 10 m to a maximum of 315 m. The mean perimeter of all the shoals was 38.5 m although a very large standard deviation was calculated (SD =38.36). The frequency distribution of perimeter is shown in Figure 4.11. It can be seen that the distribution is very highly skewed to the right with most of the shoals (70%) having a perimeter of less than 50 m and the shoals with a perimeter of greater than 100 m accounting for less than 5 % of the total. A comparison of the basic statistics calculated for perimeter for each survey is shown in Table 4.11.

Table 4.11. Basic statistics calculated for shoal perimeter for each survey.

| Survey | $\bar{x}$ | SD | CV | Min | Max |
|---|---|---|---|---|---|
| Rafos II | 35.5 | 38.22 | 1.07 | 6 | 227 |
| Intercalibration | 52.2 | 53.18 | 1.02 | 8 | 315 |
| Rafos III (grid 2) | 28.0 | 22.98 | 0.82 | 7 | 135 |
| Rafos III (grid 4) | 17.8 | 10.53 | 0.59 | 6 | 66 |
| All surveys | 35.8 | 38.36 | 1.07 | 6 | 315 |

The mean perimeter varied significantly between surveys ($P < 0.0005$) with the intercalibration survey having the highest mean perimeter and also the largest range in perimeter. The mean, standard deviation and range of the perimeter of schools recorded during the Rafos III (grid 4) survey was the lowest. A Tukey comparison amongst the means revealed that the mean of the intercalibration survey differed significantly from all other survey means.

**School density and packing density**

The average biomass per unit area of the schools varied from a minimum of 0.1 $g.m^{-2}$ to a maximum of 127.9 $g.m^{-2}$. The mean school density for all surveys was calculated to be 16.7 $g.m^{-2}$ with a standard deviation of 20.615 $g.m^{-2}$. The distribution of mean school density is highly skewed to the right (g1 =2.18) and shoals with a mean density per unit area of less than 40 $g.m^{-2}$ accounted for more than 75 % of the total. The log-transformed data are more symmetrical and not too far from a normal distribution ($0.025 < P < 0.01$). The frequency distribution of the log-transformed density data as well as the expected normal distribution are shown in Figure 4.12. An analysis of variance was done using biomass per unit area ($g.m^{-2}$) as the dependent variable to compare the means from the various surveys. These results as well as the basic statistics calculated for mean school density is shown in Table 4.12.

Table 4.12. Basic statistics calculated for fish density ($g.m^{-2}$) for each survey and results of the single factor analysis of variance between survey means.

| Survey | $\bar{x}$ | SD | CV | Min | Max | $g_1$ |
|---|---|---|---|---|---|---|
| Rafos II | 12.2 | 16.129 | 1.32 | 0.2 | 99.0 | 2.75 |
| Intercalibration | 15.8 | 22.123 | 1.39 | 0.1 | 127.9 | 2.89 |
| Rafos III (grid 2) | 24.3 | 21.818 | 0.89 | 0.5 | 95.6 | 1.11 |
| Rafos III (grid 4) | 17.7 | 22.860 | 1.29 | 0.2 | 104.5 | 2.00 |
| All surveys | 16.7 | 20.615 | 1.23 | 0.1 | 127.9 | 2.18 |

| Source of variation | SS | df | MS | F-value | p | F*crit* |
|---|---|---|---|---|---|---|
| Surveys | 12059.73 | 3 | 4019.91 | 9.86 | < 0.0005 | 2.62 |
| Error | 230437.8 | 565 | 407.85 | | | |
| Total | 242497.5 | 568 | | | | |

The analysis of variance shows that a significant difference does exist between the average biomass per unit area of the individual surveys. A Tukey test revealed that the only significant difference in mean density was between Rafos III (grid 2) and the rest of the surveys ($\mu_{\text{Rafos II}} = \mu_{\text{intercalibration}} = \mu_{\text{Rafos III (grid 4)}} \neq \mu_{\text{Rafos III (grid 2)}}$).

The average biomass per unit volume for all schools was 170.74 $g.m^{-3}$ (SD = 211.48). The distribution was extremely skewed to the right ($g_1$ = 2.08) and although the log-transformed data was more symmetrical, a Chi-squared test showed that it was far from normal ($P < 0.001$). The frequency distribution of the log-transformed mean biomass per unit volume and expected normal frequency are shown in Figure 4.13. The log-transformed histogram is slightly skewed to the left ($g_1$ = -0.43). At least 50 % of the shoals had a mean biomass per unit volume of less than 100 $g.m^{-3}$ and shoals with a mean biomass per unit volume of more than 500 $g.m^{-3}$ accounted for less than 10 % of the total number of shoals. Shoal with a mean biomass per unit volume of greater than 1000 $g.m^{-3}$ only accounted for less than 1 % of the total.

A comparison of mean shoal biomass per unit volume between surveys showed a significant difference ($P < 0.0001$). The results of the ANOVA performed on the individual survey data and a comparison of basic statistics calculated for each survey are shown in Table 4.13.

Table 4.13. Basic statistics calculated for density ($g.m^{-3}$) for each survey and results of single analysis of variance between survey means.

| Survey | $\bar{x}$ | SD | CV | Min | Max | $g_1$ |
|---|---|---|---|---|---|---|
| Rafos II | 150.37 | 202.95 | 1.35 | 0.85 | 1297.69 | 2.77 |
| Intercalibration | 233.91 | 271.83 | 1.16 | 1.27 | 1359.35 | 1.49 |
| Rafos III (grid 2) | 178.30 | 167.39 | 0.94 | 4.97 | 660.70 | 0.99 |
| Rafos III (grid 4) | 119.63 | 162.57 | 1.36 | 1.29 | 800.33 | 2.02 |
| All surveys | 170.74 | 211.48 | 1.23 | 0.85 | 1359.35 | 2.08 |

**ANOVA**

| Source of variation | SS | df | MS | F-value | p | *Fcrit* |
|---|---|---|---|---|---|---|
| Surveys | 889329.7 | 3 | 296443.2 | 6.83 | < 0.001 | 2.62 |
| Error | 24694149 | 569 | 43399.21 | | | |
| Total | 25583479 | 572 | | | | |

The distribution of mean shoal biomass per unit volume was positively skewed for all surveys and skewness ranged from a minimum of 0.99 for the Rafos III (grid 2) survey to a maximum of 2.77

for the Rafos II survey. The mean shoal biomass per unit volume for each survey ranged from 119.63 $g.m^{-3}$ for the Rafos III (grid 4 ) survey to as much as 233.91 $g.m^{-3}$ for the intercalibration survey. The only significant different mean shoal biomass per unit volume found after a Tukey test was that of the intercalibration survey with no significant differences found between the means of the other surveys.

Packing density ( individuals per cubic meter ) varied from less than 1 $ind.m^{-3}$ to a maximum of 36.2 $ind's.m^{-3}$. The distribution of packing density was positively skewed ($g_1 = 2.58$)and not too far from a log-normal distribution ($0.025 < P < 0.01$)The histogram of the log-transformed data and expected normal distribution is shown in Figure 4.14. The mean packing density for all surveys is 4.0 $ind's.m^{-3}$ and at least 50 % of the shoals had a packing density of less than 2 $ind's.m^{-3}$. When comparing the individual surveys (Table 4.14) it is evident that significant differences occurred between the mean packing density of the surveys. The intercalibration survey had the highest mean packing density followed by the Rafos II survey. The two Rafos III surveys had identical mean packing densities, but these were significantly lower than the other two surveys. In all cases the distribution of packing density was skewed to the right. A Tukey test confirmed that significant differences exist in mean packing density between all surveys except for between the two Rafos III surveys ($\mu_{\text{Rafos II}} \neq \mu_{\text{intercalibration}} \neq \mu_{\text{Rafos III (grid 2)}} = \mu_{\text{Rafos III (grid 4)}}$).

Table 4.14. Basic statistics calculated for packing density ($ind's.m^{-3}$) for each survey and results of the single factor analysis of variance between survey means.

| Survey | $\bar{x}$ | SD | CV | Min | Max | $g_1$ |
|---|---|---|---|---|---|---|
| Rafos II | 4.2 | 5.67 | 1.35 | 0.02 | 36.2 | 2.77 |
| Intercalibration | 6.2 | 7.21 | 1.16 | 0.03 | 36.1 | 1.49 |
| Rafos III (grid 2) | 2.4 | 2.22 | 0.94 | 0.07 | 8.8 | 0.98 |
| Rafos III (grid 4) | 2.4 | 3.26 | 1.36 | 0.03 | 16.0 | 2.01 |
| All surveys | 4.0 | 5.39 | 1.37 | 0.02 | 36.2 | 2.58 |
| **Source of variation** | **SS** | **df** | **MS** | **F-value** | **p** | ***Fcrit*** |
| Surveys | 1248.51 | 3 | 416.17 | 15.36 | < 0.001 | 2.62 |
| Error | 15418.49 | 569 | 27.09 | | | |
| Total | 16667 | 572 | | | | |

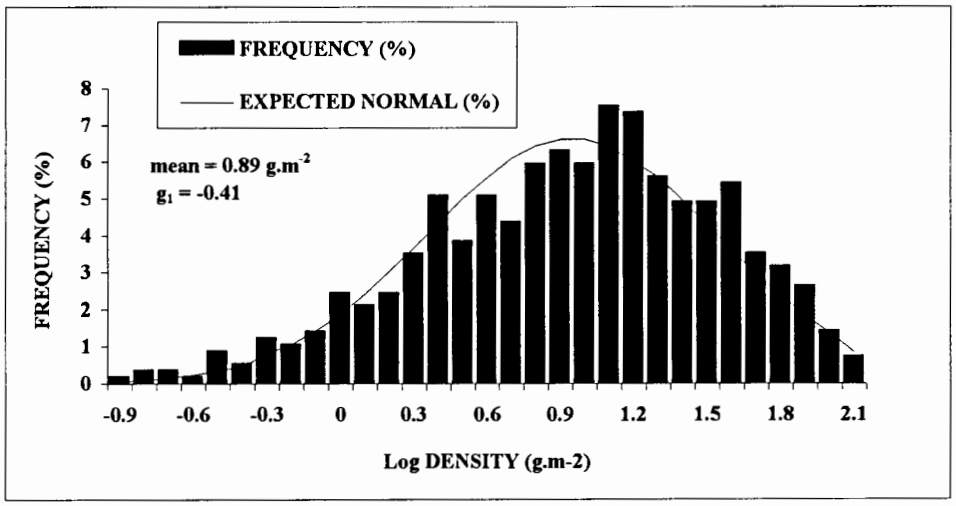


Fig 4.12. Frequency and expected normal distribution of log-transformed density per unit area ($g/m^2$).

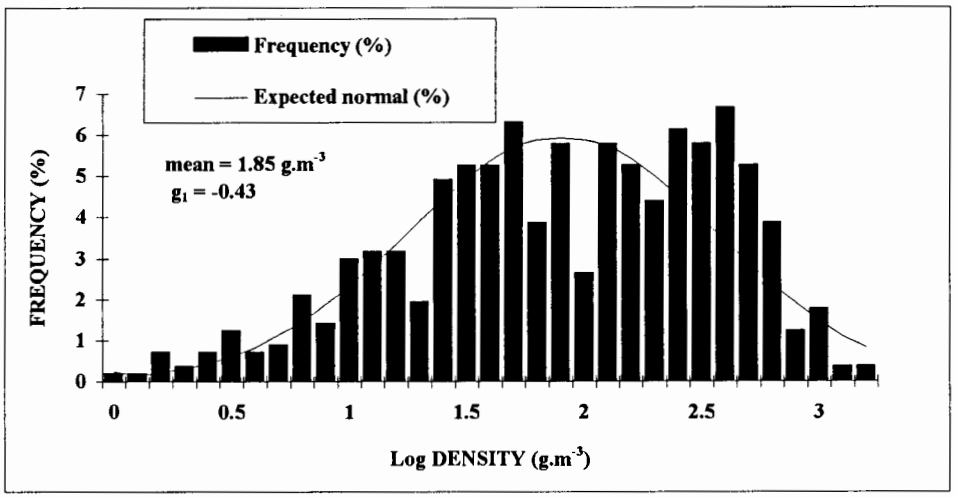


Fig 4.13. Frequency and expected normal distribution of log-transformed density per unit volume ($g/m^3$).

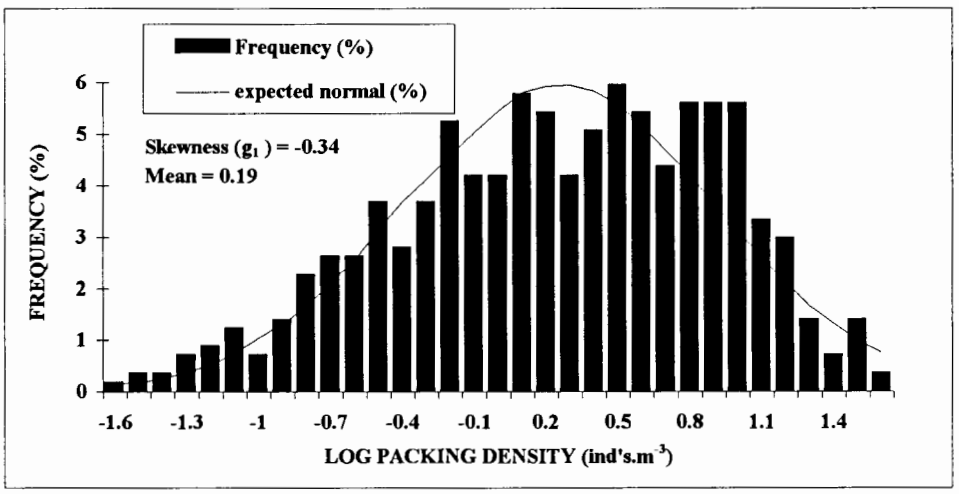


Fig 4.14. Frequency and expected normal distribution of log-transformed packing density ($ind's/m^3$).

**Horizontal and vertical roughness**

Both the histograms of horizontal and vertical roughness were positively skewed ($g_1$ = 1.88 and 2.76 respectively). The frequency distribution of the log-transformed data was more symmetrical in both cases (Figure 4.15), although still far from normal. The mean horizontal roughness was 7558.1 (SD = 12081) and the mean vertical roughness was 8033.73 (SD = 10826.88). An analysis of variance showed significant differences in both mean horizontal and vertical roughness between surveys (P = 0.0035 and P = 0.0023, respectively). A comparison of basic satistics calculated for both variables is shown in Table 4.15.

Table 4.15. Basic statistics calculated for both horizontal and vertical roughness for each survey.

| | Survey | $\bar{x}$ | SD | CV | Min | Max | $g_1$ |
|---|---|---|---|---|---|---|---|
| HORIZONTAL | Rafos II | 8679.9 | 12081.33 | 1.39 | 0.1 | 62996.7 | 1.85 |
| | Intercalibration | 8797.1 | 10252.11 | 1.17 | 3.5 | 42519.0 | 1.19 |
| | Rafos III (grid 2) | 6585.4 | 6596.61 | 1.00 | 4.3 | 32169.4 | 0.99 |
| | Rafos III (grid 4) | 4693.8 | 6534.16 | 1.39 | 0.1 | 29044.5 | 1.71 |
| | All surveys | 7558.1 | 9903.22 | 1.31 | 0.1 | 62996.7 | 1.88 |
| VERTICAL | Rafos II | 7116.38 | 8877.27 | 1.25 | 1.1 | 52466.4 | 1.98 |
| | Intercalibration | 10428.87 | 15267.79 | 1.46 | 1.6 | 94143.8 | 2.82 |
| | Rafos III (grid 2) | 8879.74 | 9219.51 | 1.04 | 4.2 | 34014.3 | 0.90 |
| | Rafos III (grid 4) | 5698.06 | 8486.45 | 1.49 | 0.6 | 45213.2 | 2.52 |
| | All surveys | 8033.73 | 10826.88 | 1.35 | 0.6 | 94143.8 | 2.76 |

Results of a Tukey test on the means of horizontal roughness showed that the only significant different mean was that of the Rafos III (grid 4) survey which was much lower than the rest ($\mu_{\text{Rafos III (grid 4)}} \neq \mu_{\text{Rafos III (grid 2)}} = \mu_{\text{Rafos II}} = \mu_{\text{Intercalibration}}$). In the case of vertical roughness the means of the Rafos II and Rafos III (grid 2) surveys were similar, but differed significantly from the other two surveys($\mu_{\text{Rafos III (grid 4)}} \neq \mu_{\text{intercalibration}} = \mu_{\text{Rafos III (grid 2)}} \neq \mu_{\text{Rafos II}}$).

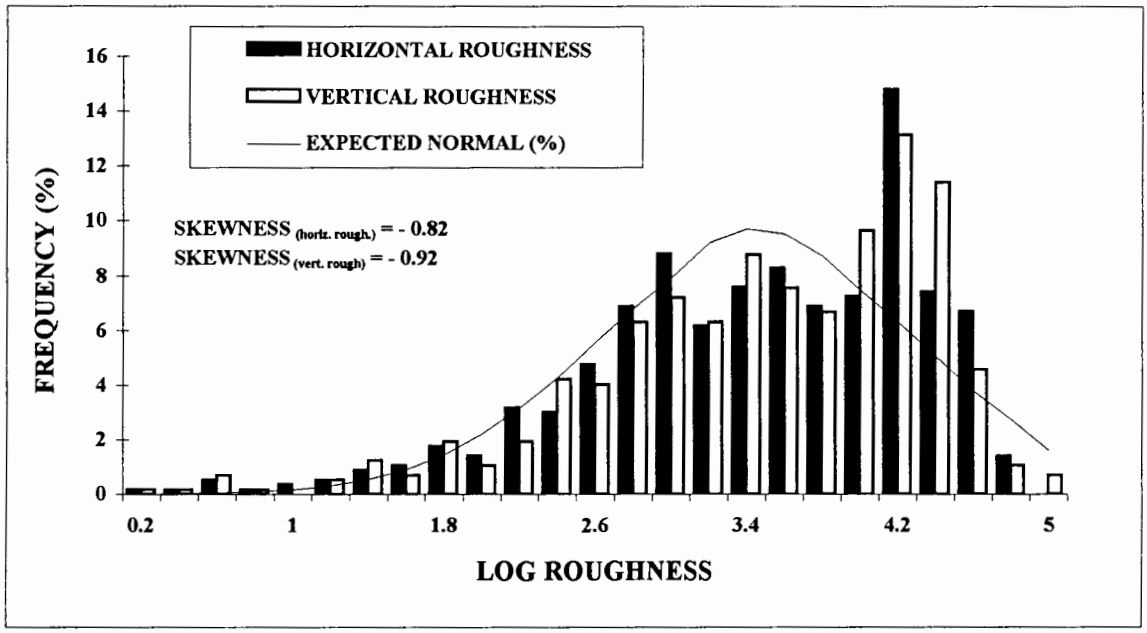


Fig 4.15. Frequency and expected normal distributions for both horizontal and vertical roughness.

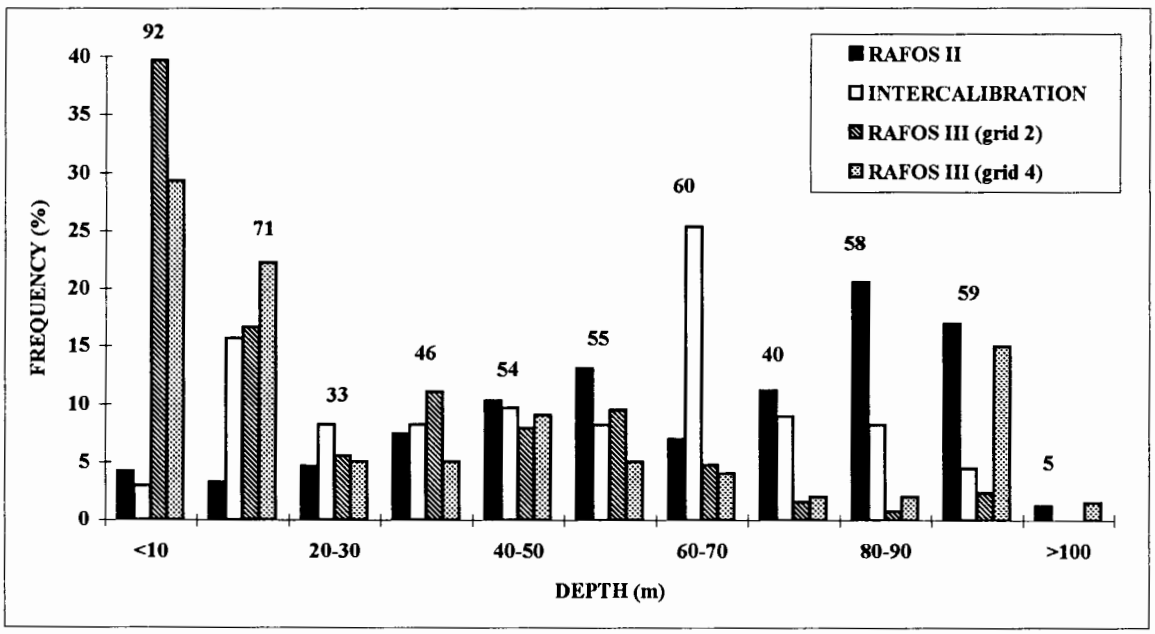


Fig 4.16. Depth distribution of shoals grouped according to surveys. Numbers on figure represent the number of shoals present per depth class.

**Shoal depth**

The mean depth at which shoals occurred varied greatly from less than 10 m below the surface to more than 100 m below the surface (Figure 4.16). It must again be emphasised that only day schools have been used in this part of the analysis and that the depth distribution of schools at night would probably be much shallower. There were also significant differences in the mean school depths between surveys. The number of schools at a depth of less than 20 m was quite high when all surveys were taken into account (30%). During the Rafos II survey, large numbers of shoals occurred at depths in excess of 70 m and very few at depths of less than 20 m. The schools recorded during the intercalibration survey were mostly at a depth of between 60 - 70 m and those recorded during the Rafos III surveys were mostly found shallower than 30 m. In all surveys, the schools were distributed throughout the entire water column. Results of a single factor analysis of variance on mean depth showed a significant difference between the survey means ($P < 0.0001$). A subsequent Tukey test to determine between which means significant differences existed, showed that all surveys means differed significantly ($\mu_{\text{Rafos II}} \neq \mu_{\text{Rafos III (grid 2)}} \neq \mu_{\text{Rafos III (grid 4)}} \neq \mu_{\text{Intercalibration}}$).

## 4.2 PRINCIPAL COMPONENT ANALYSIS

A Principal Component Analysis (PCA) was applied to the data of all schools to establish which variables best described school characteristics and to investigate whether these variables remained constant throughout the four surveys. The main purpose was to reduce the number of variables and to detect structure in the relationships between variables.

All variables except fractal dimension, skewness and kurtosis were log-transformed to assist in the normalisation of their distributions. Highly correlated variables were excluded from further analysis. To maximise the variance explained by the PCA and ease interpretation, a varimax normalised rotation was applied to the data. After computation of eigenvalues, a graphical scree test was done to establish the number of factors to extract.

The eigenvalues for the first three components are presented in Table 4.16. The first component explained 59 % of the total variance, the second explained 16 % of the variance and the third explained 10 % of the variance. Together the first three components explained 87 % of the total variance.

Table 4.16. Total variance extracted by each of the three principal components.

| STAT. FACTOR ANALYSIS | Eigenvalues Extraction: Principle components | | | |
|---|---|---|---|---|
| Component | Eigenvalue | % total var. | Cum. Eigenval | Cum. % |
| 1 | 6.5982 | 59.98 | 6.5982 | 59.98 |
| 2 | 1.8569 | 16.88 | 8.4552 | 76.86 |
| 3 | 1.1362 | 10.32 | 9.5914 | 87.19 |

When the maximised factor loadings are compared (Table 4.17) it is clear that the first factor is highly correlated with the variables describing the size and shape of the schools such as length, area and perimeter indicating the importance of school morphology in the classification of school types. The second factor mainly reflected those variables relating to the spatial distribution within schools (horizontal and vertical roughness) and the mean acoustic intensity. The third factor was highly

correlated to variables describing the distribution of the acoustic intensity such as skewness and kurtosis.

Table 4.17. Factor loadings of the first, second and third principle components.

| STAT. FACTOR ANALYSIS | Factor loadings (Varimax normalised ) Extraction: Principle components (Marked variables highly load the respective factors) | | |
|---|---|---|---|
| Variable | Factor 1 | Factor 2 | Factor 3 |
| Height | 0.77* | 0.31 | 0.10 |
| Length | 0.78* | 0.09 | 0.30 |
| Area | 0.92* | 0.23 | 0.25 |
| Volume | 0.89* | 0.17 | 0.27 |
| Perimeter | 0.88* | 0.24 | 0.21 |
| Fractal Dimension | 0.85* | 0.11 | 0.16 |
| Acoustic Intensity | 0.23 | 0.93* | -0.03 |
| Horiz. Roughness | 0.18 | 0.88* | 0.24 |
| Vert. Roughness | 0.19 | 0.92* | 0.21 |
| Skewness | 0.34 | 0.25 | 0.88* |
| Kurtosis | 0.29 | 0.10 | 0.91* |
| Variance explained | 4.70 | 2.84 | 2.03 |
| % of Total | 42.80 | 25.85 | 18.53 |

When the first and second and first and third factor loadings are plotted (Figure 4.17 a and b), it is clear that the variables describing school characteristics are grouped into three distinct sets of school descriptors. The descriptors which reflect the school morphology strongly loads the first component but only slightly weights the second and third components. Those variables describing the distribution of acoustic intensity only slightly weight both the first and second components but strongly weights the third. The descriptors which reflect the internal acoustic intensity and spatial distribution thereof strongly load the second component. From this it is clear that the PCA has successfully reduced the number of variables necessary to describe school characteristics to three.

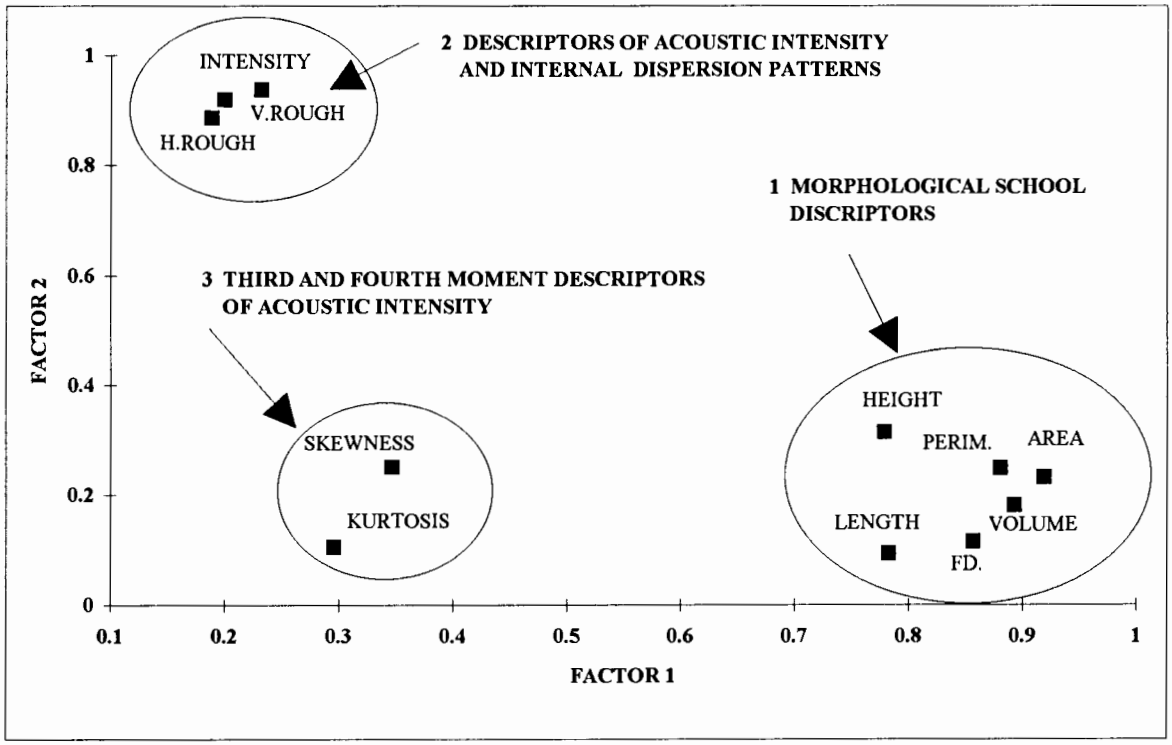


Fig 4.17(a). Plot of the first versus the second factor loadings as extracted by the PCA.

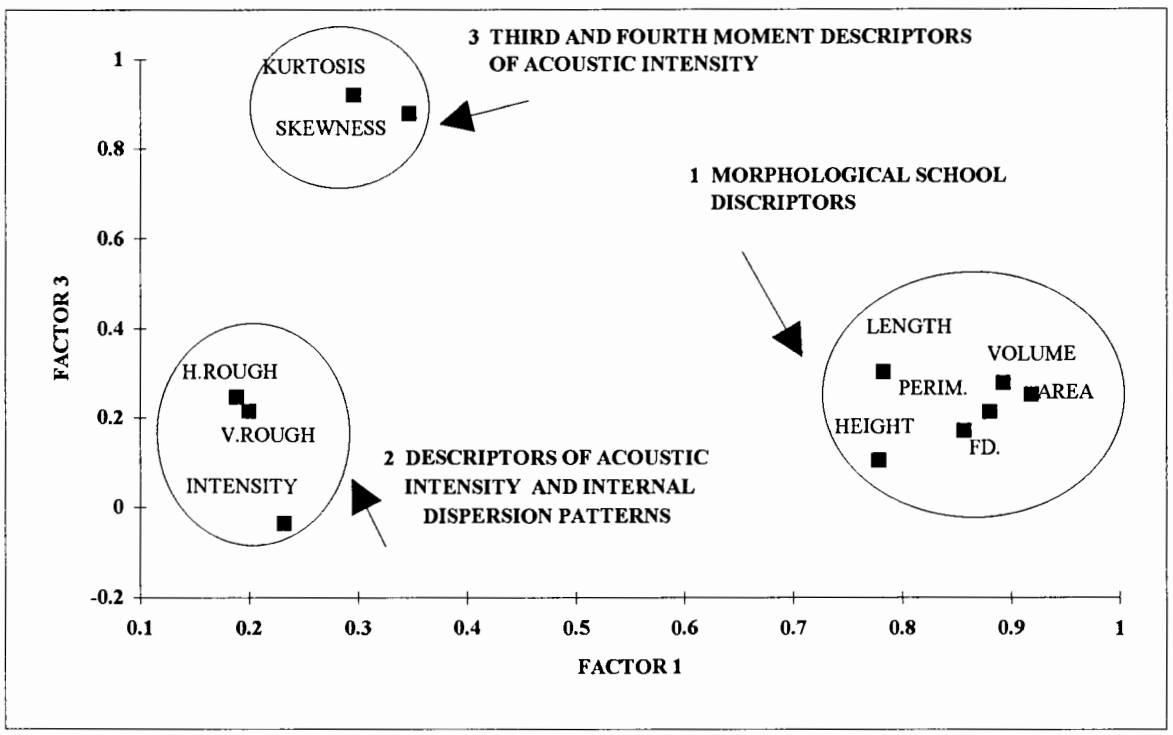


Fig 4.17 (b). Plot of the first versus the third factor loadings as extracted by the PCA.

The distribution of the schools for all surveys, classified according to the first two factors and grouped by survey showed no clear patterns (Figure 4.18). The amount of variation along both the x -axis and y-axis was similar and very few outliers were observed, indicating just as much variability in morphological characteristics as internal school characteristics. This also indicated that the four surveys were not separated by either of the two components in any significant manner. Very slight differences did, however, occur and these are described below:

a) For the Rafos II survey the fish schools were slightly more variable along the y-axis than along the x-axis indicating that for this survey the internal school structures were more variable than the morphological characteristics.

b) In the case of the intercalibration survey, the range of distribution of schools along both the axes were similar and not very different from the distribution of the Rafos II survey. Slightly more schools were distributed to the right (on the x-axis), possibly indicating more variability in morphological characteristics than that of the Rafos II survey.

c) The distribution of the Rafos III (grid 2) schools was notably more variable along the x-axis, possibly indicating more variance in internal school intensity descriptors which negatively weighted the first component. Variation along the y-axis was little and possibly indicated less variability in acoustic intensity and internal dispersion than the previous two surveys.

d) For the Rafos III (grid 4) survey, the distribution of schools was more to the left of the x-axis than for the other surveys possibly indicating higher variability in the descriptors of acoustic density. More variability was also observed along the y-axis possibly indicating greater variability in internal spatial distribution and density.

In general the above observations indicate that sardine schools are variable as the individual parameters differed between surveys, but there is a consistency in their shape, structure and density. This is probably characteristic of the species, which is independent of the time and area of the surveys.

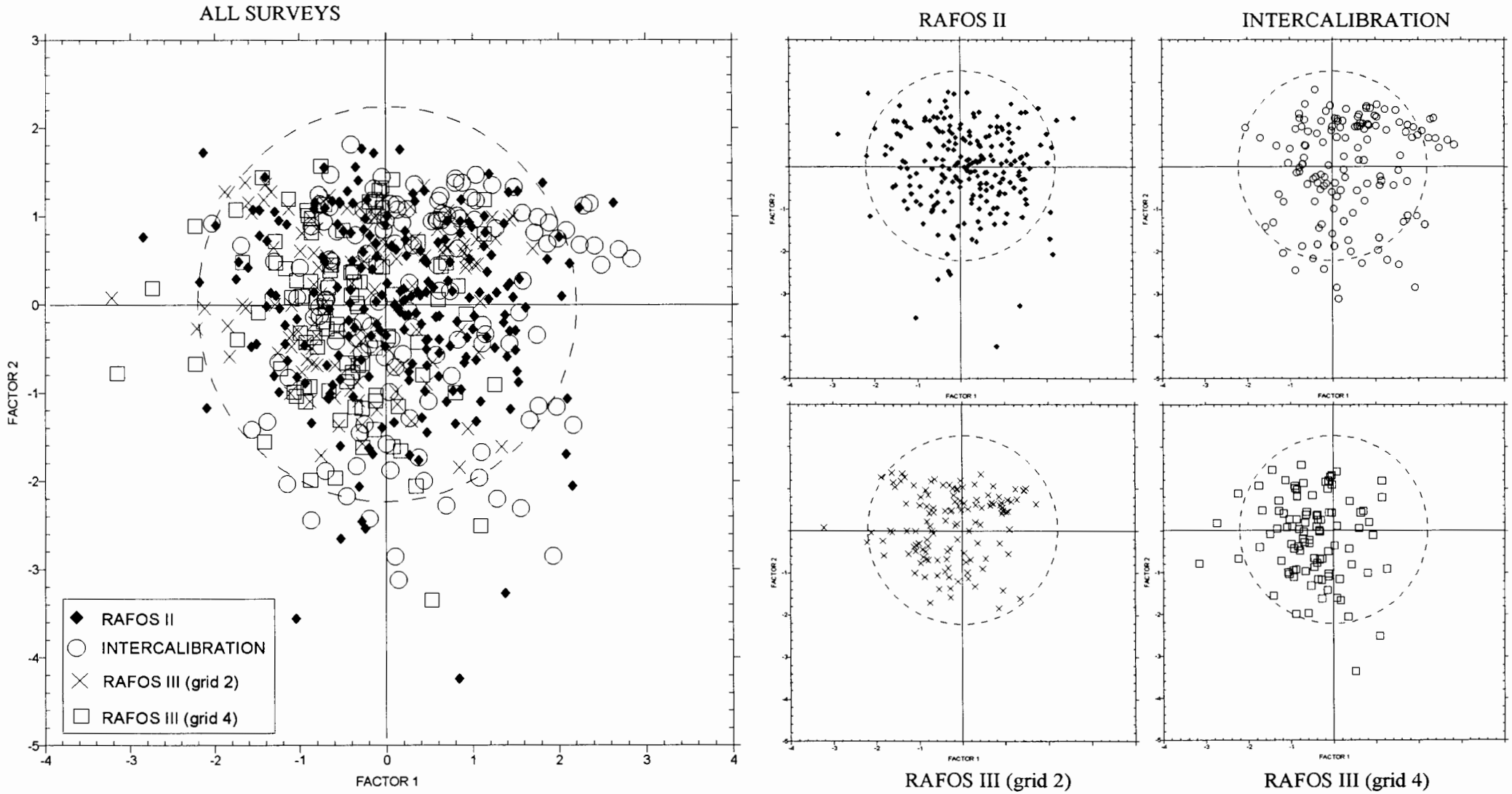


FIG 4.18. Scattergram of the shoals identified in all surveys and in each individual survey according to the values of the first two components of the PCA.

## 4.3 INTERNAL SCHOOL STRUCTURE.

To investigate the internal school structure 12 schools of various size and shape were selected after being identified by SHAPES. The frequency distribution of acoustic intensity of each shoal using the density of each cell (1 ping horizontally and 1 metre vertically) is shown in Figure 4.19. All shoals were positively skewed with a few large values in each case contributing a large proportion to the mean and the variance. Basic statistics calculated for each shoal are shown in Table 4.18.

Table 4.18. Basic statistics calculated for each shoal.

| Shoal | N cells | Acoustic Intensity (Sa) | | | | |
|---|---|---|---|---|---|---|
| | | Mean | Min | Max | SD | Skewness |
| 1 | 221 | 10496 | 10 | 111540 | 21734 | 2.67 |
| 2 | 163 | 4732 | 10 | 76371 | 10335 | 3.83 |
| 3 | 145 | 15024 | 10 | 103190 | 24493 | 1.77 |
| 4 | 271 | 2976 | 10 | 45558 | 6360 | 3.89 |
| 5 | 209 | 2173 | 10 | 33387 | 4556 | 3.58 |
| 6 | 153 | 5293 | 10 | 65038 | 9088 | 3.34 |
| 7 | 431 | 6159 | 10 | 69172 | 9976 | 2.44 |
| 8 | 290 | 20474 | 11 | 111610 | 33052 | 1.42 |
| 9 | 445 | 9984 | 10 | 106862 | 19700 | 2.50 |
| 10 | 367 | 20546 | 10 | 110824 | 32008 | 1.40 |
| 11 | 254 | 3513 | 10 | 30538 | 5768 | 2.22 |
| 12 | 514 | 3066 | 10 | 43821 | 4995 | 3.49 |

A proportional representation of the acoustic intensity within each cell for all 12 schools is shown in Figure 4.20. The diameter of the circles is proportional to the acoustic intensity of the cells. As a minimum threshold of 10 was used in the shoal detection criteria, no zero values are present. Each shoal data set includes a large proportion of small values and a smaller proportion of large values. In most cases there seems to be a clustering of larger values in high intensity areas within the schools. These core areas are present at different locations within each shoal and often towards the edges of the schools.

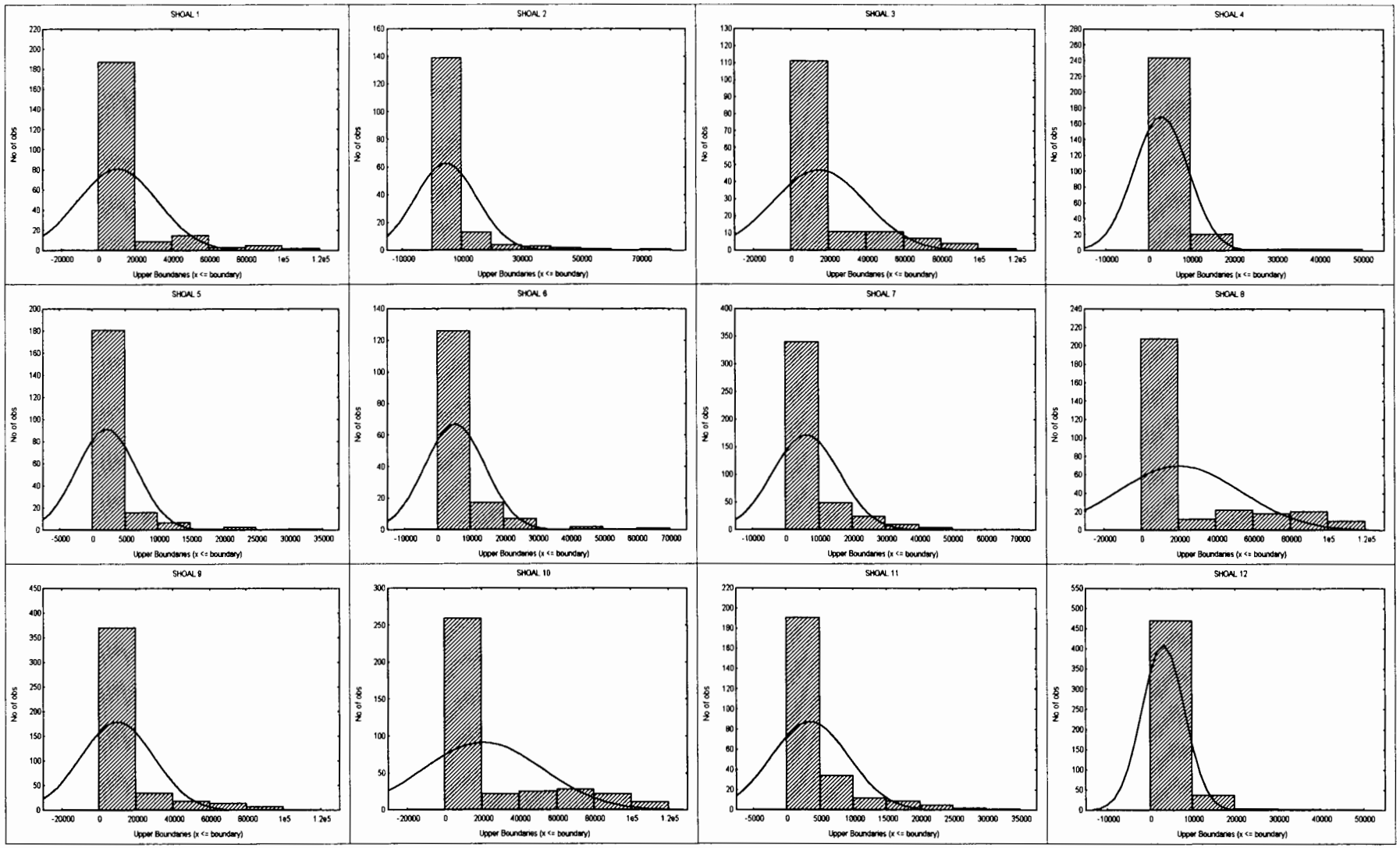


Fig 4.19. Frequency histograms with expected normal distributions for acoustic intensity within each shoal.

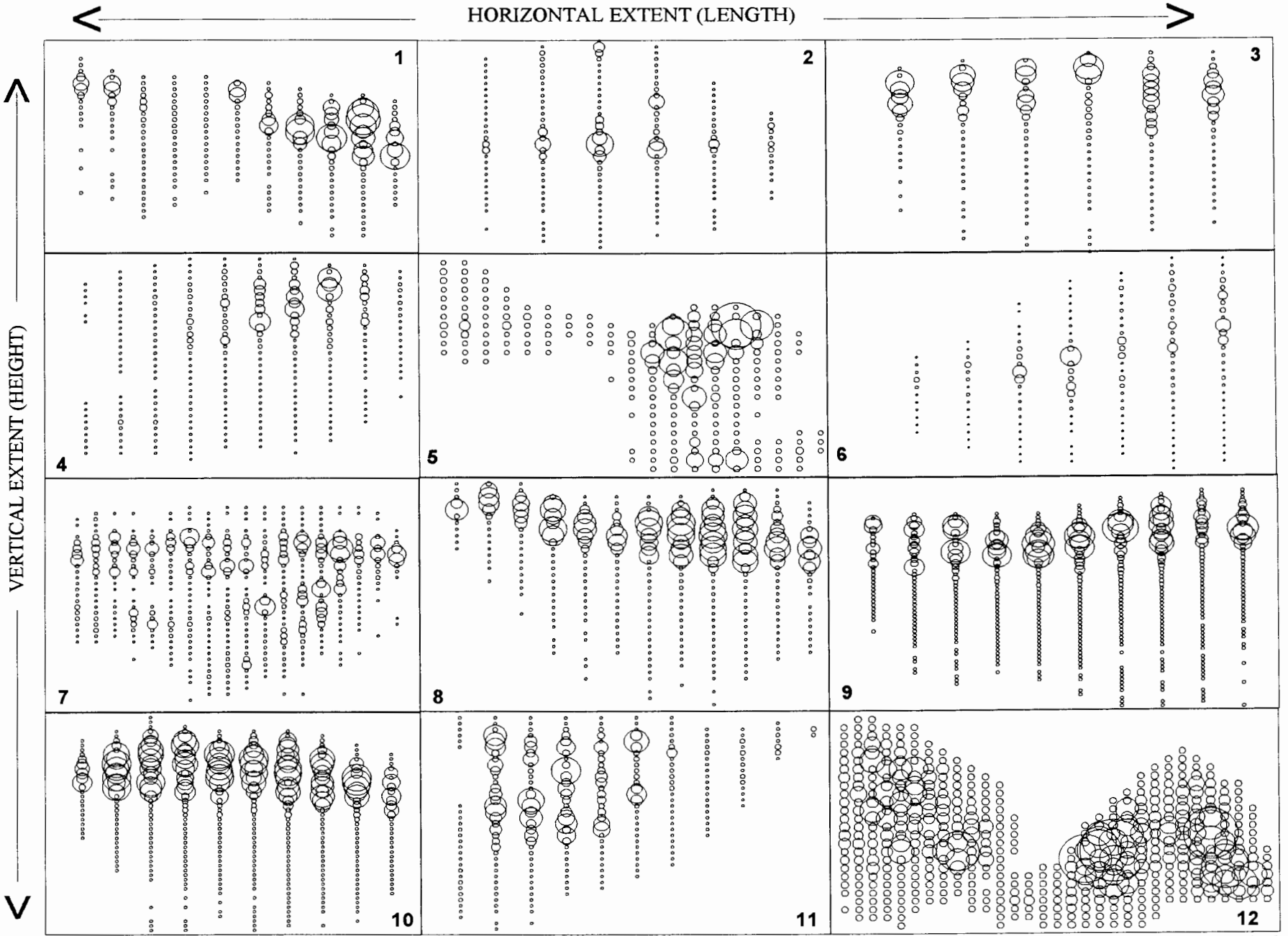


Fig 4.20. Proportional representation of acoustic intensity of each cell (1 ping in horizontal dimension and 1 m in vertical dimension) inside each shoal.

Two-dimensional variograms (horizontal dimension; 0° and vertical dimension; 90°) were computed for each school. Models fitted to each variogram are shown in Figure 4.21. A nugget effect which describes apparent discontinuity near the origin was a feature of all variograms. The nugget which is usually due to either spatial variability below the minimum lag distance and/or to experimental error was in most cases very similar in both the horizontal and vertical dimension even though the shortest distance between points was always less in the vertical dimension (1 m) compared to the horizontal dimension ( 3 or 4 m depending on the range used and the speed of the vessel). This possibly indicates that the rate of change of variance at very small scale is larger in the vertical dimension than in the horizontal dimension.

Spatial structure of varying range was observed in all variograms with a spherical model in the majority of the cases best describing the underlying structure within the schools. Details of the models such as type, nugget, range and sill fitted to the variograms for each shoal are shown in Table 4.19. Small anisotropies were noted in most cases, with the largest differences being reflected in the magnitude of the sill. In all but three of the schools the sill was larger in the vertical dimension than in the horizontal dimension. This is caused by stronger vertical gradients than horizontal gradients, probably because environmental gradients also change quicker vertically than horizontally. In most cases the range tended to be quite similar in magnitude. The mean range for all shoals was approximately 18 meters in both dimensions which gives an indication of the size of the "core" of a school. Large differences in range did occur in the variogram models of three of the schools. These differences are investigated below:

(i) In the case of shoal three a power model best described the spatial structure in the horizontal dimension indicating that the variance increases with distance but does not reach a maximum and then stabilize. When looking at the proportional representation of the data in Figure 4.20 it can be seen that the high values are spread out across the entire horizontal extent and not clumped together as in most of the other shoals.

(ii) In the case of shoal 7 where the range in the vertical dimension is less than in the horizontal dimension a layering of large values can be seen in the vertical dimension (Figure 4.20) with small values in between the two layers.

(iii) When looking at the proportional representation of the values in shoal 12 (Figure 4.20) two high density areas are observed, one close to the beginning of the shoal and the other close to the end of the shoal. In this case the range in the horizontal extent is larger than in the vertical extent as a result of the size and shape of the area of high density inside the school.

In general spatial structure was observed in both directions which supports the idea that high density core areas exist within each shoal and that fish are not randomly distributed within the shoal. This points to organization inside the shoals where individuals are performing synchronised activities as a group.

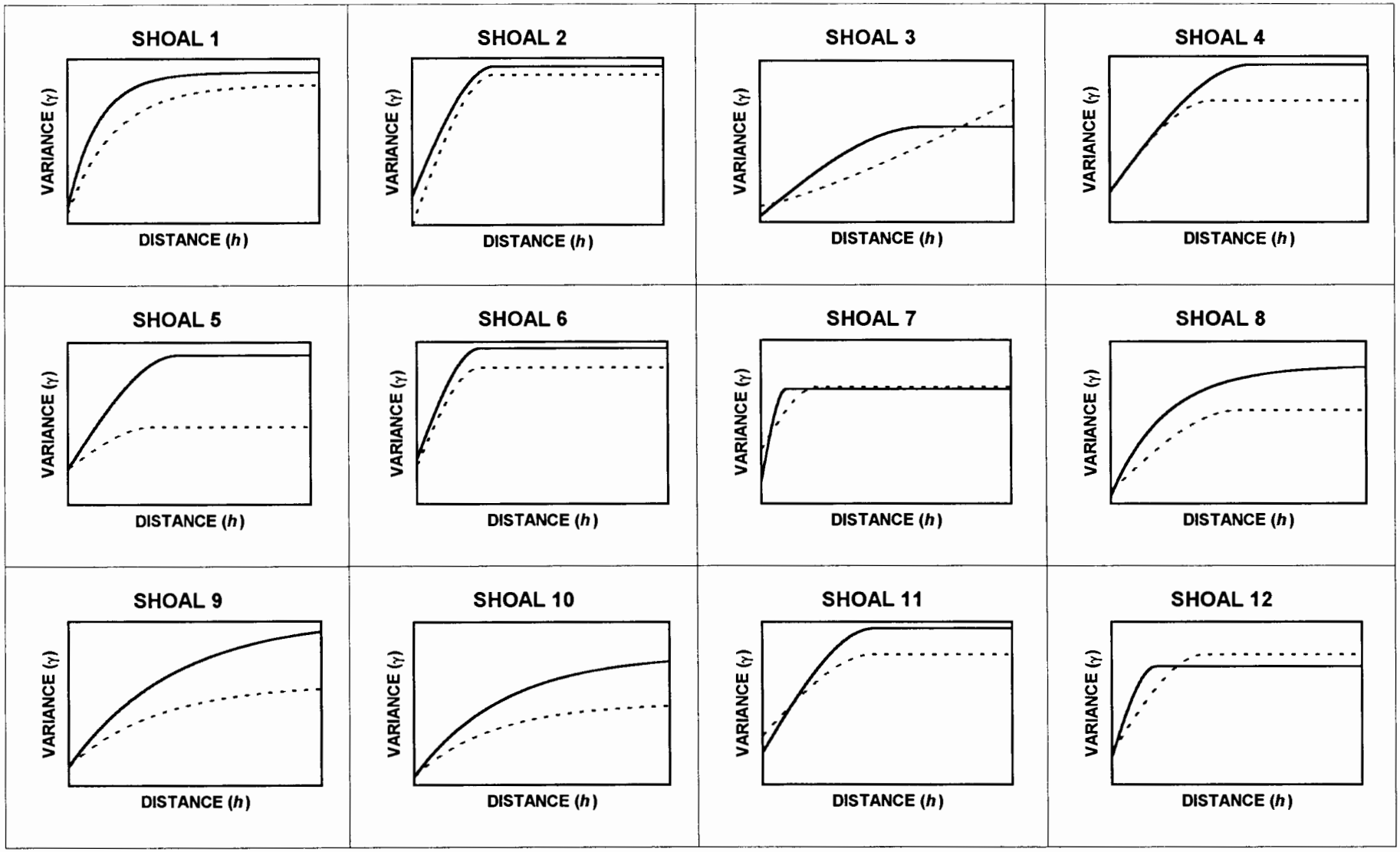


Fig 4.21. Simplified 2-dimensional variogram models for shoals 1 to 12 (solid line = vertical; dotted line = horizontal)

Table 4.19. Details of models fitted to the variograms of each shoal.

| Shoal | Model type | | Nugget effect ($s^2$) | | Sill ($s^2$) | | Range (m) | |
|---|---|---|---|---|---|---|---|---|
| | 0° | 90° | 0° | 90° | 0° | 90° | 0° | 90° |
| 1 | exp | exp | $3.5x10^7$ | $5x10^7$ | $4.7x10^8$ | $5x10^8$ | 17 | 11 |
| 2 | sph | sph | 0 | $3.5x10^7$ | $1.8x10^8$ | $1.5x10^8$ | 13 | 13 |
| 3 | power | sph | $2x10^8$ | $0.8x10^8$ | $1.3x10^7$ | $1.1x10^9$ | exp 1.25 | 26 |
| 4 | sph | sph | $1.1x10^7$ | $1.1x10^7$ | $3.3x10^7$ | $4.6x10^7$ | 16 | 22 |
| 5 | sph | sph | $1.1x10^7$ | $1.1x10^7$ | $1.3x10^7$ | $3.5x10^7$ | 14 | 18 |
| 6 | sph | sph | $3x10^7$ | $3.5x10^7$ | $7.5x10^7$ | $8.5x10^7$ | 10 | 10 |
| 7 | sph | sph | $5x10^7$ | $2x10^7$ | $5.7x10^7$ | $8.5x10^7$ | 9 | 4 |
| 8 | sph | exp | $1.5x10^8$ | $1x10^8$ | $1x10^9$ | $1.6x10^9$ | 20 | 20 |
| 9 | exp | exe | $7x10^7$ | $7x10^7$ | $3x10^8$ | $5.4x10^8$ | 32 | 38 |
| 10 | exp | exp | $1x10^8$ | $1x10^8$ | $9x10^8$ | $1.5x10^9$ | 28 | 32 |
| 11 | sph | sph | $1.5x10^7$ | $1x10^7$ | $2.5x10^7$ | $3.8x10^7$ | 18 | 18 |
| 12 | sph | sph | $8x10^6$ | $7x10^6$ | $2.4x10^7$ | $2.2x10^7$ | 15 | 7 |

Model equations used (Cressie, 1991):

(i) Spherical model

$$\gamma(h:\theta) = 0 \text{ or } C_o \{ \text{when } h = 0,$$
$$\gamma(h:\theta) = C_o + C_s\{(1.5)(|h| / \alpha_s) - (0.5)(|h| / \alpha_s)^3\} \text{ when } 0 < |h| \leq \alpha_s,$$
$$\gamma(h:\theta) = C_o + C_s \text{ when } |h| \geq \alpha_s,$$

where $\gamma(h:\theta)$ is the semi-variogram for distance h and direction $\theta$, $C_o$ is the nugget effect, $C_s$ is the sill due to the spherical structure and $\alpha_s$ is the range of the spherical structure.

(ii) Exponential model

$$\gamma(h:\theta) = 0 \text{ or } C_o \{ \text{when } h = 0,$$
$$\gamma(h:\theta) = C_o + C_e\{1 - 10^{(-|h|/\alpha e)}\} \text{ when } h \neq 0$$

where $C_e$ is the sill due to the exponential structure and $\alpha_e$ is the range parameter of the exponential structure.

(iii) Power model

$$\gamma(h:\theta) = 0 \text{ or } C_o \text{ when } h = 0,$$
$$\gamma(h:\theta) = C_o + Ch^a \text{ when } h > 0$$

where a is the exponent and $1 < a < 2$ (tangent more and more horizontal when a approaches 2.

# CHAPTER 5

# TEMPORAL DYNAMICS OF SARDINE

## 5.1 VERTICAL PATTERNS OF DISPERSION

Extensive vertical migration was noted during all five surveys. A typical reconstructed echogram, illustrating the difference in vertical distribution as observed by day and by night on a repeated transect, is shown in Figure 5.1. During the day shoals are observed throughout the water column and in many cases close to or on the bottom. Just before sunset, these shoals then tend to disperse close to the surface in a sound scattering layer. Very few shoals are present at night. The density values are based on integration of the whole mile and not on individual shoals/layers.

To quantify the extent of vertical migration, the depth of the maximum backscattering strength for each 1 nm interval for all surveys was grouped together for each hour class (Figure 5.2 a). Each observation is represented by a black dot. It is very clear from this plot that during the night, fish tend to be found in the upper 30 metres of the water column with very few observations at depths in excess of 30 m. During the day the fish tend to be distributed throughout the water column and in a few cases were detected at depths in excess of 100 m. A large proportion of the daylight observations were, however, also made in the upper 40 m of the water column and it is clear that during the day there is far greater variation in the depth at which sardine were detected.

This fact is further illustrated in Figure 5.2 (b) in which are plotted the mean depth and standard deviation of mean depth for each hour. During the night, the mean depths are all shallower than during the daylight hours and during the day, the standard deviations are much greater than during the night hours. When all observations are grouped together in a day class and a night class the difference between the variances are significant. The results of an F-test done to compare day and night variances is shown in Table 5.1. A Tukey test to test for differences between the means of each hour class also revealed that significant differences existed between the day hour classes and the night hour classes, but no significant differences between individual day hour classes and no significant differences between night hour classes, with the exception of hour class 5 which was significantly different from the rest of the day classes. This could possibly indicate that the split between night and day should have been an hour later in the morning, or that the fish are not reacting very fast to a change in light level in this transition from darkness to light.

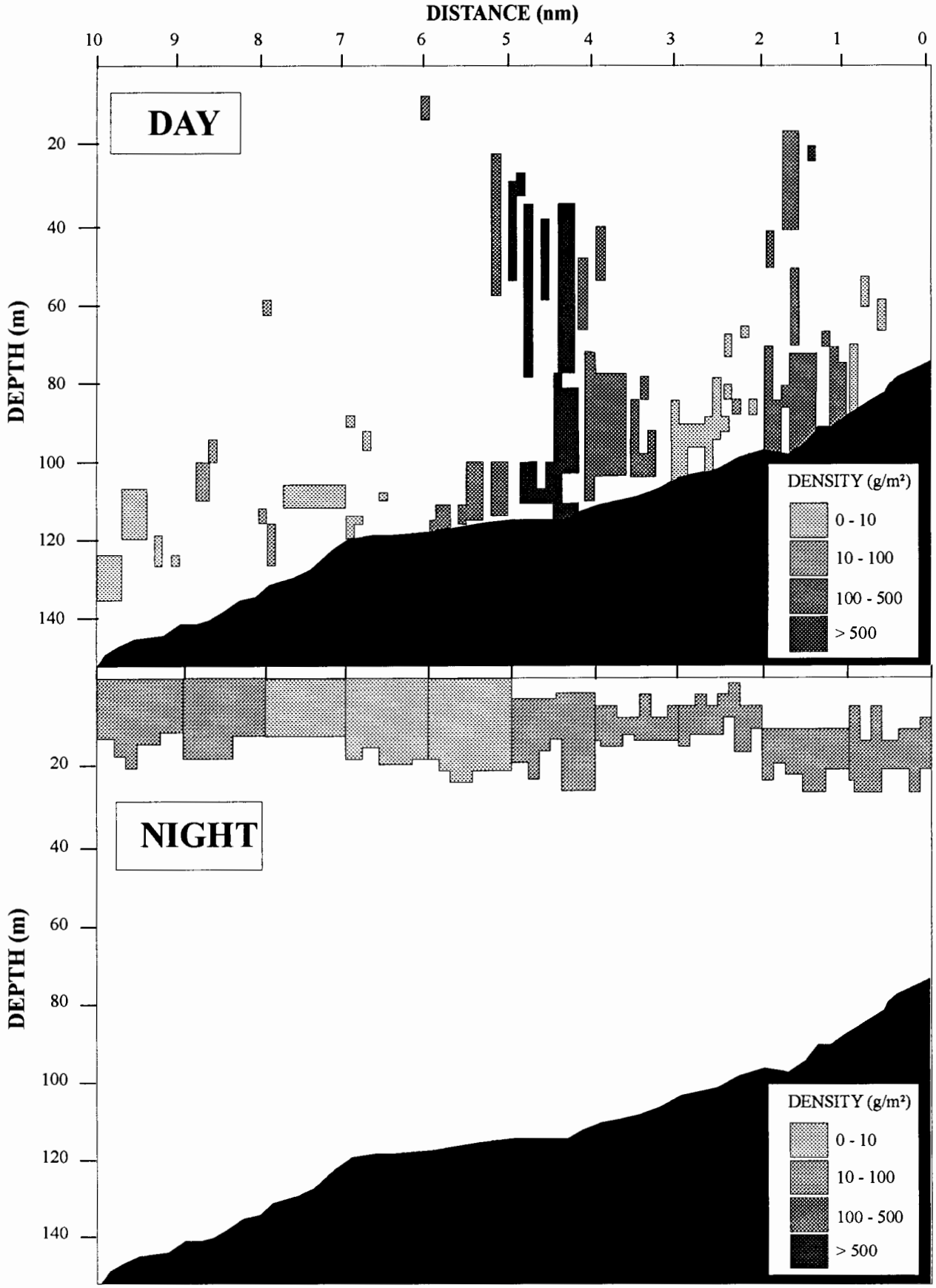


Fig 5.1. Vertical distribution of sardine as observed on a repeated transect by day and by night during the RAFOS II meso-scale survey.

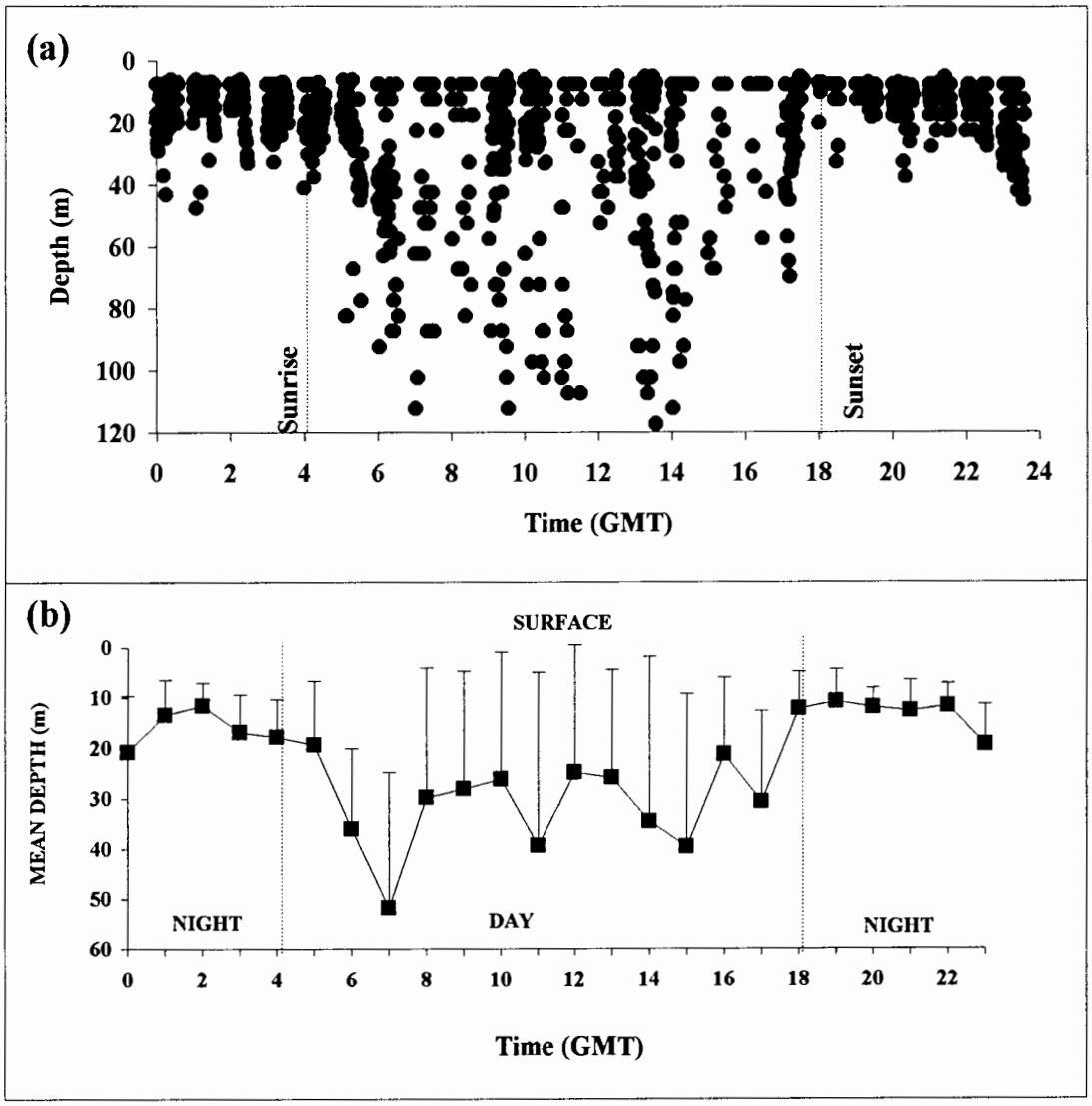


Fig 5.2. (a) Shows the raw data where the depth of the maximum backscattered energy is plotted against time for each 1 nm segment of transect; (b) reflects the mean and the standard deviation of depth for each hour class. Both figures use all data from all of the meso-scale surveys.

Table 5.1. Results of the F-test to compare day and night variances of mean fish depth.

| | Mean Depth (m) | Variance | N | df | F | *Fcrit* |
|---|---|---|---|---|---|---|
| Day | 33 | 591.29 | 627 | 626 | 10.03 | 1.14 |
| Night | 14 | 58.94 | 625 | 624 | | |
| $P(F \leq 10.03) < < 0.0001$ | | | | | | |

A significant difference in mean depth between day and night was also found for each individual survey. The mean depth for each survey as well as the coefficient of variance and probability of accepting the null hypothesis that mean depth is equal during day and night is shown in Table 5.2.

Table 5.2. Mean depth by day and night and coefficient of variance for each survey.

| SURVEY | DAY | | NIGHT | | P ($\alpha$ 0.05) |
|---|---|---|---|---|---|
| | Mean Depth (m) | CV | Mean Depth (m) | CV | |
| RAFOS II | 56 | 0.07 | 18 | 0.04 | $4.7 \times 10^{-17}$ |
| INTERCALIBRATION | 37 | 0.12 | 12 | 0.11 | $1.5 \times 10^{-7}$ |
| RAFOS III (1 st grid) | 26 | 0.11 | 9 | 0.04 | $2.8 \times 10^{-6}$ |
| RAFOS III (2 nd grid) | 27 | 0.13 | 9 | 0.06 | $8.1 \times 10^{-6}$ |
| SHOALING BEHAVIOUR | 26 | 0.06 | 20 | 0.06 | $4.7 \times 10^{-17}$ |
| All SURVEYS | 33 | 0.05 | 14 | 0.04 | $3.2 \times 10^{-26}$ |

In all cases the mean depth at night was less than that recorded during daytime. During the night the mean depth was consistently less than 20 m whilst during the day the mean depth was always deeper than 25 m. The CV's also tended to be slightly lower at night than during the day, indicating less variability in depth during the night.

## 5.2 DIURNAL VARIATION IN SARDINE DENSITY

The mean density calculated for day and night coverages of each survey from the raw density data is presented in Figure 5.3 (a). Error bars indicate the standard errors of the means. In four of the five surveys, the mean recorded density is higher during the day with the largest difference being that of the intercalibration survey where the mean density during the day is nearly nine times higher than that recorded during the night. The differences between the day and night values are highly significant using any of the non-parametric tests, except for the Rafos III (2 nd grid) survey, (Wilcoxon, Kolmogorov-Smirnov and Mann Whitney tests give $p < 0.05$). The combined mean density of all surveys recorded during the night is at least 250 % lower than that recorded during the day and the difference is again highly significant ($p < 0.005$).

The multifactorial analysis of variance on the acoustic densities was applied to the log-transformed data to normalise their distributions. The ANOVA indicated that the survey had a strong influence as did the hour intervals. The effect of the day/night period was also significant although not as important. The interaction between survey and day/night period was highly significant (Table 5.3). The influence of the survey is to be expected for obvious reasons such as different areas, timing and setting. The effect of day/night is probably obscured by the one survey in which the mean density at night was higher than that recorded during the day.

Table 5.3. Results of a multifactorial analysis of variance on acoustic density after logarithmic transformation.

| Source of Error | SS | df | MS | F | P-level |
|---|---|---|---|---|---|
| Survey | 89.58 | 9 | 9.95 | 4.57 | <0.0001 |
| Day/night | 6.097 | 1 | 2.2 | 2.8 | <0.05 |
| Hour period | 328.612 | 23 | 14.29 | 6.56 | < 0.0001 |
| Survey x day/night | 59.58 | 5 | 14.897 | 6.851 | < 0.0001 |

The mean relative density estimated for each hour class from all surveys shows a regular pattern with the highest densities during the day and lower densities at night (Figure 5.3 b) in spite of the large standard errors observed for most hour classes. Four peaks are seen during the day: the

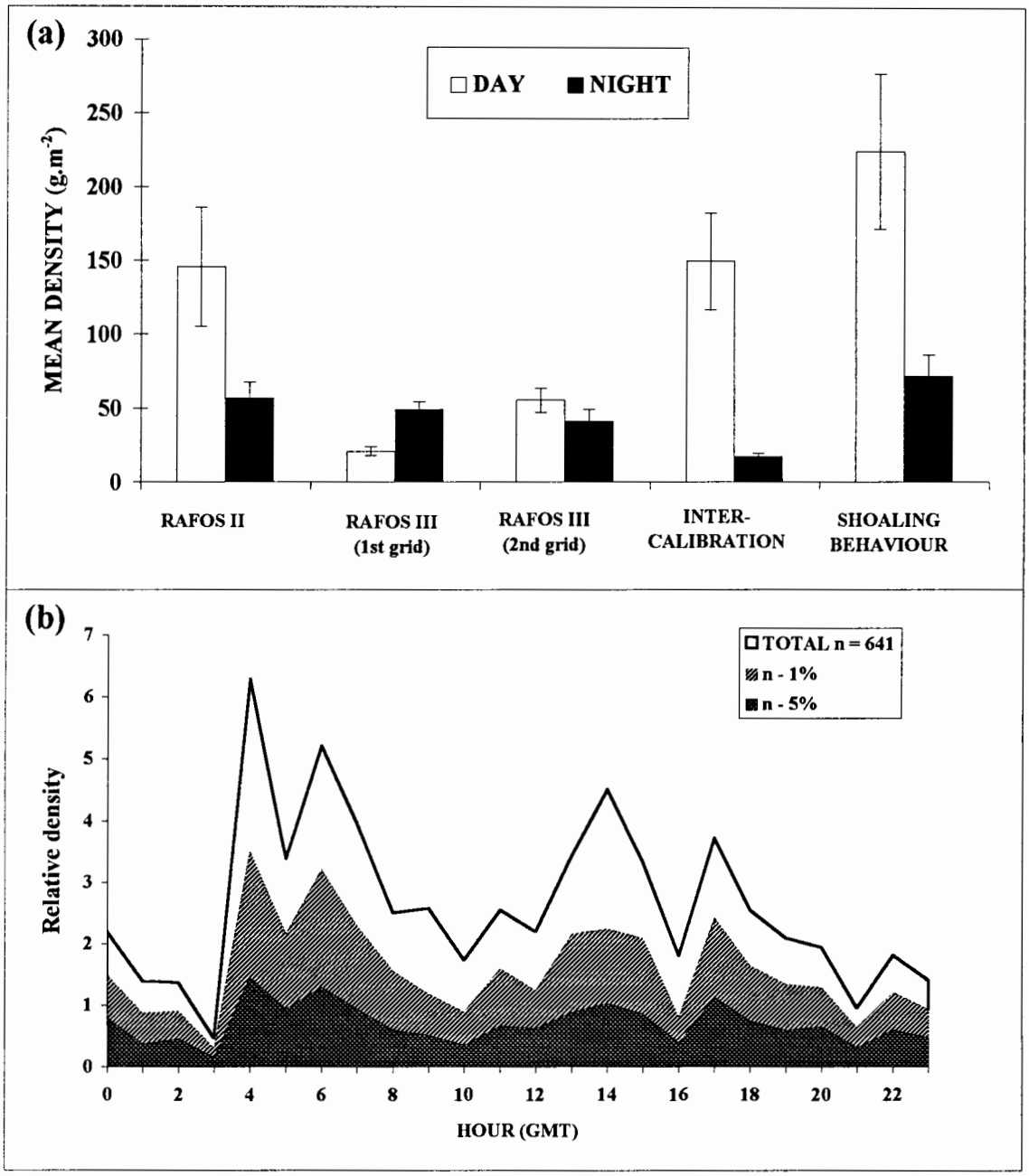


Fig 5.3. The differences in mean density estimated by day and by night for the same area is demonstrated in (a) while (b) reflects on the contributions of high values to the relative density changes with time using data from all the surveys.

highest occurs around the time of sunrise (04:00 GMT). The next peak occurs two hours after sunrise and the third in the late afternoon. The fourth peak occures just before sunset (17:00 GMT). The first and fourth peaks are of short duration and last only for one hour. The second and third peaks lasts for 2 and three hours respectively. Around mid-day the mean densities are much lower and almost resemble those recorded at night. These effects are maintained even when removing the highest values (outliers) from the data set. The largest effect is seen in the amplitude of the peaks whereas at night less difference is observed when the highest 5 % of values are removed. The difference between day and night still remains highly significant ($p < 0.005$).

The frequency distributions of the log transformed data for both day and night are shown in Figure 5.4 (a). Because of the varying spatial patterns found between day and night distributions of sardine it is expected that the frequency distributions of day and night density values will be very different. After logarithmic transformation, the frequency distribution of the night densities is close to a normal distribution. The day time distribution is, however, not normal (Kolmogorov-Smirnov and Chi-square goodness of fit procedures give $p < 0.01$). The predominance of very low and very high values during the day is attributed to the higher spatial variability during the day due to fish aggregating in schools. The skewness of both the day and the night frequency distributions (raw density values), is also evident in Figure 5.4 (b) in which a small proportion of the densities contribute significantly to the mean. This is much more pronounced during the day, when the removal of only 5 % of the highest values decreases the mean density estimate by 50 %. The decrease in mean density is, however, quite constant after the initial decline between day and night, and the difference never reaches that observed for the total averages (250%). Although not shown, the removal of the lowest densities indicates that there is no difference in rate of increase in mean density between day and night up to the removal of 20 % of the lowest densities. Even after the removal of 50 % of the lowest densities, the increase in density during the day is only 12 % higher than that at night.

The autocorrelation function (AFC) performed on individual surveys showed very few significant positive correlation coefficients for lags of more than 2 hours. It was not possible either to detect any diurnal cycle. This is probably due to the method used to deal with missing values and the large number of missing values for each individual survey. The AFC computed on the artificial time series indicated a clear diurnal cycle (Figure 5.5) of approximately 12 hours with some significant correlations even after 48 lags.

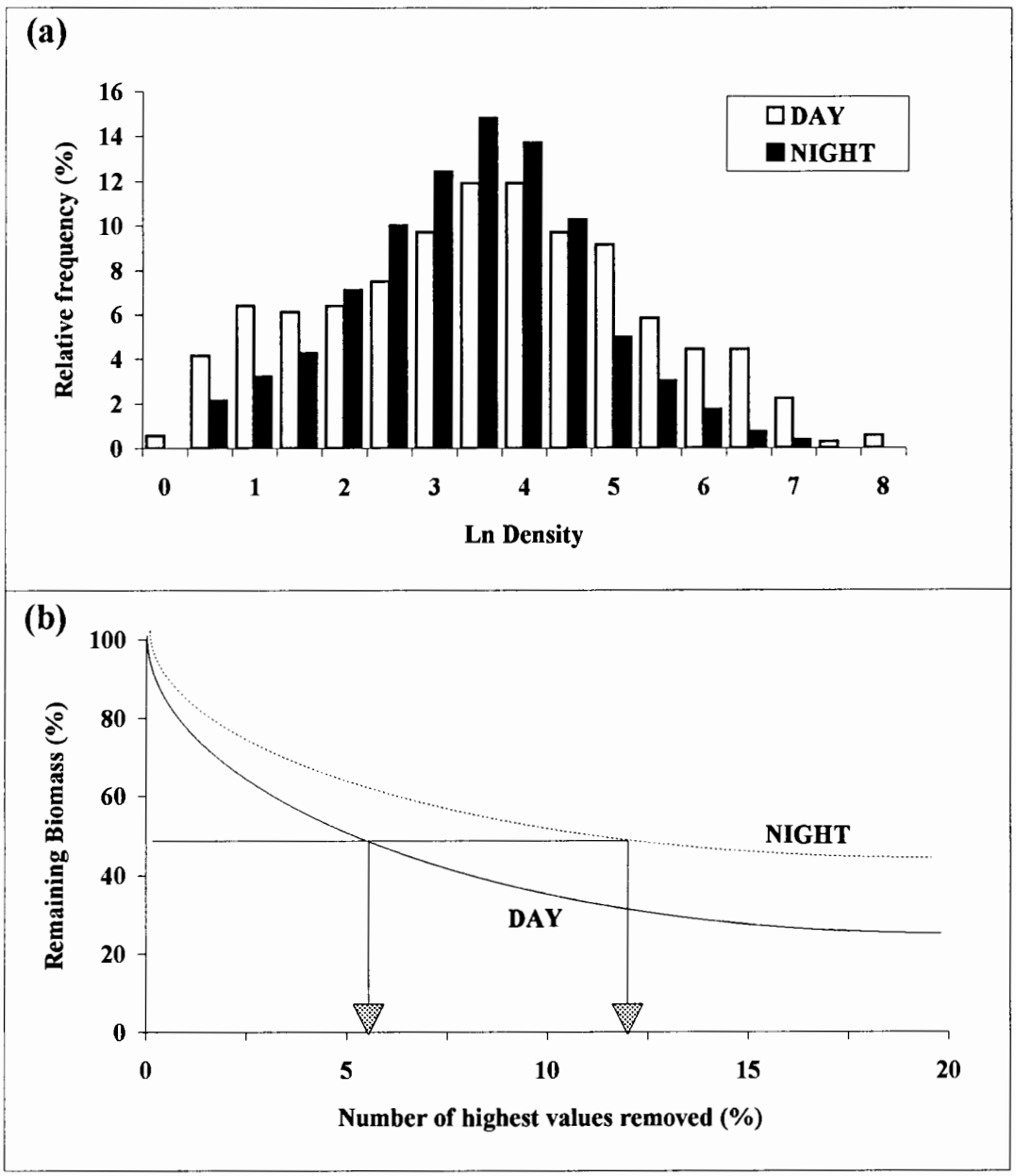


Fig 5.4. (a) Shows the frequency of the log transformed data for both day and night of all the surveys combined and (b) indicates the effects on the remaining biomass by day and night when the highest values are removed.

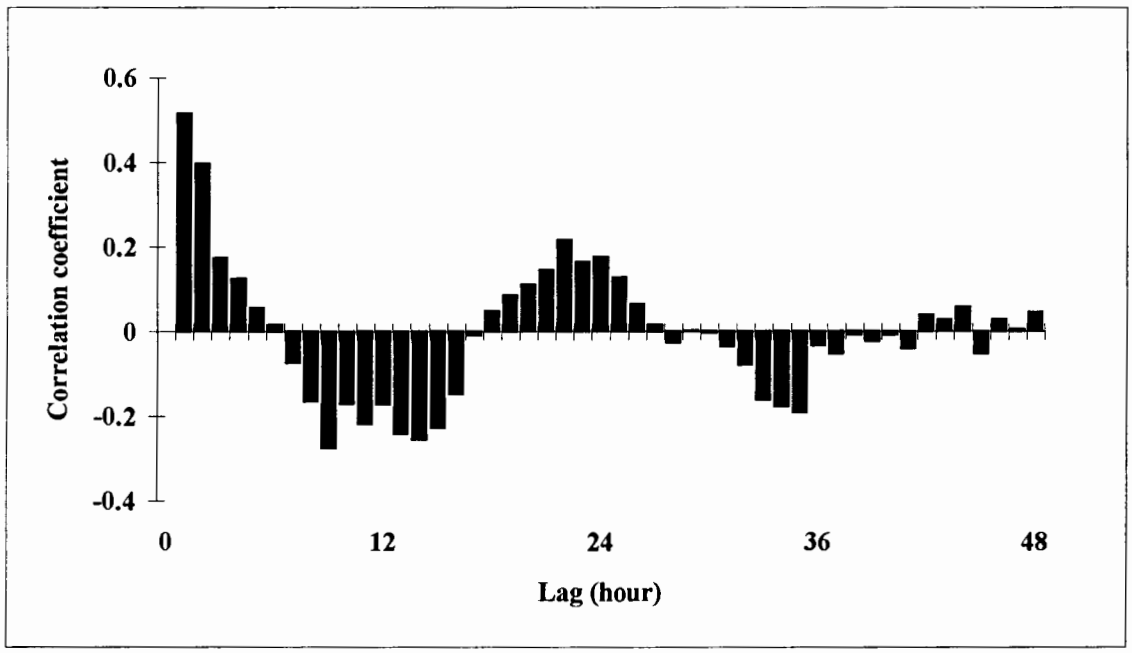


Fig 5.5. Autocorrelation function of relative acoustic density using all survey data.

# CHAPTER 5. DISCUSSION

Marine ecosystems and particularly upwelling regions are generally characterised by large spatial and temporal environmental variability. It is therefore expected that organisms inhabiting such variable environments would over time have developed various mechanisms or strategies for dealing with an ever-changing environment. That pelagic fish distributions are influenced by their environment has often been demonstrated empirically (Swartzman *et al.*, 1995) A large amount of variation is therefore expected in any study regarding the distribution and behaviour of pelagic fish.

## SPATIAL STRUCTURE OF SARDINE AT MESO-SCALE LEVEL

Although spatial structures are fundamental characteristics of marine organisms it has until recently been very difficult to explain or characterise them, mainly due to the difficulties that appear when trying to observe the aquatic ecosystem *in situ*.

The application of acoustic methods (echo sounders and sonar) has overcome these limitations and allowed the direct observation of the three-dimensional structures of the populations as well as their reactions to hydrological characteristics. Hence enabling a better understanding of the relationships between the population distributions and the environment. As a matter of fact these methods are the only ones that allow a remote, continuous and synoptic observation of the individuals in their own space (GEOSPACE, 1993).

### Distribution in relation to temperature

Previous hydroacoustic surveys off southern Africa have shown that sardine, round herring and anchovy are mostly absent where the sea surface temperature is above 20° C, suggesting that the offshore and eastern boundaries of these populations will be strongly influenced, if not controlled, by warm Agulhas Current water over the shelf (Armstrong et al 1991). Results from the SARP surveys and analysis of all November spawner biomass surveys, confirm these findings. Only in a very few instances were sardine found further offshore than the 20 °C isotherm and that was usually in cases where a strong temperature front was

present. Although the distribution of sardine in relation to the vertical structure was not investigated in the course of this study, it was on occasion noted that sardine were found beneath a strong thermocline at great depth. This has also previously been demonstrated by Armstrong *et al.*, (1991). They showed that, during winter, sardine on the South African South Coast can migrate below the 20 °C isotherm into cooler water, and consequently may be found distributed father east than the 20°C isotherm would suggest. No distinct hydrological features were present during any of the meso-scale surveys, mainly due to the small scale of these surveys. It is important to see the results of this study in that light, as changes in the environmental conditions show that the distribution of sardine is strongly influenced by them.

**Horizontal patterns of dispersion**

Variograms suggested the existence of some spatial structure at the meso-scale level during four of the five day surveys and three of the five night surveys. Sardine distributions were generally characterised by relatively short autocorrelation ranges ($<10$ nm) which suggest very little spatial structure. Barange and Hampton (in press) found similar autocorrelation ranges of night time data for sardine in a study which covered the entire distribution of sardine on a much larger scale. These short autocorrelation ranges are probably a consequence of the patchiness of sardine distributions at a range smaller than the ranges studied.

However, these surveys were not designed specifically for this type of study and in some instances did not adequately cover the distribution of sardine in a particular area. It is therefore difficult to speculate as to why there is a lack of structure in some of the surveys. Lack of structure could possibly be attributed to fish migration in and out of the survey area between successive coverages or to fish migrating to the surface at night. This is supported by the mean depth of fish being shallower at night than during the day during two of the surveys when no structure at night was apparent. Auto-correlation ranges for day time surveys where structure was present, varied from 3 to 7 nm. Large nugget effects were evident in all cases. Auto-correlation ranges at night were slightly larger and ranged from 7 to 10 nm for surveys where structure was observed. Nugget effects were also noted

although mostly smaller than during the day surveys. This difference is likely to be due to the greater patchiness in sardine distribution during the day than during the night. The generally small structure observed in all variograms suggests that there is a lower chance of encountering a shoal during the day than during the night and even when a shoal is encountered, it is not possible to predict where the next one may be found (Petitgas, 1993).

Barange and Hampton (in press) compared the spatial structure of sardine and anchovy and found that the variograms computed from anchovy distributions were fairly well behaved with smaller nugget effects and larger ranges. They attributed this difference to two main factors: Firstly that sardine are more patchy than anchovy on their spawning grounds and secondly that sardine do not have a single strategy of occupying space. This second factor they linked to the protracted spawning period of sardine which, unlike anchovy, lasts throughout the year. Another possible explanation is the much broader age structure of sardine than that of anchovy where different size classes of sardine would for example display varying feeding strategies.

A significant finding was that distributions of density were extremely positively skewed, particularly during the day when a very small proportion of the values contributed greatly to the mean and the variance. The structure of the variograms would therefore be strongly influenced by these dense areas. Some authors have preferred to lessen the effects of outliers by truncation of the raw data (Maravelias and Haralabous, 1995; Simmard *et al.*, 1993). Truncation is probably not the best way to get rid of the effects of outliers because the small number of high values are genuine and not simply statistical outliers which can be ignored.

In cases where structure was observed using 2-D variograms, the autocorrelation range in the along track direction tended to be larger than in the across track direction. The autocorrelation range in the along track direction also tended to be similar to the omnidirectional variogram. This indicates that small scale changes in variogram structure probably reflect along track trends more than across track trends which is to be expected due to the different sampling frequency in the two directions. Some of the directional variograms were highly erratic due to the small number of pairs of observations. Consequently not all the directional variograms can be regarded as a representative description of the structure.

Further investigation into the spatial heterogeneity of the day and night distributions as measured by the skewness of the density histograms (Petitgas, 1994) indicated more selectivity at night than during the day. As selectivity represents a measure of the concavity of cumulative frequency plots of fish density and therefore the dispersion relative to the global mean, conclusions can be drawn about diel changes in aggregation structure. It is clear that for the night time values the curve is more convexed than for the day surveys, indicating that fish were more dispersed during the night. This is supported by transition period studies (Misund *et al.* in prep.) using a sector scanning sonar, which showed that schools were dispersed in a layer around half an hour after sunset and resumed schooling around sunrise. Nevertheless, some big shoals still existed inside the layer late at night. The fact that schooling persists during the night although not at the same level as during the day, is also clear from the skewed distribution of fish density at night.

Furthermore, it may be assumed that because fish were more dispersed during the night, the probability of encountering sardine aggregations should be larger than during the day. This is not reflected in the mean densities as measured by day and night and it is therefore suggested that at night a part of the population was not available for echo integration by being too close to the surface. Similar selectivity curves plotted for sardine by Barange and Hampton (in press) showed little difference between the convexity of day and night curves. They therefore concluded that little diel dispersal of sardine aggregations occurred. In their study of a much larger scale, they also found that mean densities recorded at night were higher than those recorded during the day. It is suggested that these contrasting findings are due to differences in the scales of these respective studies as well as sampling variance which would have been high given the patchiness of sardine aggregations.

For both the means and the variances to be accurately sampled it would be necessary to increase sampling effort with a more homogenous spread of effort over the entire distribution of sardine. This would imply that inter-transect spacing would have to be reduced and should be related to the variogram range of high density aggregations. From this study it is clear that the autocorrelation range is small ($<10$ nm). The similar findings by Barange and Hampton (in press) suggest that reducing the inter-transect spacing to at least 10 nm would increase the probability of sampling high density areas. This would in turn lead to improved sampling of

the mean and the variance. If time or financial constraints rendered this unfeasible a different sampling strategy would have to be employed whereby sampling effort is increased in high density areas. It would, however, still be essential to ensure that an unbiased measure of the mean and the variance is maintained.

### Spatial structure between shoals

Using variograms, the number of schools per $nm^2$ was found to be spatially structured. In addition, a Chi-square goodness-of-fit test for a Poisson (i.e. random) distribution also revealed that shoals were not randomly distributed within the survey area for all four surveys. Similar structure between fish schools was found by Marchal and Petitgas, (1993). They also suggest that the information in this variable may relate biologically to occupation of the habitat which indicates that schools are located in space in an aggregated and structured manner. Variograms computed using the number of schools per $nm^2$ tended to show more structure and were better behaved than variograms computed using density ($g.m^{-2}$). This is probably due to the difference in skewness of the histograms, with the histograms of fish density generally being much more skewed than those of number of schools. It could therefore be feasible in the future to make more use of the number of schools per $nm^{-2}$ when analysing the spatial structure of a population. This also makes sense in that most of the biomass is usually contained within schools, particularly during the day. At night, the problem of correctly delineating schools within a dense scattering layer could possibly be overcome by identifying dense aggregations or patches and using these in the same manner as schools are used during the day.

## SPATIAL STRUCTURE OF SARDINE SHOALS

### Shoal characteristics and descriptors

Results of this study suggest a general trend in which horizontal dimensions are significantly larger than the vertical extent. Pitcher and Partridge (1979) noted that schools of herring in a 10 m diameter tank were discoid, having similar length to width ratios, but were of shallow

depth; the ratio of length and width to depth being 3.0: 3.1: 1.0. Cullen *et al.* (1965) gave similar values of 2.1: 1.7: 1.0 for *Harengula* schools in the wild. During the present study shoals were presumed to have identical width and length and therefore only the ratio of length to depth is of relevance for comparisons to earlier studies. Results of this study indicate different average length to depth ratios for individual surveys (RAFOS II, 3:1; Intercalibration , 2:1; RAFOS III, 4:1). The average ratio for all surveys was 3.0:1.0(S.E ±0.12).. This is identical to the ratio of length:depth of 3:1 concluded by Pitcher and Partridge (1979) from all available literature. This also gives an indication of the shape of sardine schools, with a length:depth ratio (elongation) of greater than 1 indicating an elliptical shape and a value of 1 indicating a circular shape. The fractal dimension which is determined from the perimeter length to area relationship and is a measure of the shape complexity of schools revealed that sardine schools had a regular shape.

Many factors can, however, affect school shape. Breder (1959) and Radakov (1973), both suggested than faster swimming schools would be more elongated than slower swimming schools. Partridge *et al.*(1980) found that this was not the case for saithe schools. Saithe schools in their study tended to become more spherical with an increase in swimming speed. During this study swimming speed of schools was not mentioned and therefore it is not possible to determine whether swimming speed was a factor contributing to the variability of school shape. A factor which may possibly have played a role in the variability of elongation between surveys is the difference in size of the fish. During the RAFOS III surveys the mean length of fish was larger than mean length of fish during the intercalibration and RAFOS II surveys. If the swimming speed of sardine is proportional to body length as has been suggested by Hunter (1972) for northern anchovy and by Blaxter and Staines (1971, cited in Blaxter and Hunter 1982) for herring, this would indicate more elongation of schools during the RAFOS III surveys. Breder (1965) also suggested that the nearest neighbour distance (NND) of fish in a school increased linearly with body length. If this is the case for sardine, then the NND during the RAFOS III surveys would have been greatest and would explain the larger elongation of schools. Several authors have also found that the (NND) decreases as a function of the number of fish in a school (Breder (1954), Keenleyside (1955), Partridge (1980) and Partridge *et al.* 1980)). Once again if this were the case in sardine schools, it would imply that NND was greatest during the RAFOS III surveys when the

packing density within schools was less than during the other surveys.

Investigations into the relationships between school geometry and school biomass revealed significant relationships between the back-scattered echo energy and the area or volume of the schools during all surveys. An underlying principle for such relationships to be observed, is that individuals performing synchronized and polarized swimming, form compact high-density units (Partridge *et al.* 1980), which create proportionality between the biomass and geometric dimensions. School dimension to school biomass relationships found during this study are in accordance with the findings of Pitcher and Partridge (1979), who concluded that school volume is proportional to the number of individuals in a school. The existence of such relationships also supports the "behavioural rules" that apply to schooling individuals as suggested by (Partridge, 1982 and Partridge *et al.*, 1980). They state that individuals in a school maintain a minimum approach distance to each other and prefer a certain distance and direction to their neighbours. It is therefore obvious that proportionality must exist between the total volume occupied and the number of fish in a school.

The variations seen in the correlations between school geometry and school biomass are probably to some extent as a result of the positions of transects through schools that are not circular. In addition large variations in packing density exist between schools as a consequence of the internal dynamics of a moving mass of individuals (Misund, 1990). The fact that the area to biomass and volume to biomass relationships are equally strong, indicates that both the horizontal and vertical dimensions are important determinants of school size. In a similar analysis of herring, sprat and saithe schools, Misund et al. (1992) found that the horizontal dimension is the most important determinant of school size. In another study focusing on sardine schools, Misund et al., (in prep) found stronger relationships between school volume and school biomass than school area and school biomass, indicating the importance of the vertical dimension on the size of schools. The existence of relationships between school geometry and school biomass is of significance if comparative echo-sounder and sonar studies are to be performed in the future.

The "shadow effect" has long been considered an important acoustic limitation. Several authors have studied this problem Olsen, (1986); Foote, (1982,1990) and have suggested that

the shadow effect occurs only in schools in which the packing density is greater than 3000 $g.m^{-3}$. Misund (1990) has shown that these cases are very rare and therefore the problem of shadowing is almost negligible. In this study, shoals with a mean biomass per unit volume exceeding 1000 $g.m^{-3}$ accounted for less than 1 % of the total. In a few instances, the density within a nucleus of a large school reached as much as 6500 $g.m^{-3}$. Results of this study therefore indicate that overall the mean packing density would rarely reach the density at which it would result in significant shadowing. Mean packing densities measured during this study are very similar to those measured for herring (Misund *et.al.* 1995). The mean packing density of all schools analyzed in this study was four individuals.$m^{-3}$ which is almost identical to the value of 4.25 herring.$m^{3}$ given by Misund. The mean packing density of sardine schools is, however, much lower than that measured for sardine by Misund *et.al.* (in prep) which indicated a mean density of 29.5 fish.$m^{-3}$. School dimensions during that study, were measured by means of sector scanning sonar and threshold values for shoal recognition were higher.

The packing density observed during this study is suspected to be slightly low due to the low threshold set in the shoal recognition criteria. The threshold used corresponds to a packing density of 0.1 individuals per $m^3$. This value is very low when compared to similar studies elsewhere and would tend to reduce the mean packing density of schools. Nevertheless, the most recent target strength data available for sardine (Barange *et al.*, 1996) indicates that the mean biomass per unit volume would decrease when compared to the target strength equation used in this study. It is therefore assumed that these two effects would counter each other and that the reported packing density in this study is not too far from correct for sardine.

**Principal Component Analysis**

Use of shoal and patch recognition software during this study has taken full advantage of the two-dimensional image provided by acoustics at a scale (1 metre) which is much closer to that encountered in nature as apposed to the artificial scale (1 nautical mile) traditionally imposed by the echo-integrator.

The comparison of shoal characteristics has allowed for the determination of those acoustic variables which best describe the nature of sardine schools. In this study, it was apparent from multivariate analysis that shoal identification was dominated by two descriptors, the morphology and energetics, the former being the most dominant. Other studies concerning the discrimination of patches have shown similar results with geometry and intensity being the principle discriminant factors (Souid, 1986; Rose and Leggett, 1988; Vray *et al.*, 1990; Scalabrin, 1991).

Acoustic measurements of fish distribution and abundance require knowledge of the backscatter's taxonomic or community group. Traditionally, hydroacoustic biomass surveys have depended on concurrent fishing to identify the fish species observed. This method of species identification may be problematic. Catchability may vary between species and the trawl cannot achieve the same spatial and temporal sampling comparable with that of acoustic sampling. Fishermen and experienced users can often distinguish schools of different fish species based on echogram characteristics, but this approach remains subjective. Several recent advances in fisheries science, acoustic technology, digital signal processing and digital image processing have, however, made the possibility of semi-automated fish classification a more realistic goal. Several authors have recently used the information present in the digitized backscattered signal to discriminate between different species, with varying degrees of success. (Rose and Leggett, 1988; Haralabous and Georgakarakos, 1996; Scalabrin et al., 1996).

The manner in which fish occupy space may not always be the same. The shape, size and density of schools may vary appreciably from species to species and within species, from age class to age class. Within species school characteristics might also be dependent on external factors such as hydrological features and the presence or absence of predators and prey. Massé *et al.*, (1996) found that both the vertical distribution and schooling behaviour of pelagic fish may be influenced by the species composition of schools. They also found that acoustic characteristics of schools were modified in the case of a two-species mixture. Internal and external factors may therefore interact in a complex way making the modelling of school structures and behaviour very challenging.

However, the multivariate analysis of sardine shoal characteristics in this study showed no large difference in shoal descriptors amongst all surveys. This could indicate an inherent temporal and spatial stability in sardine school structure, which would facilitate this kind of identification process. It should be noted that all surveys were done during the same season, in similar areas with no strong hydrological features and where sardine were the dominant species present. It is therefore essential that this study be expanded to cover wider geographic and hydrological ranges as well as situations where species compositions are different in order to validate the results. It is suspected that in the future a combination of shoal characteristics and measures of instantaneous echo structure within schools should prove beneficial for species identification and therefore stock assessment.

**Internal school structure**

Most studies on school structure deal with the mean distance between neighbours and their spatial distribution, but few deal with the heterogeneity of the distribution and its significance (Fréon *et al.* 1992). This spatial heterogeneity within wild schools was first mentioned by Cushing (1977). A study of the geometrical characteristics of fish schools by Breder (1976) suggested that the organisation of fish in schools is not stochastic but highly structured. Partridge *et al.*, (1980) showed that schools of three different species i.e.,herring, saithe and cod do not position themselves at random within schools and could be ranked in terms of the degree of structure present. They showed that saithe schools are better organised than cod schools and that herring schools are better organised than saithe schools.

In this study the investigation into the presence or absence of structure within sardine schools was done by making use of the high resolution capabilities of acoustic sampling coupled with the use of variograms. Results of this study confirmed previous suggestions of non-randomness within schools. Existence of a spatial structure within all shoals analyzed suggests that the internal structure is heterogeneous, sometimes including large vacuoles and nuclei of high density. Auto-correlation ranges were generally similar in both the horizontal and vertical dimensions with no large anisotropies noted. Because structure was observed within most shoals analyzed, it may possibly be concluded that sardine schools are cohesive units, within which individuals are performing synchronised and similar activities such as

feeding and spawning. It is therefore also reasonable to suggest that sardine schools consist of fish of a similar size (for feeding and speed maintenance) and reproductive state. Several laboratory and field studies have indeed shown that fish prefer the company of individuals matching in body size (Pitcher, 1993). Breder (1976) stated that the variation in the lengths of individuals in a school usually reaches no more than 30 %.

## TEMPORAL DYNAMICS OF SARDINE

### Vertical patterns of distribution

Since the advent of the echo-sounder it has been possible to follow the variations and extent of vertical migration of fish populations. Since the pioneering work done by Runnstrøm in the early 1940's (Runnstrøm, 1941, cited in Blaxter and Holliday, 1963) numerous authors have reported on the phenomenon of vertical migration particularly by clupeoids. The general pattern of vertical migration seems to be an upward movement at night followed by a spreading out of the fish. Several reasons have been suggested as to why fish migrate vertically. These include changes in vertical distribution in relation to changes in food availability, avoidance of predators, the following of a preferred light intensity and changes in the thermal and salinity structure of the water column (Blaxter and Holliday, 1963). It seems likely that the control of vertical migration is extremely complex, depending on a number of external factors, the effect of which will be modified by internal factors such as the age and physiological state of the fish.

In this study it has been found that the extent of vertical migrations of sardine is very variable. Definite extensive vertical migration of sardine from the surface at night to depths of up to 100 metres during the day were sometimes noted. The mean depth at which fish were observed was shallower than 20 m for all night surveys and greater than 20 m for all day surveys. When mean densities of successive day and night surveys were compared in conjunction with the depth distribution, it was found that during four of the five surveys the density measured during the day was higher than that measured at night. In all four of these surveys, the fish were shallower at night than during the day and possibly indicated that fish were missed above the transducer.

The use of sonar to detect when fish are too close to the surface has increased in recent years (Misund *et al.*, 1996). As it would probably be inappropriate to survey sardine only during the day due to time constraints, the use of sonar may be useful in alerting scientists during routine surveys as to the presence of surface shoals. In these instances surveys should be temporarily halted. Recent developments in sonar software and the establishment of linear relationships between geometric dimensions and biomass of fish shoals, also leads the way to comparative echo sounder and sonar estimates. It is expected that future acoustic surveys of fish abundance will increasingly be facilitated by sonar observations.

**Diurnal variation in sardine density**

A strong diurnal cycle in fish density was observed. Large variations also existed in the measurement of biomass between successive surveys, with densities being lower on average at night than during the day. Both day and night distributions of density were strongly positively skewed with a few high values contributing largely to both the mean and the variance. This emphasises the importance of making use of the spatial structure of sardine aggregations to increase the probability of sampling the tail of the histogram if reliable density estimates are to be obtained.

Fréon *et al.*, (1993) found that lower densities were recorded by day than by night in an analysis of acoustic data from tropical locations covering 18 surveys. They concluded that lateral avoidance of the survey vessel by near surface shoals is the primary reason for underestimation by day. Preliminary findings by Hampton et al., (in prep), however, suggest that sardine schools in South Africa show very little or no signs of avoidance reaction to the presence of a research vessel. Fréon *et al.*, (1993) also concluded that in their analysis of acoustic data, the bias owing to fish being too close to the surface at night could account for only about 10 % of the day/night difference. Other explanations offered by Fréon *et al.*, (1993) for underestimation of fish at night included the decrease in tilt angle of the fish which is greater during the night than during the day and the light on a vessel which produces a strong reaction, and in some cases changes the echo abundance below the vessel. They, however, speculated that the variability of the tilt angle during the night was probably limited to deep schools which were very few. This is because fish close to the surface are probably

in polarized position due to the noise of the vessel passing over them.

In this case, variability of tilt angle would not have played a major role in the underestimation of sardine at night during this study as most of the biomass was in the upper 20 m. Furthermore, the bias resulting from light on a vessel is assumed to be minimal as most of the surveys were done with minimum lighting. It is evident from the present study that differences in day and night densities are so large and cannot be ascribed to these biases alone. It is therefore suspected that unless large scale migration of sardine out of or into the survey area took place between successive day and night coverages, the bias as a result of sub-surface fish is much larger than 10 %. Further studies in the comparison of sonar and echo-sounder estimates of fish biomass could assist in highlighting vertical migration biases and well as those caused by avoidance. This would, however, depend on the availability of a high resolution multi-beam sector scanning sonar.

## CONCLUSIONS

The use of acoustic data has enabled a synoptic study of the spatial dynamics of sardine populations. Although much variation between surveys was noted throughout this study in terms of spatial structures, variables describing shoals and diurnal behaviour of sardine, the following conclusions may be drawn.

The use of variograms to describe spatial structure at the meso-scale level indicated the existence of relatively small spatial structure. Spatial structure was generally larger at night as a consequence of the dispersion of fish. In some instances though, the lack of spatial structure at night may be attributed to fish migration out of the survey area or above the transducer. Increased survey precision and accuracy may, however, be obtained by making use of this spatial structure in the design of sardine biomass surveys.

A clear 12 hour diurnal cycle in sardine density was noted with sardine density being lower at night than during the day. Linked with this is the finding that sardine undergo significant diel vertical migrations and may not always be available for acoustic sampling at night. It is suggested that future surveys incorporate the use of sonar to detect when fish are too close

to the surface in which case surveying should be temporarily halted.

It was clear from this study that sardine are mostly dispersed at night, although limited shoaling still persists. This was evidenced from the skewness of both the day and night density histograms. A decrease in inter-transect spacing would lead to a greater probability of accurately sampling a sufficient number of high density areas, leading to a more normal distribution of fish density and therefore and increase in survey precision.

The use of the digitised backscattered signal provided useful information on sardine shoal characteristics in an automated manner. In addition the Principal Component Analyses was successful in decreasing the number of variables describing sardine shoal characteristics to three factors. These factors appeared to be both spatially and temporally stable. An analysis of the internal structure of sardine shoals also indicated the existence of a spatial structure which could be inherent of sardine shoals. Similar future studies on other species, in other seasons and temperature environments may lead the way to eventual identification of pelagic species based on shoal characteristics. This would also increase the precision of sardine and all other pelagic biomass surveys.

From this study it is therefore concluded that sardine are not randomly distributed, but present organized structures at any scale, from one metre up to several kilometres. Such a deterministic occupation of space depends on physiological and behavioural reactions, as well as on spatio-temporal structurations of the environmental characteristics. The aquatic space is three-dimensional, and the vertical dimension is very important, thus the shape that the spacial organization may present is complex. This present study is a good example of the amount of variation that can occur in a study of the spatial distribution of fish populations in both the horizontal and vertical dimension as well as in the behaviour of fish populations in relation to time and the environment. Failure to take this spatial structure into account risks omission of fundamental characteristics of the biology of the species, and serious errors in the population analysis.

The following diagram (Figure 6.1) attempts to summarize the findings of this study and includes suggestions for improvements to current acoustic methods of abundance estimation of sardine.

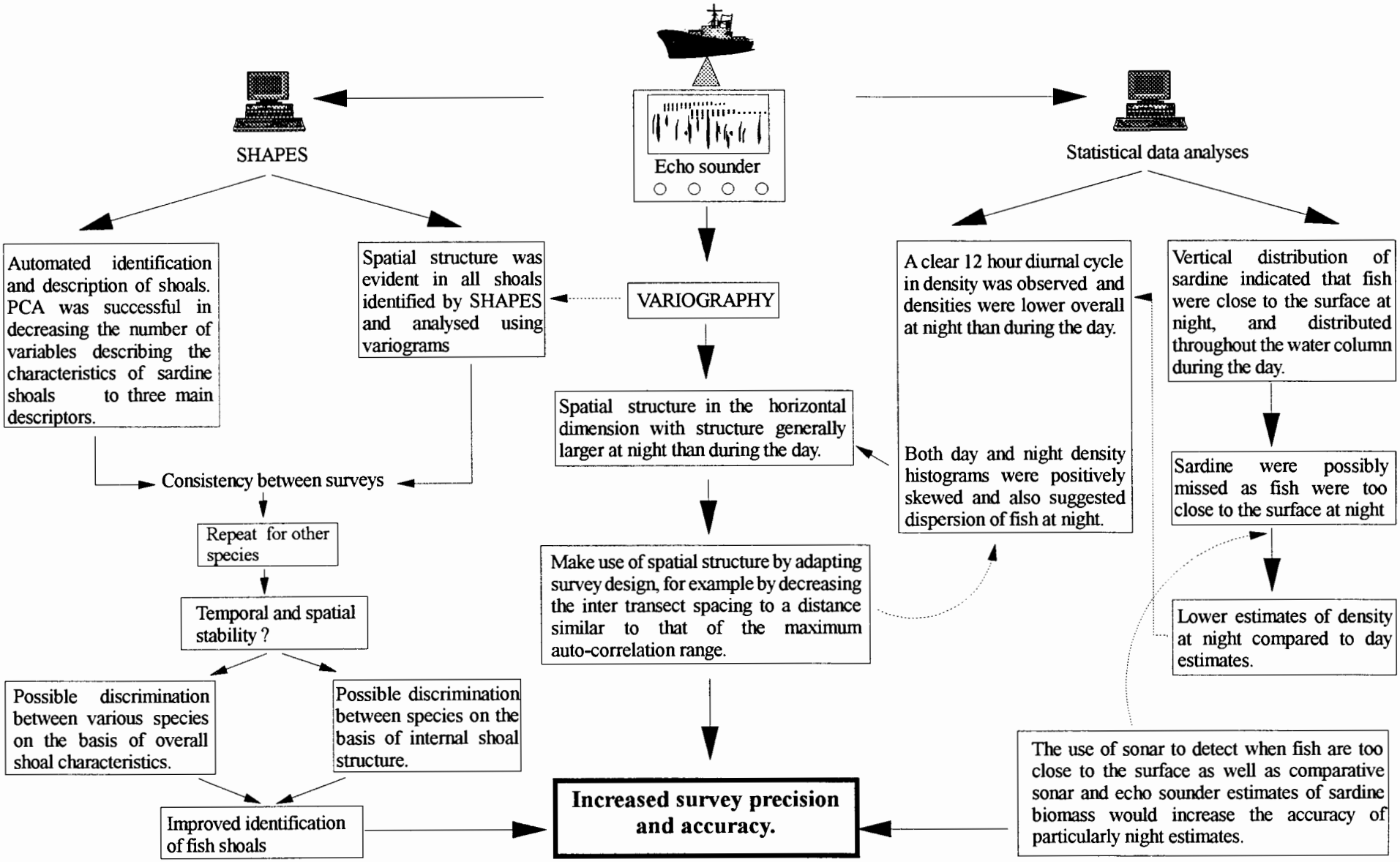


Fig. 6.1. Schematic summary of this study, highlighting important findings and suggestions to improvement in the methods of sardine stock assessment by acoustics.

## REFERENCES


Armstrong, M.J., Chapman, P., Dudley, S.F.J. and I. Hampton 1991. Occurence and population structure of pilchard *Sardinops ocellatus*, round herring *Etrumeus whiteheadi* and anchovy *Engraulis capensis* off the East Coast of southern Africa. *S. Afr. J. Mar. Sci.* 11:227-249.

Armstrong, M.J.,Shelton, P.A.,Prosch, R.M. and W.S. Grant 1983. Stock assessment and population dynamics of anchovy and pilchard in ICSEAF Division 1.6 in 1982. *Colln scient. Pap. int. Commn SE. Atl. Fish.* **10**(1):7-25.

Barange, M. and C. van der Lingen 1996. (Eds.) WOSAS - Workshop on southern African sardine: Proceedings and recommendations. *BEP Rep.* **29**:107 p.

Barange, M. 1994. Acoustic identification, classification and structure of biological patchiness on the edge of the Agulhas Bank and its relation to frontal features. *S. Afr. J. mar. Sci.* **14**:333-347.

Barange, M. and I. Hampton 1996. Structural analysis of co-existing anchovy and sardine populations from acoustic data: Implications for survey design. *In press.*

Barange, M., Hampton, I. and M. Soule 1996. Empirical determination of in situ target strengths of three loosely aggregated pelagic fish species. *ICES J. Mar. Sci.* **53**: 225-232.

Blaxter, J.S.H and J.R. Hunter 1982. The biology of the clupeoid fishes. *Adv. mar. Biol.* **20**:1-223.

Blaxter, J.S.H and F.G.T.Holliday. 1963. The behaviour and physiology of herring and other clupeoids. *Advances in Marine Biology.* **1**:261-393.

Breder, C.M 1954. Equations descriptive of fish schools and other animal aggregations. *Ecology.* **35**:361-370.

Breder, C.M. 1976. Fish schools as operational structures. *Fishery Bulletin. U.S.* **74**:471-502.

Breder, C.M 1959. Studies on social groupings in fish. *Bull. Am. Mus. Nat. Hist.* **117**:397-481.

Butterworth, D.S. 1983. Assessment and management of pelagic stocks in the southern Benguela region. In: *Proceedings of the Expert Consultation to Examine Changes in Abundance and Species Composition of Neritic Fish Resources, San José, Costa Rica, April 1983.* Sharp, G.D. and J. Csirke (Eds.). *F.A.O. Fish. Rep.* **291**(2):329-405.

Crawford, R.J.M.,Shannon, L.V. and D.E. Pollock 1987. The Benguela ecosystem. 4. The major fish and invertebrate resources. In *Oceanography and Marine Biology. An Annual Review* **25**. Barnes, M. (Ed.). Aberdeen University Press: 353-505.

Cressie, N.A.C. 1991. *Statistics for spatial data.* John Wiley &Sons Inc., New York 900 pp.

Cullen, J.M., Shaw, E. and H. Baldwin 1965. Methods for measuring the 3-D structure of fish schools. *Anim. Behav.* **13**:534-543.

Cushing, D.H. 1977. Observations on fish shoals with the arl scanner. *Rapp. P.-v. Réun. Cons. int. Explor. Mer.* **170**:15-20.

FAO. 1994. Fishery statistics, catches and landings, 1992. *Food and Agricultural Organization of the United Nations. Rome, Italy*, 677 pp.

FAO. 1993 Trends in catches and landings. Atlantic fisheries: 1970-1991. *FAO Fisheries Circular No. 855.1, Rome, FAO*, 1993. 223 pp.

Foote, K.G. 1990. Correcting acoustic measurements of scattered density for extinction. *J. Acoustic. Soc. Am.* **75**:612-616.

Foote, K.G. 1982. Energy in acoustic echoes from fish aggregations. *Fish. Res.* **11**:129-140.

Fréon, P., Soria, M., Mullon, C. and Gerlotto, F. 1993 Diurnal variation in fish density estimate during acoustic surveys in relation to spatial distribution and avoidance reaction. *Aquat. Living. Resour.* **6**:221-234.

Fréon, P., F. Gerlotto and O.A. Misund 1993. Consequences of fish behaviour for stock assessment. *ICES Mar. Sci. Symp.* 178-183.

Fréon, P., F. Gerlotto and M. Soria. 1992. Changes in school structure according to external stimuli: description and influence on acoustic assessment. *Fisheries Research.* 15:45-66.

GEOSPACE Group, Monpellier, France. 1993. Forword: The spatial organization of aquatic populations as observed using hydroacoustic methods. *Aquat. Living. Resour.* **6**:171-174.

GLOBEC 1994. International GLOBEC small pelagic fishes and climate change program. Report of the first planning meeting. La Paz, Mexico, June 20-24, 1994.

Halldórsson, O. and P. Reynisson 1983. Target strength measurements of herring and capelin in situ at Iceland. In: *Symposium on Fisheries Acoustics. Selected Papers of the ICES/F.A.O.Symposium on Fisheries Acoustics, Bergen, Norway, June 1982.* Nakken, O. and S.C. Venema (Eds.). *F.A.O. Fish. Rep.* **300**:78-84.

Hampton, I. 1992. The role of acoustic surveys in the assessment of pelagic fish resources

on the South African continental shelf. In: *Benguela trophic functioning*. Payne, A.I.L., Brink, K.H., Mann, K.H. and R. Hilborn (Eds.). *S. Afr. J. Mar. Sci.* **12**:1031-1050.

Hampton, I. 1987. Acoustic study on the abundance and distribution of anchovy spawners and recruits in South African waters. In: The Benguela and Comparable Ecosystems. Payne, A.I.L.,Gulland, J.A. and K.H. Brink (Eds.). *S. Afr. J. Mar. Sci.* **5**:901-917.

Hampton, I., Shelton, P.A. and M.J. Armstrong 1985. Direct estimates of anchovy spawner biomass off SA. *S. Afr. Shipp. News Fishg Ind. Rev.* **40**(4):31,33.

Hampton, I., Misund, O.A.,Coetzee, J.C.,Freon, P., Olsen, K. and I. Svellingen. Comparison of echo-sounder and sonar estimates of sardine (*Sardinops sagax*) biomass in False Bay, South Africa. (In prep.)

Hampton, I. 1996. Acoustic and egg-production estimates of South African anchovy biomass over a decade: comparisons, accuracy and utility. *ICES J. Mar. Sci.* **53**: 493-500.

Haralabous, J. and S. Georgakarakos 1996. Artificial neural networks as a tool for species identification of fish schools. *ICES J. Mar. Sci.* **53**:173-180.

Hoar, W.S., and D.J. Randall 1978. *Fish physiology. Locomotion*. **7**:576 p.

Hunter, J.R. 1972. Swimming and feeding behaviour of larval anchovy *Engraulis mordax*. *Fishery Bulletin U.S.* **70**:821-838.

Keenleyside, M 1955. Aspects of schooling behaviour in fish. *Behavior*. **8**:83-248

MacLennan D.N.and E.J.Simmonds 1992. *Fisheries Acoustics*. London; Chapman & Hall: ix +325 pp. +4 pp. Plates.

Maravellias, C.D. and J. Haralabous. 1995. spatial distribution of herring in the Orkney/Shetland area (Northern North Sea): a geostatistical analysis. *Neth. J. Sea. Res.* **34**:319-329.

Marchal, E. and P. Petitgas. 1993. Prescision of acoustic fish abundance estimates: separating the number of schools from the biomass in the schools. *Aquat. Living. Resour.* **6**:211-219.

Massé, J., Koutsikopoulos, C. and W. Patty. 1996. The structure and spatial distribution of pelagic fish schools in multispecies clusters: an acoustic study. *ICES. J. Mar. Sci.* **53**:155-160.

Matheron, G 1971. The theory of regionalized variables and its applications. *Ecole Nationale Supérieure de Mines de Paris, Fontainebleau, France*. 211 pp.

Misund, O.A., Aglen, A., Hamre, J., Ona, E., Rottingen, I., Skagen, D. and J.W. Valdemarsen. 1996. Improved mapping of schooling fish near the surface: comparison of abundance estimates obtained by sonar and echo integration. *ICES J. Mar. Sci.* **53**:383-388.

Misund, O.A., Fréon, P., Coetzee, J., Gardener, M., Olsen, K. and I. Hampton. Schooling behaviour of sardine (*Sardinops sagax*) in False Bay, South Africa. (In prep).

Misund, O.A. 1990. Dynamics of moving masses: variability in packing density and shape among pelagic schools. *ICES. CM 1990*/**B:40**.

Misund, O.A., Aglen, A., Beltestad, A.K. and J. Dalen. 1992. Relationships between the geometric dimensions and biomass of schools. *ICES. J. Mar. Sci.* **49**:305-315.

Misund, O.A., Aglen, A. and E. Frønæs. 1995. Mapping the shape, size, and density of fish schools by echo integration and a high resolution sonar. *ICES. J. Mar. Sci.* **52**:11-20.

Nero, R.W. and J.J. Magnuson. 1989. Characterization of patches along transects using high resolution 70-kHz integrated acoustic data. *Can. J. Fish. Aquat. Sci.* **46**:2056-2064.

Olsen, K. 1990. Fish behaviour and acoustic sampling. *Rapp. P.-v. Réun. Cons. int. Explor. Mer.* **189**:147-158.

Partridge B.L. The effect of school size on the structure and dynamics of minnow schools. *Anim. Behav.* **28**:68-77.

Partridge, B.L. Structure and function of fish schools. *Scientific American.* **245**:114-123.

Partridge, B.L., Pitcher, T., Cullen, J.M. and J. Wilson 1980. The three dimensional structure of fish schools. *Behav. Ecol. Sociobiol.* **6**:277-288.

Petitgas, P. and A. Prampart 1993. EVA: a geostatistical software on IBM-PC for structure characterization and variance computation. *ICES CM 1993/D*: **65**. 55 pp.

Petitgas, P. 1993. Use of disjunctive kriging to model areas of high pelagic fish density in acoustic fisheries surveys. *Aquat. Living. Res.* **6**: 201-209.

Petitgas, P. 1994. Spatial strategies of fish populations. *ICES. C.M. 1994*/**D:14**

Pitcher, T.J. and B.L. Partridge 1979. Fish school density and volume. *Mar. Biol.* **54**:383-394.

Pitcher, T.J. 1993. *Behaviour of teleost fishes*. Fish and Fisheries Series 7. Chapman and Hall, London. 715 pp.

Roel, B.A. and M.J. Armstrong 1991. The round herring *Etrumeus whiteheadi*, an abundant, underexploited clupeoid species off the coast off southern Africa. *S. Afr. J. Mar. Sci.* **11**:267-287.

Rose, G.A. and W.C. Leggett 1988. Hydroacoustic signal classification of fish schools by species. *Can. J. Fish. Aquat. Sci.* **45**:597-604.

Rossi, R.E., Mulla, D.J., Journel, A.G. and E.H. Franz 1992. Geostatistical tools for modeling and interpreting ecological spatial dependence. *Ecological Monographs*. **62**(2):227-314.

Scalabrin, C., Diner, N., Weill, A., Hillion, A. and M-C. Mouchot. 1996. Narrowband acoustic identification of monospecific fish shoals. *ICES. J. Mar. Sci.* **53**:181-188.

Shelton, P.A.,Armstrong, M.J. and B.A. Roel. 1992. An overview of the application of the eff production method in the assessment of anchovy in the Southeast Atlantic. *Contr. Sci. nat. Hist. Mus. Los Angeles Cty.*

Simmard, Y., Marcotte, D. and G. Bourgault. 1993. Exploration of geostatistical methods for mapping and estimating acoustic biomass of pelagic fish in the Gulf of St Lawrence: size of echo-integration unit and auxiliary environmental variables. *Aquat. Living. Resour.* **6**:185-199.

Swartzman, G., Stuetzle, W., Kulman, K. and M. Powojowski. 1994. Relating the distribution of pollock schools in the Berring Sea to environmental factors. *ICES J. Mar. Sci.* **51**:481-492.

Thompson, C.J. 1990. The market for fish meal and oil in the United States: 1960-1988 and future prospects. *Calif. Coop. Oceanic Fish. Invest. Rep.* **31**:124-131.

Vray, D., Gimenez, G. and R. Person. 1990. Attempt at classification of echo-sounder signals based on linear discriminant function of Fisher. *Rapp. P.-v. Réun. Cons. int. Explor. Mer.* **189**:388-393.

Weston, D.E.,and H.W. Andrew 1990. Seasonal sonar observations of the diurnal shoaling times of fish. *J. Acoust. Soc. Am.* **87**:673-680.

Zar, J.H. 1984. *Biostatistical analysis*. London; Prentice-Hall International, Inc: xiv +718 pp.